E-ISSN: 2148-6247

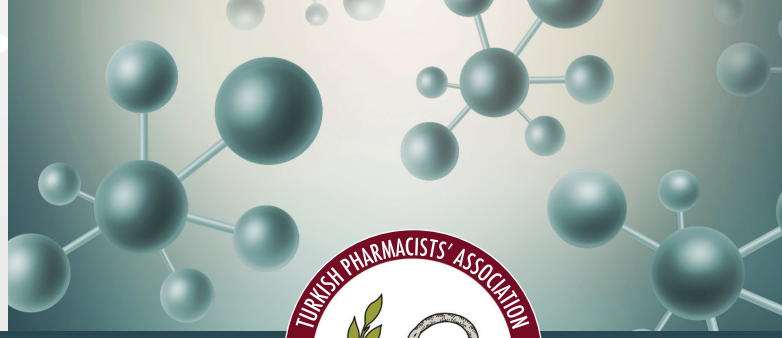

Turkish Journal of PHARMACEUTICAL SCIENCES

An Official Journal of the Turkish Pharmacists' Association, Academy of Pharmacy

Volume: 21 Issue: 2 April 2024

www.turkjps.org

PubMed Central PubMed Scopus TR DİZİN

galenos Publishing House

Turkish Journal of
PHARMACEUTICAL SCIENCES

Turkish Journal of
PHARMACEUTICAL SCIENCES

Turkish Journal of
PHARMACEUTICAL SCIENCES

Please refer to the journal's webpage (https://www.turkjps.org/) for "Editorial Policy" and "Instructions to Authors".

The editorial and publication process of the **Turkish Journal of Pharmaceutical Sciences** are shaped in accordance with the guidelines of ICMJE, WAME, CSE, COPE, EASE, and NISO. The Turkish Journal of Pharmaceutical Sciences is indexed in **PubMed, PubMed Central, Thomson Reuters / Emerging Sources Citation Index, Scopus, ULAKBİM, Türkiye Atıf Dizini, Embase, EBSCO Host, Türk Medline, Cabi, CNK**I.

The journal is published online.

Owner: Turkish Pharmacists' Association, Academy of Pharmacy

Responsible Manager: İlkay Erdoğan Orhan

galenos yayınevi

Publisher Contact
Address: Molla Gürani Mah. Kaçamak Sk. No: 21/1
34093 İstanbul, Türkiye
Phone: +90 (530) 177 30 97
E-mail: info@galenos.com.tr/yayin@galenos.com.tr
Web: www.galenos.com.tr | **Publisher Certificate Number:** 14521

Publication Date: May 2024
E-ISSN: 2148-6247
International scientific journal published bimonthly.

Turkish Journal of
PHARMACEUTICAL SCIENCES

CONTENTS

Original Articles

Turk J Pharm Sci 2024;21(2):88-94
DOI: 10.4274/tjps.galenos.2023.90846

ORIGINAL ARTICLE

Potential Hepatoprotective Effects of Irbesartan, an Accessible Angiotensin II Receptor Blocker, Against Cisplatin-Induced Liver Injury in a Rat Model

Onur ERTUNÇ[1]*, Yalçın ERZURUMLU[2], Mehtap SAVRAN[3], Deniz ÇATAKLI[3], Eltaf DOĞAN KIRAN[4], Şakir PEKGÖZ[1]

[1]Süleyman Demirel University Faculty of Medicine, Department of Pathology, Isparta, Türkiye
[2]Süleyman Demirel University Faculty of Pharmacy, Department of Biochemistry, Isparta, Türkiye
[3]Süleyman Demirel University Faculty of Medicine, Department of Pharmacology, Isparta, Türkiye
[4]Süleyman Demirel University Faculty of Medicine, Department of Biochemistry, Isparta, Türkiye

ABSTRACT

Objectives: Drug-induced liver injury is a common adverse reaction that frequently occurs with chemotherapeutic agents, such as cisplatin (CIS). This study seeks to enhance our understanding of drug actions and their associated adverse effects by examining the toxicity of CIS on rat liver tissue. We aimed to investigate the potential hepatoprotective effects of irbesartan (IRB), an easily accessible angiotensin II receptor blocker, in mitigating CIS-induced hepatotoxicity.

Materials and Methods: Wistar albino rats were divided into four groups. These groups included a control group [saline, *per* oral (*p.*o.)] for seven days, and 1 mL saline intraperitoneal [(i.p.) on the fourth day]; a CIS group (1 mL saline for seven days and 7.5 mg/kg CIS *i.p.* on the fourth day); a CIS + IRB group (IRB: 50 mg/kg *p.o.* for seven days and 7.5 mg/kg CIS *i.p.* on the fourth day), and an IRB group (50 mg/kg IRB *p.o.* for seven days). The effect of IRB on interleukin-1 beta (IL-1β) and caspase 3 levels was evaluated by immunohistochemical analysis, and its effects on mRNA expression levels of CCAAT/enhancer-binding protein homologous protein (CHOP) and immunoglobulin-heavy-chain-binding protein (BiP) were tested by quantitative real-time polymerase chain reaction.

Results: IRB administration mitigated CIS-induced liver toxicity by inhibiting endoplasmic reticulum (ER) stress. Specifically, this drug reduced the mRNA expression of ER stress markers, including CHOP and BiP. In addition, IRB treatment decreased oxidative stress, inflammatory responses, and apoptotic markers.

Conclusion: These findings suggest that IRB is a promising therapeutic option for preventing CIS-induced liver injury, potentially by modulating ER stress-related pathways.

Keywords: Cisplatin, ER-stress, irbesartan, liver toxicity.

INTRODUCTION

Cisplatin (CIS) (*cis*-diamminedichloroplatinum) is one of the most commonly preferred chemotherapeutic agents for treating malignancies. Several adverse effects can be observed with CIS treatment, such as nephrotoxicity, gastrointestinal disorders, neurotoxicity, ototoxicity, hepatotoxicity, and cardiotoxicity.[1,2] CIS-induced hepatotoxicity is the most frequently encountered adverse effect that reduces therapeutic efficacy and limits the usage of this drug in cancer therapy.[3] Studies have shown that CIS-induced toxicity might result from mitochondrial dysfunction, excessive reactive oxygen species (ROS) production, increased tumor necrosis factor-alpha (TNF-α) levels, and induction of endoplasmic reticulum (ER) stress. Although there are predictable links between ER stress and anticancer drug-induced liver injury, the underlying mechanism remains unclear.[4,5]

*Correspondence: onurertunc@hotmail.com, Phone: +90 542 220 66 21, ORCID-ID: orcid.org/0000-0002-4159-1711
Received: 06.11.2022, Accepted: 06.05.2023

ER is a multifunctional organelle found in eukaryotic cells and consists of sac-like structures and branched tubules. It regulates numerous pivotal functions, including protein biosynthesis, folding, trafficking, calcium storage, and lipogenesis.[6,7] Altering physiological conditions affect ER homeostasis for various reasons, such as genetic mutations, heat shock, oxidative stress, and multiple pathophysiologies. Furthermore, increased protein synthesis requirement, glucose deprivation, or imbalance in ER calcium stock levels can cause impaired functionality of the ER, termed ER stress.[8]

Unfolded protein response (UPR) signaling is responsible for re-establishing cellular homeostasis against ER stress, and it is regulated by three ER-membrane-localized transmembrane proteins: inositol-requiring kinase 1 alpha (IRE1α), protein kinase R-like endoplasmic reticulum kinase (PERK), and activating transcription factor 6 (ATF6). It coordinates the ER protein folding capacity, proteostasis, and programmed cell death under prolonged UPR activation. Additionally, UPR has been associated with drug resistance in numerous pathologies.[7,9]

Protein aggregation in the ER lumen or insufficient ER capacity causes the release of glucose-regulated protein 78, also regarded as immunoglobulin-heavy-chain-binding protein (BiP), from the UPR sensors to which it is attached. BiP is a member of the heat shock protein family and is a key player that manages ER stress responses.[10] Thus, BiP levels in the ER pool play a critical role in managing ER stress. Furthermore, progesterone receptor regulates the expression level of various cell death-associated inducers, such as CCAAT/enhancer-binding protein homologous protein (CHOP), also known as GADD153.[11] CHOP is a pro-apoptotic transcription factor induced by ER stress and mediates apoptosis.[12] Because of the critical roles of BiP and CHOP proteins, changes in their levels are frequently evaluated in investigating ER stress at the cellular level.

Metabolic dysregulation induced by excessive numbers of lipids, glucose, cytokines, neurotransmitters, or exposure to chemotherapeutic agents leads to ER stress. This disruption in normal cellular function can contribute to the exacerbation of inflammatory responses and other associated pathologies.[13] Recent studies suggest that ER stress management is a potential target for new therapeutic approaches to be developed against cancer or tissue injuries.[14,15]

Irbesartan (IRB) is an angiotensin II receptor blocker that is commonly used for treating hypertension. It acts on the renin-angiotensin system (RAS) and exerts protective effects on diverse organs in the body, such as the heart, kidney, and liver. In addition, IRB has anti-inflammatory, antioxidant, and antifibrotic effects.[16] Emerging research has demonstrated that various pharmaceutical agents used in cancer treatment can induce a robust ER stress response. This novel insight may offer new avenues for developing more effective therapeutic strategies.[17,18] In addition, the efficacy of drug or chemoresistance occurrence can be alleviated by modulation of ER stress. This approach can be an important factor that could alter the treatment of adverse responses.[18] However, the relationship between ER stress and the action of anticancer drugs remains unclear. In this study, we shed light on the potential protective mechanisms underlying IRB against CIS-induced hepatotoxicity. To achieve this, we evaluated the impact of IRB on ER stress, oxidative stress parameters, and anti-inflammatory cytokine expression. The present findings may offer valuable insights into the therapeutic potential of IRB in managing drug-induced liver injury.

MATERIALS AND METHODS

Animals

Adult male Wistar albino rats (n= 32) with an average weight of 250-300 g were obtained from the Animal Research Laboratory. They were group-housed (eight rats *per* cage) under a 12/12 hours light/dark cycle at room temperature (24 ± 1 ˚C) with a relative humidity of 50 ± 10% and access to food and water *ad libitum*. Animals were acclimatized for at least seven days before experimentation (Figure 1). All experimental procedures were permitted by the National Institutes of Health and the Committee on Animal Research according to the ethical rules (approval number: 09/03, date: 23.09.2021).

All rats were randomly separated into four groups as follows:

1) The control group was given mL saline [*per* oral (*p.o.*)] for seven days. On the fourth day, 1 mL of saline was given [intraperitoneal (*i.p.*)].

2) The CIS group was administered 1 mL saline *p.o.* for seven days, and 7.5 mg/kg *i.p.* CIS (CIS, Koçak Farma, Türkiye) was administered on the fourth day.[19]

3) The CIS + IRB group was administered 50 mg/kg IRB (Sandoz, Switzerland) *p.o.* for 7 days, and 7.5 mg/kg CIS *i.p.* was administered on the fourth day.[20]

4) The IRB group was administered 50 mg/kg IRB *p.o.* for seven days, and 1 mL saline *i.p.* was administered on the fourth day.

The sacrifice of animals was performed 6 hours after the last drug administration under ketamine (80-100 mg/kg) (Alfamin, Alfasan International Besloten Vennootschap) and 8-10 mg/kg xylazine bio 2% solution (Bioveta, Czech Republic) anesthesia. Liver tissue were then removed. One part of the tissues converged for total antioxidant status (TAS), total oxidant status (TOS), and immunoblotting assay. The remaining tissue was fixed in 10% buffered formaldehyde for histopathological examination and immunohistochemical (IHC) analysis.

Histopathological analysis

The liver was removed, fixed in 10% buffered formalin during necropsy, and taken for routine pathology processing after macroscopic sampling using an automatic tissue processor (Leica ASP300S, Wetzlar, Germany) and embedded in a paraffin block. 5 µ thick sections were taken from blocks using a microtome (Leica RM2155, Leica Microsystems, Wetzlar, Germany). Then, hematoxylin-eosin staining was used to stain the sections and monitored by a light microscope.

IHC analysis

Two sections were taken from all groups of the liver samples and placed in poly-L-lysine coated slides. Then, IHC staining

of slices with anti-caspase-3 [sc-7272, 1:100, Santa Cruz (Texas, USA) and anti-interleukin-1 beta (IL-1β) [sc-52012, 1:100 dilution, Santa Cruz (Texas, USA)] was performed using the streptavidin-biotin technique consistent with the manufacturer's protocol. The incubation of sections with primary antibodies for 60 min was performed, and then immunohistochemistry using biotinylated secondary antibody and streptavidin-alkaline phosphate conjugate was performed. The secondary antibodies of the EXPOSE mouse and rabbit specific horseradish peroxidase/diaminobenzidine (HRP/DAB) Detection IHC kit (ab80436) (Abcam, Cambridge, UK) were used. DAB was used as the chromogen. Antigen dilution solution was used as a negative control. Blinding was performed in the examination of samples. Semiquantitative analysis was performed to quantify the intensity of the IHC markers using a grading score ranging from (0) to (3) as follows: (0) = negative, (1) = weak focal staining, and ≤ 10%, (2) = diffuse weak staining and ≥ 10%, and (3) = intense diffuse staining and ≥ 10%.[21] Independent ten different areas of each section were analyzed under 40X objective magnification by an experienced pathologist. The Database Manual Cell Sens Life Science Imaging Software System (Olympus Co., Tokyo, Japan) was used for morphometric analysis and microphotography.

Quantitative real-time polymerase chain reaction

Total RNA was extracted from rat tissues using a column-type minipress kit (Bio-Rad, Hercules, CA, USA) following the manufacturer's protocol. Complementary DNA was then synthesized with a cDNA Synthesis kit (Bio-Rad Laboratories, Hercules, CA). cDNA was amplified using the iTaq Universal SYBR Green Supermix in a CFX96 instrument (Bio-Rad Laboratories, Hercules, CA). In the polymerase chain reaction (PCR) processes, pre-denaturation at 95 °C for 10 min, followed by 40 cycles at 95 °C for 10 seconds, and at 60 °C for 30 seconds were followed. Melting curve analysis was performed to confirm the specificity of the PCR amplicons. Specific primers were designed to amplify BiP (Forward 5'-*TGT GAC TGT ACC AGC TTA CTT C-3'*, Reverse 5'-*TCT TCT CTC CCT CTC TCT TAT CC-3'*), CHOP (Forward 5'-*GGA GGC TAC ACT CTA CAA AGA AC-3'*, Reverse 5'-*CCT TCT AAC GCT TCC CAA AGA-3'*), and GAPDH (forward 5'-*CAA GGT CAT CCC AGA GCT GAA-3'*, Reverse 5'-*CAT GTA GGC CAT GAG GTC CAC-3'*). The housekeeping gene GAPDH was used to normalize relative gene expression. Relative mRNA expression levels were analyzed using the Livak method.[22]

Detection of oxidative stress markers

Biochemical analyses included measurements of TAS, TOS, and Open Systems Interconnection (OSI) levels. For oxidant-antioxidant analysis, liver tissue samples were homogenized. The spectrophotometric measurement of the TAS and TOS was performed using commercial kits consistent with the manufacturer's instructions (Rel Assay Diagnostics, Gaziantep, Türkiye), and the TOS/TAS ratio was noticed as OSI value.[23,24]

Liver function parameter measurement

Serum samples were obtained from the blood of rats by centrifugation at 3000 rpm for 10 min. The levels of aspartate transaminase (AST) and alanine aminotransferase (ALT) in serum were determined using the spectrophotometric technique on an autoanalyzer (Beckman Coulter, USA) with the instrument's kit.

Statistical analysis

Statistical analysis was performed using GraphPad Prism 5 software (San Diego, California, USA). Results were expressed as mean ± standard deviation (SD). One-way analysis of variance (ANOVA) followed by Bonferroni multiple comparison test was used to compare the groups. $p < 0.05$ were considered significant.

RESULTS

Histopathological finding

In hematoxylin-eosin staining, ten fields at 40X magnification were evaluated in the same way IHC expressions were assessed. The liver is typically organized into hexagonal lobules containing the central vein at the center and the portal vein, hepatic artery, and bile duct at the corners. Hepatic sinusoids connect the central vein to the portal vein (as depicted in Figure 2E). Following four days of CIS treatment, rats exhibited liver congestion, increased Kupffer cells, and reactive changes such as nucleolar prominence, as observed in liver sections (Figures 2A, 2B). However, in the group treated with both CIS and IRB, congestion in the hepatic sinus was reduced, as demonstrated by the H&E slides (Figure 2C). Interestingly, in the IRB-treated group, there was an increase in cytoplasmic eosinophilia (Figure 2D).

IHC findings

IHC evaluation showed that CIS administration caused a significant increase in caspase 3 and IL-1β expressions in the liver tissues of rats ($p < 0.001$). IRB treatment reversed the CIS-induced increment in caspase -3 and IL-1β expressions ($p < 0.01$, $p < 0.001$, respectively) (Figures 3, 4).

Quantitative reverse transcriptase polymerase chain reaction results

Elevated mRNA expression levels of CHOP and BiP were detected in the CIS group compared with the control ($p < 0.05$, $p < 0.001$; respectively). The combined treatment of CIS and

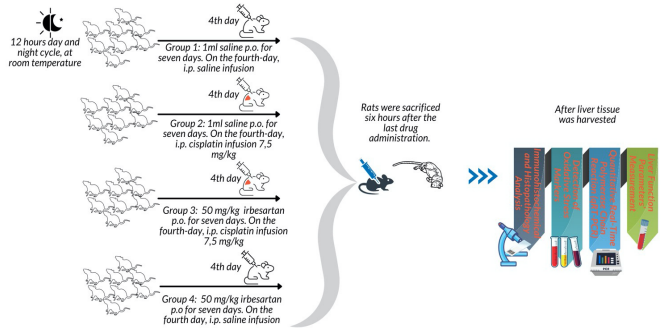

Figure 1. Experimental procedures are depicted as in the drawing

IRB significantly decreased the expression levels of CHOP and BiP compared with the CIS group ($p < 0.01$). Only IRB treatment significantly reduced CHOP and BiP levels compared with the CIS group ($p < 0.001$, $p < 0.01$, respectively) (Figure 5).

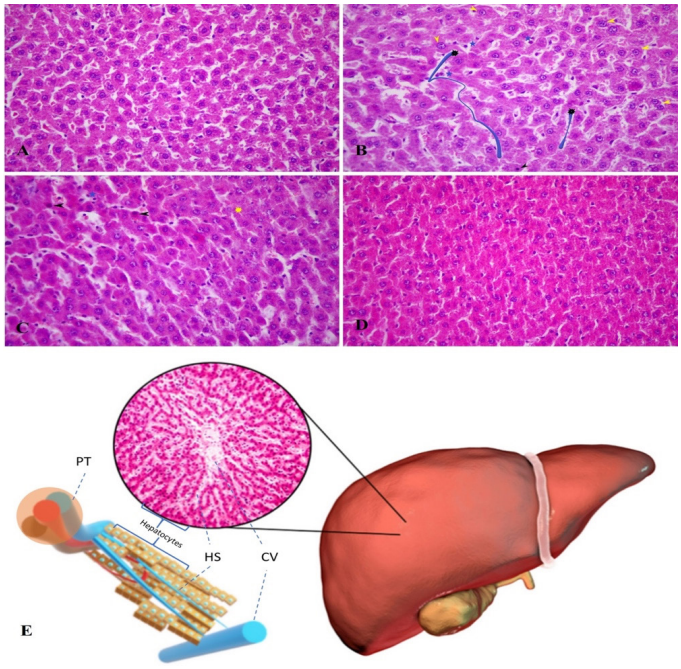

Figure 2. Histopathological findings in the liver tissue. Normal parenchymal hepatocytes in control mouse (A), CIS-treated group; sinusoidal spacing (shown in 3D line), sinusoidal Kupffer cells (blue star), reactive cellular alterations and nucleolar prominence (yellow arrows), and occasional apoptosis (black arrows) (B), CIS + IRB group; congestion, and sinusoidal spaces, increased eosinophilic cytoplasm (yellow mark), and sinusoidal Kupffer cells (blue star) and sporadic apoptotic hepatocytes (black arrow) (C), IRB group; eosinophilic cytoplasm (D), hepatic lobule schema (E) (all H&E slides were captured by the microscope Nikon Ni-U at 200x magnification)

HS: Hepatic sinus, CV: Central vein, PT: Portal triad, CIS: Cisplatin, IRB: Irbesartan

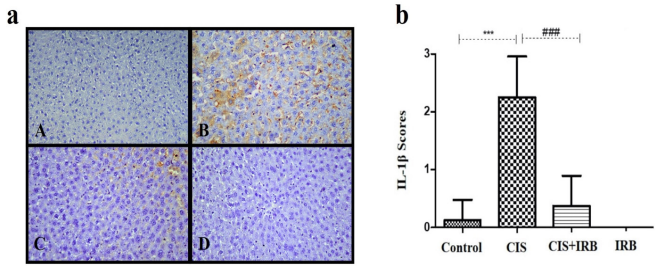

Figure 3. A) IHC evaluation of IL-1β levels. Negative expression in the control group (A), marked increase in expression in the CIS group (B), decreased expression in the CIS + IRB group (C), and lack of expression in the IRB group (D). B) Statistical analysis of IL-1β levels. In the CIS group IL-1β scores were significantly higher than those in the control group ($p < 0.001$). In the CIS + IRB group, IL-1β scores significantly decreased compared with those in the CIS group ($p < 0.001$). In the IRB group, IL-1β scores were significantly lower than those in the CIS group ($p < 0.001$). Comparison between groups was assessed by One-Way ANOVA test followed by *post-hoc* Bonferroni multiple comparison test.

IHC: Immunohistochemical, IL-1β: Interleukin-1 beta, CIS: Cisplatin, IRB: Irbesartan, ANOVA: Analysis of variance

Biochemical results

Oxidative stress parameters

A significant decrement in TAS levels was determined in the CIS group compared with the controlgroup ($p < 0.01$, Figure 6). In the CIS + IRB and IRB groups, TAS levels increased compared with the CIS group ($p < 0.001$ for both). OSI levels were elevated in the CIS group compared with the control group ($p < 0.01$). In the CIS + IRB group, OSI level was attenuated compared with the CIS group ($p < 0.01$) (Figure 6).

Liver function parameters

The ALT and AST levels of the CIS group were significantly higher than the control ($p < 0.001$, $p < 0.01$, respectively). In the CIS + IRB group, ALT and AST levels were attenuated compared with the CIS group ($p < 0.001$, $p < 0.01$, respectively). In contrast, ALT levels were attenuated in the IRB group compared with the CIS + IRB group ($p < 0.05$) (Figure 7).

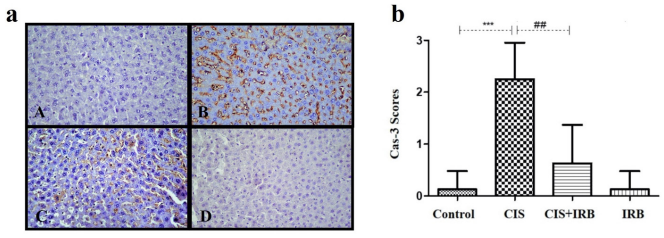

Figure 4. a) IHC evaluation of caspase-3 levels. Negative expression in the control group (A), marked increase in expression in the CIS group (B), decreased expression in the CIS + IRB group (C), and lack of expression in the IRB group (D). b) Statistical analysis of caspase-3 levels. In the CIS group, caspase-3 scores were significantly higher than those in the control group ($p < 0.001$). In the CIS + IRB group, caspase-3 scores significantly decreased compared with those in the CIS group ($p < 0.01$). Comparison between groups was assessed by One-Way ANOVA followed by *post-hoc* Bonferroni multiple comparison test

IHC: Immunohistochemical, IL-1β: Interleukin-1 beta, CIS: Cisplatin, IRB: Irbesartan, ANOVA: Analysis of variance

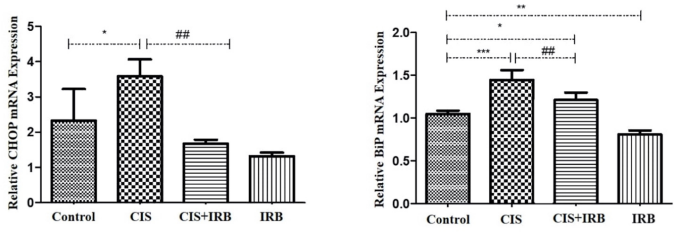

Figure 5. Evaluation of the relative mRNA expression levels of CHOP and BiP. mRNA expression levels of CHOP and BiP were analyzed by qRT-PCR. Relative mRNA expression values were calculated using $2^{-\Delta\Delta CT}$ and GAPDH was used as a housekeeping marker. Data represent the mean of four independent biological replicates in triplicates, and error bars represent SD. Comparison between groups was assessed by One-Way ANOVA followed by *post-hoc* Bonferroni multiple comparison test. Values are represented as means ± SD.

(n=3), $^{*}p < 0.05$, $^{**}p < 0.01$, $^{***}p < 0.001$, * represents comparison with control group, $^{\#}p < 0.05$, $^{\#\#}p < 0.01$, $^{\#\#\#}p < 0.001$, # represents comparison with CIS group, CIS: Cisplatin, IRB: Irbesartan, CHOP: CCAAT/enhancer-binding protein homologous protein, BiP: Immunoglobulin-heavy-chain-binding protein, qRT-PCR: Quantitative reverse transcriptase polymerase chain reaction, SD: Standard deviation, ANOVA: Analysis of variance

DISCUSSION

IRB is a commonly used angiotensin-converting enzyme-II blocker and is effective in treating hypertension-related cardiovascular diseases.[25] The RAS plays a pivotal role in the physiological system, especially in blood pressure regulation and its components, including angiotensin II, which is highly expressed in various tissues, such as the kidney, adipose, and liver.[26-28] Moreover, inhibition of RAS by angiotensin-converting enzyme (ACE) inhibitors or angiotensin receptor antagonists has been presented as a therapeutic approach for liver fibrosis.[29] It has been shown that the effects of these drugs are not limited to angiotensin blockage; they also have ameliorative activity on oxidative stress, glutathione depletion, and lipid peroxidation.[30-32] *In vivo* and *in vitro* studies performed on cardiomyocytes have shown that angiotensin II induces ER stress.[33] A study conducted on human pancreatic islet cells demonstrated a protective effect of Losartan, another ACE inhibitor, against glucose-induced ER stress responses.[34] Although detailed examinations of the anti-inflammatory and antioxidant effects of IRB have been conducted in various studies, the ER stress-related outcomes of IRB still need to be clearly understood.[25] Kabel et al.[16] demonstrated that IRB exhibited hepatoprotective effects by inhibiting apoptosis in hepatic tissues.[16] Thus, we investigated the underlying mechanism of IRB in CIS-induced hepatotoxicity by evaluating ER stress-related responses.

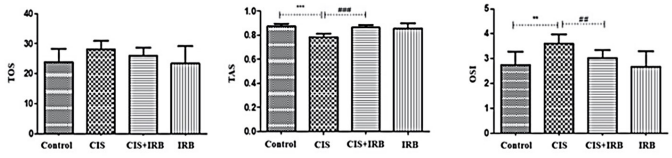

Figure 6. Oxidative stress parameters of the liver tissue. Values are presented as means ± SD.

Comparison between groups and results of oxidative stress markers were assessed by One-Way ANOVA test followed by *post-hoc* Bonferroni multiple comparison test

**p* < 0.05, ***p* < 0.01, ****p* < 0.001,* represents comparison with control group, #*p* < 0.05, ##*p* < 0.01, ###*p* < 0.001, # represents comparison with CIS group, CIS: Cisplatin, IRB: Irbesartan, SD: Standard deviation, ANOVA: Analysis of variance, TAS: Total antioxidant status, TOS: Total oxidant status, OSI: Open Systems Interconnection

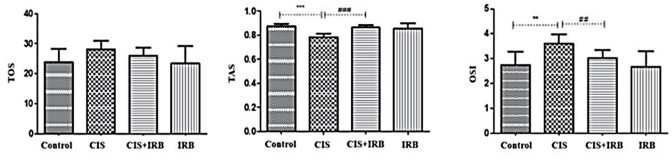

Figure 7. Evaluation of liver function parameters. Values are presented as means ± SD. Comparison between groups and results of oxidative stress markers were assessed by One-Way ANOVA test followed by *post-hoc* Bonferroni multiple comparison test

**p* < 0.05, ***p* < 0.01, ****p* < 0.001, * represents comparison with control group, #*p* < 0.05, ##*p* < 0.01, ###*p* < 0.001, # represents comparison with CIS group, CIS: Cisplatin, IRB: Irbesartan, SD: Standard deviation, ANOVA: Analysis of variance, ALT: Alanine aminotransferase, AST: Aspartate aminotransferase

CIS is a chemotherapeutic drug that shows efficiency against various cancer types such as testicular, gastric, ovarian, lung, and breast.[4] However, almost 30% of patients may face the adverse effects of CIS, which limits drug usage in therapy.[3] There are numerous side effects of CIS, but hepatotoxicity is still the most common. To date, the proven mechanisms of CIS-induced hepatotoxicity are mitochondrial dysfunction, oxidative stress, inflammatory apoptosis, and disrupted Ca^{+2} homeostasis.[35]

Recent studies have shown that possible ER stress-mediated mechanisms may have a critical role in hepatotoxicity progression.[36] ER membrane-localized sensor proteins (IRE1α, PERK, and ATF6) fine-tune the ER stress responses for the cells to adapt to changing physiological conditions.[11] In particular, releasing BiP protein from ER stress sensors activates UPR signaling. When the cells cannot overcome prolonged ER stress, the expression levels of CHOP, which is a downstream effector of the PERK branch of UPR, increase, and programed cell death is triggered through CHOP-controlled apoptotic proteins.[37] Thus, cell survival or programmed cell death decisions are made under ER stress. Herein, we evaluated the mRNA expression levels of CHOP, a pro-apoptotic factor, and found that its high expression levels lead cells to mediate programed cell death. In addition, we tested the mRNA expression levels of BiP, which is an ER chaperone and is frequently used as a marker to monitor ER stress.[38]

In studies that investigated the protective effects of IRB against CIS-induced hepatotoxicity, our findings indicated that IRB administration significantly restores CIS-induced tissue damage by decreasing ER stress induction (Figure 6). We determined that IRB significantly reduced the CIS-induced mRNA expression levels of BiP and CHOP. These results suggest that IRB plays a protective role in CIS-induced hepatotoxicity by reducing CIS-mediated elevation of BiP and CHOP levels.

The CHOP protein is also associated with one of the mechanisms that leads to ROS production linked to ER stress.[39] For this reason, to better understand the protective role of IRB against CIS-induced tissue damage, we evaluated the TAS, TOS, and OSI levels. As expected, CIS treatment caused a decrease in the TAS level and an increase in the OSI level (Figure 7).

The feedback between inflammatory cell responses and the ER stress response might trigger apoptosis in several pathological conditions.[40] ER stress may lead to activation of nuclear factor kappa-light-chain-enhancer of activated B cells (NF-κB) phosphorylation and increment in the proinflammatory and apoptotic cytokine synthesis and release from the cell, contributing to the inflammatory and apoptotic cycle progression.[41] As known, IL-1β and Cas-3 are common inflammatory and apoptotic mediators, respectively. In addition, they cross-talk with each other through the NF-κB pathway.[42] Previous studies have indicated that IRB could prevent inflammation by inhibiting the NF-κB pathway.[25]

Our findings suggested that CIS administration strongly increased CHOP and BiP mRNA expressions, resulting in increased IL-1 and Cas-3 levels; in contrast, IRB administration

significantly decreased IL-1 and Cas-3 levels, as seen in the results of immunohistochemistry. In addition, the present histopathologic findings overlapped with the literature.[25,43] Consistent with immunostaining results, our histological findings support the protective role of IRB against CIS-induced liver tissue damage. In the CIS group, sinusoidal dilatation and apoptotic bodies increased compared with the normal group. In addition, we detected a significant increase in eosinophilic cytoplasm in the IRB + CIS and IRB groups, which might result from cellular hypertrophy or peroxisomal and smooth ER or mitochondrial enhanced activity in the liver cells. Collectively, these results suggest that IRB effectively reverses CIS-induced hepatocellular tissue damage by decreasing ER stress and inflammatory responses triggered by CIS administration.

Moreover, we measured the impact of IRB on hepatic tissue-related biochemical parameters. ALT and AST are serological markers of pathologies in liver tissue. Biochemical detection of ALT is particularly susceptible to detecting liver injury.[44] In addition, AST is found in the mitochondria of hepatocytes, and when injury of hepatocytes occurs, it is released into the blood.[45] Our results showed that CIS administration elevated ALT and AST levels (Figure 7). These results suggest that IRB significantly reverses CIS-induced liver injury and inflammation in hepatocellular tissue. In addition, consistent with the literature, our findings indicate that IRB might protect the hepatocellular tissue against CIS-induced tissue damage by regulating ER stress and oxidative stress status.

Main points

- IRB reverses CIS-induced oxidative stress.
- IRB modulates CIS-induced liver dysfunction by reorganizing the main liver enzymes.
- IRB reduces CIS-induced ER stress.

Study limitations

The present study tested the effects of IRB on mRNA levels of CHOP and BiP. Therefore, further detailed analyses are required for a better understanding of the effect of IRB on ER stress modulation and its protective roles against CIS-induced liver injury.

CONCLUSION

Herein, we investigated the possible effects of IRB on CIS-induced hepatotoxicity. Our findings suggest that IRB may play protective roles against CIS-induced liver toxicity. However, further studies are needed to elucidate the mode of action of IRB in liver toxicity.

Ethics

Ethics Committee Approval: All experimental procedures were permitted by the National Institutes of Health and the Committee on Animal Research according to the ethical rules (approval number: 09/03, date: 23.09.2021).

Informed Consent: Not necessary.

Authorship Contributions

Surgical and Medical Practices: O.E., M.S., Concept: O.E., Y.E., M.S., Design: O.E., Y.E., M.S., Data Collection or Processing: O.E., Y.E., D.Ç., Ş.P., E.D.K., Analysis or Interpretation: O.E., Y.E., D.C., Literature Search: O.E., Y.E., D.C., Writing: O.E., Y.E., D.C.

Conflict of Interest: The authors declare no competing financial interests.

Financial Disclosure: This research was supported by Süleyman Demirel University Scientific Research Projects Unit.

REFERENCES

1. Lee HY, Mohammed KA, Goldberg EP, Kaye F, Nasreen N. Cisplatin loaded albumin mesospheres for lung cancer treatment. Am J Cancer Res. 2015;5:603-615.
2. Breglio AM, Rusheen AE, Shide ED, Fernandez KA, Spielbauer KK, McLachlin KM, Hall MD, Amable L, Cunningham LL. Cisplatin is retained in the cochlea indefinitely following chemotherapy. Nat Commun. 2017;8:1654.
3. Lebwohl D, Canetta R. Clinical development of platinum complexes in cancer therapy: an historical perspective and an update. Eur J Cancer. 1998;34:1522-1534.
4. Dasari S, Tchounwou PB. Cisplatin in cancer therapy: molecular mechanisms of action. Eur J Pharmacol. 2014;740:364-378.
5. Foufelle F, Fromenty B. Role of endoplasmic reticulum stress in drug-induced toxicity. Pharmacol Res Perspect. 2016;4:e00211.
6. Berridge MJ. The endoplasmic reticulum: a multifunctional signaling organelle. Cell Calcium. 2002;32:235-249.
7. Hetz C. The unfolded protein response: controlling cell fate decisions under ER stress and beyond. Nat Rev Mol Cell Biol. 2012;13:89-102.
8. Li A, Song NJ, Riesenberg BP, Li Z. The Emerging roles of endoplasmic reticulum stress in balancing immunity and tolerance in health and diseases: mechanisms and opportunities. Front Immunol. 2019;10:3154.
9. Storm M, Sheng X, Arnoldussen YJ, Saatcioglu F. Prostate cancer and the unfolded protein response. Oncotarget. 2016;7:54051-54066.
10. Wang M, Wey S, Zhang Y, Ye R, Lee AS. Role of the unfolded protein response regulator GRP78/BiP in development, cancer, and neurological disorders. Antioxid Redox Signal. 2009;11:2307-2316.
11. Bertolotti A, Zhang Y, Hendershot LM, Harding HP, Ron D. Dynamic interaction of BiP and ER stress transducers in the unfolded-protein response. Nat Cell Biol. 2000;2:326-332.
12. Oyadomari S, Mori M. Roles of CHOP/GADD153 in endoplasmic reticulum stress. Cell Death Differ. 2004;11:381-389.
13. Lin YD, Chen S, Yue P, Zou W, Benbrook DM, Liu S, Le TC, Berlin KD, Khuri FR, Sun SY. CAAT/enhancer binding protein homologous protein-dependent death receptor 5 induction is a major component of SHetA2-induced apoptosis in lung cancer cells. Cancer Res. 2008;68:5335-5344.
14. Erzurumlu Y, Dogan HK, Cataklı D, Aydogdu E. Tarantula cubensis extract induces cell death in prostate cancer by promoting autophagic flux/ER stress responses and decreased epithelial-mesenchymal transition. Rev Bras Farmacog. 2022;32:575-582.
15. Ashrafizadeh M, Tavakol S, Ahmadi Z, Roomiani S, Mohammadinejad R, Samarghandian S. Therapeutic effects of kaempferol affecting autophagy and endoplasmic reticulum stress. Phytother Res. 2020;34:911-923.

16. Kabel AM, Alzahrani AA, Bawazir NM, Khawtani RO, Arab HH. Targeting the proinflammatory cytokines, oxidative stress, apoptosis and TGF-β1/STAT-3 signaling by irbesartan to ameliorate doxorubicin-induced hepatotoxicity. J Infect Chemother. 2018;24:623-631.
17. Jeon YJ, Khelifa S, Ratnikov B, Scott DA, Feng Y, Parisi F, Ruller C, Lau E, Kim H, Brill LM, Jiang T, Rimm DL, Cardiff RD, Mills GB, Smith JW, Osterman AL, Kluger Y, Ronai ZA. Regulation of glutamine carrier proteins by RNF5 determines breast cancer response to ER stress-inducing chemotherapies. Cancer Cell. 2015;27:354-369.
18. Cubillos-Ruiz JR, Bettigole SE, Glimcher LH. Tumorigenic and immunosuppressive effects of endoplasmic reticulum stress in cancer. Cell. 2017;168:692-706.
19. Alibakhshi T, Khodayar MJ, Khorsandi L, Rashno M, Zeidooni L. Protective effects of zingerone on oxidative stress and inflammation in cisplatin-induced rat nephrotoxicity. Biomed Pharmacother. 2018;105:225-232.
20. Anjaneyulu M, Chopra K. Effect of irbesartan on the antioxidant defence system and nitric oxide release in diabetic rat kidney. Am J Nephrol. 2004;24:488-496.
21. Calhoun BC, Collins LC. Predictive markers in breast cancer: An update on ER and HER2 testing and reporting. Semin Diagn Pathol. 2015;32:362-369.
22. Livak KJ, Schmittgen TD. Analysis of relative gene expression data using real-time quantitative PCR and the 2(-Delta Delta C(T)). Methods. 2001;25:402-408.
23. Erel O. A novel automated direct measurement method for total antioxidant capacity using a new generation, more stable ABTS radical cation. Clin Biochem. 2004;37:277-285.
24. Erel O. A new automated colorimetric method for measuring total oxidant status. Clin Biochem. 2005;38:1103-1111.
25. Helal MG, Samra YA. Irbesartan mitigates acute liver injury, oxidative stress, and apoptosis induced by acetaminophen in mice. J Biochem Mol Toxicol. 2020;34:e22447.
26. Yvan-Charvet L, Quignard-Boulangé A. Role of adipose tissue renin-angiotensin system in metabolic and inflammatory diseases associated with obesity. Kidney Int. 2011;79:162-168.
27. Kalupahana NS, Moustaid-Moussa N. The renin-angiotensin system: a link between obesity, inflammation and insulin resistance. Obes Rev. 2012;13:136-149.
28. Ramalingam L, Menikdiwela K, LeMieux M, Dufour JM, Kaur G, Kalupahana N, Moustaid-Moussa N. The renin angiotensin system, oxidative stress and mitochondrial function in obesity and insulin resistance. Biochim Biophys Acta Mol Basis Dis. 2017;1863:1106-1114.
29. Bataller R, Brenner DA. Liver fibrosis. J Clin Invest. 2005;115:209-218. Erratum in: J Clin Invest. 2005;115:1100.
30. Khaper N, Singal PK. Modulation of oxidative stress by a selective inhibition of angiotensin II type 1 receptors in MI rats. J Am Coll Cardiol. 2001;37:1461-1466.
31. Jahovic N, Ercan F, Gedik N, Yüksel M, Sener G, Alican I. The effect of angiotensin-converting enzyme inhibitors on experimental colitis in rats. Regul Pept. 2005;130:67-74.
32. Kedziora-Kornatowska K. Effect of angiotensin convertase inhibitors and AT1 angiotensin receptor antagonists on the development of oxidative stress in the kidney of diabetic rats. Clin Chim Acta. 1999;287:19-27.
33. Yang C, Wang Y, Liu H, Li N, Sun Y, Liu Z, Yang P. Ghrelin protects H9c2 cardiomyocytes from angiotensin II-induced apoptosis through the endoplasmic reticulum stress pathway. J Cardiovasc Pharmacol. 2012;59:465-471.
34. Madec AM, Cassel R, Dubois S, Ducreux S, Vial G, Chauvin MA, Mesnier A, Chikh K, Bosco D, Rieusset J, Van Coppenolle F, Thivolet C. Losartan, an angiotensin II type 1 receptor blocker, protects human islets from glucotoxicity through the phospholipase C pathway. FASEB J. 2013;27:5122-5130.
35. Ezz-Din D, Gabry MS, Farrag ARH, Moneim AEA. Physiological and histological impact of *Azadirachta indica* (neem) leaves extract in a rat model of cisplatin-induced hepato and nephrotoxicity. J Med Plants Res. 2011;5:5499-5506.
36. Pandey VK, Mathur A, Khan MF, Kakkar P. Activation of PERK-eIF2α-ATF4 pathway contributes to diabetic hepatotoxicity: Attenuation of ER stress by Morin. Cell Signal. 2019;59:41-52.
37. Ohoka N, Yoshii S, Hattori T, Onozaki K, Hayashi H. TRB3, a novel ER stress-inducible gene, is induced *via* ATF4-CHOP pathway and is involved in cell death. EMBO J. 2005;24:1243-1255.
38. Pobre KFR, Poet GJ, Hendershot LM. The endoplasmic reticulum (ER) chaperone BiP is a master regulator of ER functions: Getting by with a little help from ERdj friends. J Biol Chem. 2019;294:2098-2108.
39. Zhang K, Kaufman RJ. From endoplasmic-reticulum stress to the inflammatory response. Nature. 2008;454:455-462.
40. Zeeshan HM, Lee GH, Kim HR, Chae HJ. Endoplasmic reticulum stress and associated ROS. Int J Mol Sci. 2016;17:327.
41. Baeuerle PA, Baichwal VR. NF-kappa B as a frequent target for immunosuppressive and anti-inflammatory molecules. Adv Immunol. 1997;65:111-137.
42. Lamkanfi M, Declercq W, Vanden Berghe T, Vandenabeele P. Caspases leave the beaten track: caspase-mediated activation of NF-kappaB. J Cell Biol. 2006;173:165-171.
43. Taghizadeh F, Hosseinimehr SJ, Zargari M, Karimpour Malekshah A, Mirzaei M, Talebpour Amiri F. Alleviation of cisplatin-induced hepatotoxicity by gliclazide: Involvement of oxidative stress and caspase-3 activity. Pharmacol Res Perspect. 2021;9:e00788.
44. Heydrnejad MS, Samani RJ, Aghaeivanda S. Toxic effects of silver nanoparticles on liver and some hematological parameters in male and female mice (*mus musculus*). Biol Trace Elem Res. 2015;165:153-158.
45. Ennulat D, Magid-Slav M, Rehm S, Tatsuoka KS. Diagnostic performance of traditional hepatobiliary biomarkers of drug-induced liver injury in the rat. Toxicol Sci. 2010;116:397-412.

Turk J Pharm Sci 2024;21(2):95-103
DOI: 10.4274/tjps.galenos.2023.03746

ORIGINAL ARTICLE

Determination of the Effects of Ankaferd Wound Dressing on the Wound Healing Process in Rats

Erhan ŞENSOY[1], Eda GÜNEŞ[2]*, Mehmet Okan ERDAL[3]

[1]Karamanoğlu Mehmetbey University Faculty of Medicine, Department of Midwifery, Karaman, Türkiye
[2]Necmettin Erbakan University Faculty of Tourism, Department of Gastronomy and Culinary Arts, Konya, Türkiye
[3]Necmettin Erbakan University Meram Vocational School, Department of Property Protection and Security, Konya, Türkiye

ABSTRACT

Objectives: The effects of a composite nanofiber wound dressing material consisting of a polyvinylidene alcohol and polyvinylidene pyrrolidone polymer mixture with a hemostatic agent doped with Ankaferd Blood Stopper (ABS) on the healing of experimentally induced dermal wounds in rats were examined.

Materials and Methods: Rats were divided into 4 groups (n= 6). Histological material was examined on tissues taken from the wound site, whereas total antioxidant status (TAS), total oxidant status (TOS), and oxidative stress index (OSI) analyses were performed on blood samples taken from the cardia. The material that was produced had hydrophilic properties, and both the ABS-doped and-undoped forms of the material positively affected wound healing.

Results: In the histopathological examinations, macroscopic evaluations revealed a statistically significant difference between the groups in terms of wound diameter, reepithelialization, and inflammation formation (p= 0.019). In parallel with wound healing and histological outcomes, TAS values increased in the ABS-doped groups, and TOS and OSI values decreased in the wound dressing groups ($p < 0.05$).

Conclusion: It was concluded that the ABS-dopped dressing did not have a negative effect on wound healing, it accelerated healing, and it could be used effectively and safely to treat skin injuries. However, further studies are needed to evaluate the clinical and histopathological benefits and potential adverse effects of wound dressings produced using ABS-doped polymers on wound healing.

Keywords: Ankaferd, nanofiber, wound, rat, oxidative stress index

INTRODUCTION

A skin wound is an injury that compromises the integrity of the epidermis as a physical barrier, thus disrupting its normal anatomical composition and physiology.[1] Today, millions of people are injured due to various causes, and many hemostatic agents are used to stop bleeding, with different levels of action and duration of stopping bleeding. The Ankaferd Blood Stopper (ABS), which is used after surgery and is effective in many cases such as bleeding gums, is an antibacterial hemostatic agent without additives consisting of various ratios of dried roots and leaves of *Thymus vulgaris L., Glycyrrhiza glabra L., Vitis vinifera L., Alpinia officinarum Hance,* and *Urtica diocia L.,* which are plants that are used in traditional Turkish medicine.[2-4]

In the intermediate recovery step, hemostasis is a natural process consisting of the inflammation, proliferation, and maturation stages.[5,6] In this process, the general characteristics of the injured tissue should be well known, and tissue-specific treatment methods should be applied. The aim of these methods is to create an ideal environment for epithelial formation in the injured area by stimulating the inflammatory cells, platelets, and extracellular matrix involved in wound healing.[5] Wound dressings are among the treatment methods that can create an ideal environment for proliferation by mimicking the extracellular matrix, protect the wound against microorganisms and infections, and contribute to the healing process.

*Correspondence: egunes@erbakan.edu.tr, Phone: +90 506 491 34 80, ORCID-ID: orcid.org/0000-0001-7422-9375
Received: 30.01.2023, Accepted: 13.05.2023

Today, with the discovery of new-generation biopolymers and the development of novel production techniques, modern wound dressings are being produced as an alternative to conventional wound dressings.[7] Polyvinyl alcohol (PVA) and polyvinylidene pyrrolidone (PVP), which are non-toxic, bio-based, renewable, and sustainable polymers, are used in biomedical, pharmaceutical, and regenerative medicine.[8] They can be converted into biocompatible and biodegradable, water-retaining, water-soluble, and nanofiber forms.[9] As natural synthetic polymers, PVA and PVP are easy to process because they have controllable physical properties and mechanical strength, and so, they are widely used for wound dressings.[10-12] Electrospinning, which is a nanofiber production technique, is a preferred method aimed at producing nanodiameter fibers by the electric field effect of polymer-based gels, and it is preferred because fibers that are one hundred times smaller (with an average radius of 10 nm-500 nm) can be produced compared to those produced by the classical method.[13-15] It is stated that the products used in treatments with experimental practices reduce oxidative stress (TOS/TAS = OSI) by increasing the total antioxidant status (TAS).[16,17] OSI analysis is used to determine oxidative stress levels as an easy, precise, automated, and inexpensive method.

Although various polymers and methods are used in nanofiber production, there is no study in the literature in which ABS-doped PVA and PVP polymers were produced by the electrowinning method. The aim of this study was to investigate the healing process and biochemical effects of a medical textile product containing an ABS-added polymer that can stop bleeding and heal wounds quickly in a rat model with experimentally induced wounds. Scanning electron microscopy (SEM) and Fourier transform infrared spectrophotometry (FTIR) analyses were carried out to characterize ABS dopped and non-dopped ABS polymers in the production of the material.

MATERIALS AND METHODS

The study was initiated by obtaining the approval of the ethics committee of Selçuk University, Experimental Medicine Research and Application Center (decision date: 25.01.2019 and decision number: 2019-2). All chemical materials used in the study were supplied by Sigma and Merck.

Preparation of the nanofibers

In this study, nanofibers were prepared to form a homogeneous wound dressing surface and provide a longer-lasting effect by the slow release of the drug additive. In addition, a control group was formed to examine the effects of the nanofiber surface with and without the drug additive and show the effects of the drug. The electrowinning process was performed for nanofiber wound dressing production.[12,18,19] Sterile gauze was used for fiber collection, and two different solutions were used as polymer solutions.[9] First, 10% by mass PVA (Mw: 72.000) in pure water was obtained by stirring at 70 °C for 1 h. Then, 10% PVP (MW: 58.000) in ethanol was prepared using a magnetic stirrer at room temperature for 30 min. These two polymer solutions were mixed at room temperature at a ratio of 3/4 PVA and 1/4 PVP to obtain a carrier polymer solution. 10 mL of the carrier polymer solution was used to make nanofiber without any additive. Taking 10 mL of the same polymeric solution, 1 mL of Ankaferd was added and nanofibers were produced. The unhopped fiber was collected on sterile gauze with a rotary collector at a speed of 400 rpm under the influence of an electric field of 1.7 kV/cm at a flow rate of 1 mL/h. The ABS-doped fiber was collected with a rotary collector at a speed of 400 rpm under an electric field of 1.9 kV/cm at a flow rate of 0.6 mL/h.

Experiments on material characterization

The experiments in this context were conducted at Necmettin Erbakan University, Science and Technology Research and Application Center (BITAM).

SEM micrographs of polymers

SEM was used to examine the morphology of the produced materials. The surface morphologies of the polymers were examined at magnifications of 1.000 and 5.000.

FTIR analysis

FTIR analyses were performed to determine the interaction between the drug mixture and the polymer structure.[20]

Animal materials and treatments

Twelve-week-old female Wistar albino rats with an average weight of approximately 295 g were used in this study. Female rats were preferred because the skin of females is thinner than that of males, and the lack of estrogen in males would negatively affect cutaneous wound healing.[21,22] The rats were housed without any water or feed restriction at room temperature in a 24 hours light-dark cycle.[23] The study was planned to include 24 rats, with four groups (n= 6 each) (Table 1).

After the groups were formed, the rats were administered 70 mg/kg ketamine and 10 mg/kg xylazine through the intraperitoneal (*i.p.*) route.[24,25] In each rat whose back area was shaved, a wound with a diameter of 15 mm was created using a biopsy needle. Group I was not treated. Group II received a single dose of local ABS in spray form. ABS-dopped wound dressing was used for group III, non-dopped ABS wound dressing was used for group IV (Figure 1), and the study was completed on day 14.[26]

Histological evaluation

The skin tissue samples were embedded in paraffin after routine tissue processing steps, and the samples were fixated in 10% formaldehyde for histological analyses.[27] Sections of paraffin blocks with thicknesses of 6 µm each were stained

Table 1. Groups

Groups (n= 6)
Group I Control
Group II ABS local application
Group III ABS-doped wound dressing
Group IV ABS non-doped wound dressing

ABS: Ankaferd blood stopper

with hematoxylin-eosin to determine their general histological structures.[28] The sections were examined at 40x magnification under a light microscope equipped with a digital camera (Nikon Eclipse, E-400 equipped with Nikon DS Camera Control Unit DS-L1 with DS Camera Head DS-5M), and digital images of the relevant areas were taken.[29-32]

Scoring evaluation scale

Wound scoring was performed as 0 (no inflammation), 1 (mild inflammation), 2 (moderate inflammation), and 3 (severe inflammation). Wound diameter was recorded in millimeters.[25,26] The scoring process was performed according to the evaluation scale shown in Table 2.

Biochemical analysis

On the last day of the study, 1.5 mL of blood was intracardially taken from each rat. After the blood samples were centrifuged for 3000 cycles at +4 °C for 10 min, the serum parts were separated. TAS and TOS measurements of sera were performed using commercial kits (Rel Assay Diagnostics). Using a spectrophotometer (Biochrom Libra S22), the absorbances of the samples were measured at 660 nm, and OSI was determined according to the standard reference.[33,34]

Statistical analysis

The Statistical Package for the Social Sciences (SPSS, version 21.0, IBM Corporation, Armonk, NY) software was used for all statistical analyses. One-way analysis of variance and the least significant difference method were used for pair-wise comparisons ($p < 0.05$). Statistical analysis was performed on the 14th day in the scoring of wound diameters.

RESULTS

Materials and characterization

SEM micrographs of polymers

Using the SEM images, the average fiber diameters were calculated with the help of the "Fiji ImageJ for Windows V 1.8.0" program from National Institutes of Health images, and the plots shown in Figure 3 were obtained. The fiber diameters ranged from 400 nm to 2 µm. The average diameter of the unadulterated fibers was 1.066 µm, and the average diameter of the doped fibers was 0.974 µm. The determined average diameter values were sufficient to provide permeability.[35-37] While a mesh structure was detected at the points where the fibers overlapped on the surfaces of the doped fibers, no droplet or clump-like formation was observed on the surfaces (Figure 2).

FTIR analysis

In the FTIR spectra of the PVA-PVP polymer mixture, an O-H stretching vibration peak was observed at approximately 3290 cm^{-1}. The spectrum band corresponded to a C-H stress that occurred at a peak of asymmetrical stretching vibration of approximately 2862 cm^{-1}.[35,37] PVA and PVP had C=O groups showing a vibration band at about 1716 cm^{-1}. The C-N stretching vibration peak of the amine structure was observed at 1242 cm^{-1}. The spectrum bands for the C-O groups, which are

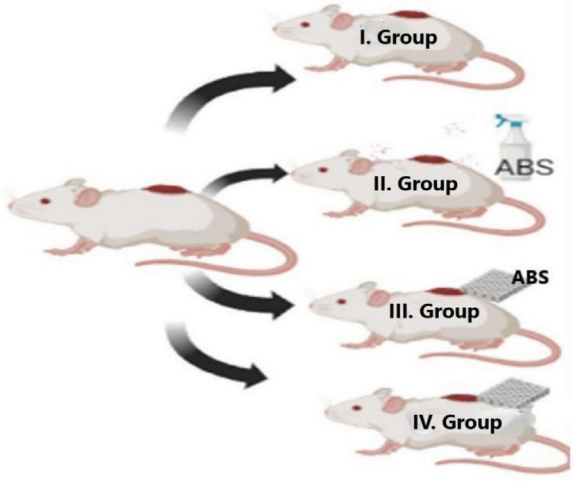

Figure 1. Stages of wound formation and treatment in rats
ABS: Ankaferd blood stopper

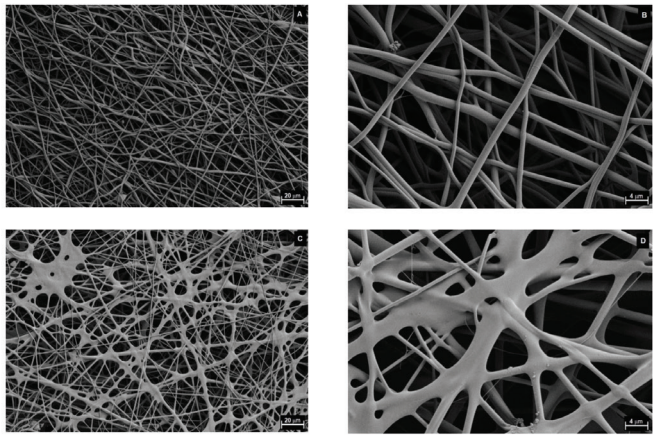

Figure 2. SEM micrographs of polymers, A) ABS non-doped (1000 x), B) ABS non-doped (5000 x), C) ABS-doped (1000 x), D) ABS-doped (5000)
SEM: Scanning electron microscopy, ABS: Ankaferd blood stopper

Table 2. Scoring evaluation scale

Ulcer (unit)	Reepithelization (unit)	Inflammation (unit)
0: None	0: None	0: None
1: At 1/3 of the wound site	1: At 1/3 of the wound site	1: Lightweight
2: At 2/3 of the wound site	2: At 2/3 of the wound site	2: Medium
3: The entire wound site	3: The entire wound site	3: Severe

acetyl groups, appeared at 1100 cm^{-1}. The plane for the C-H bend was outside the rings and formed an absorption band of approximately 720 cm^{-1}.[36] In the case of the ABS-dopped fibers, a soft formation of around 1645 cm^{-1} was observed instead of the peak loss at 1716 cm^{-1}. Here, the oxygen band in the C=O group was transformed into a C=C stretching vibration by a free reaction. It was concluded that an oxidation reaction occurred by the binding of oxygen atoms in the ABS additive (Figure 4).

Body weights

It was determined that there was no statistically significant difference between the mean body weights of the rats in the groups (p= 0.643). The statistics of the test were found to be F_{23}= 0.497 ($p > 0.05$) (Table 3).

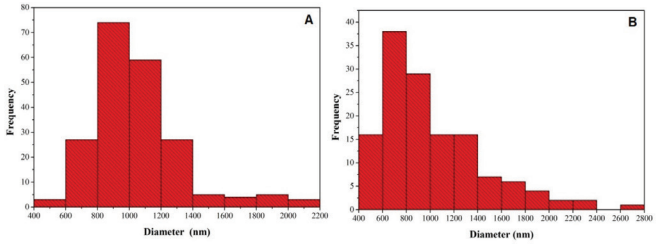

Figure 3. A) ABS non-doped and B) ABS-doped wound dressing fiber diameters (nm). Average values of ABS-doped (A) and ABS-undoped (B) fibers made with "Fiji ImageJ Program" depending on the density of the polymer

ABS: Ankaferd blood stopper

Wound scores

There was no loss of animals in the groups. In the evaluations of the median scores on the last day of the study, the average wound diameter was found to be reduced by half compared with the first day of the study in the rats in group I, whereas the recovery in group II was more limited. In group III, where the best healing process was observed, almost all wounds were closed, and there was even hair growth in the injured area. It was determined that the recovery rate in group IV was faster than that in groups I and II (Table 4). In the Tukey and Duncan tests, the test statistics were found to be p= 0.019, degree of freedom= 23, and F=4.144. When the wound diameters were compared, it was seen that the 1st and 4th groups were nearly similar. It was observed that the wound diameter in the second group did not decrease. It was determined that the wound diameter in the 3rd group decreased statistically significantly (wound diameter: group II > I > V > III; $p < 0.05$).

Table 3. Average body weights of the rats

Groups (n= 6)	Average body weight (gr) ± SD		
	First day	Day three	Last day
Group I	283 ± 4.60	288 ± 4.58	270 ± 4.30
Group II	297 ± 3.34	295 ± 1.12	295 ± 4.39
Group III	286 ± 2.24	287 ± 5.31	267 ± 1.66
Group IV	292 ± 2.38	292 ± 3.39	287 ± 6.42

SD: Standard deviation

Table 4. Values obtained from wound scores on different days of the study

Group (n= 6)	Day	Ulcer (mm)*	Reepithelization (mm)*	Inflammation (unit)*	Wound diameter (mm)
Group I	Day 0	3	0	0	15 x 15
	Day 3	3	0	0	14 x 14
	Day 7	2	2	0	10 x 10
	Day 14	2	2	0	7 x 7
Group II	Day 0	3	0	0	15 x 15
	Day 3	3	0	0	12 x 12
	Day 7	2	1	0	11 x 11
	Day 14	2	1	0	10 x 10
Group III	Day 0	3	0	0	15 x 15
	Day 3	2	1	0	10 x 10
	Day 7	1	2	0	6 x 6
	Day 14	0	3	0	1 x 1
Group IV	Day 0	3	0	0	15 x 15
	Day 3	2	1	0	10 x 10
	Day 7	2	2	0	7 x 7
	Day 14	1	2	0	6 x 6

*Scoring was performed according to the "Scoring Evaluation Scale" specified in Table 2

There was no significant difference among the groups in the macroscopic wound measurements performed on day 3 (Figure 5, $p > 0.05$). In the evaluation made on the seventh day, brown-colored scab formation was observed in all groups. The wound healing rate was the highest in group III, and the healing rate in group IV was higher than those in groups I and II ($p < 0.05$). In the histopathological evaluations, reepithelization was found to occur at a high rate in groups III and IV, at a moderate rate in group I, and at a minimum rate in group II ($p < 0.05$). On the 14th day, the wounds were completely closed in all rats in group III, whereas the wounds of the rats in group IV were substantially closed. The wounds were partially closed in group I, and healing was more limited in group II (Figure 5). In summary, reepithelization occurred at the maximum level in group III, at a high level in group IV, at a moderate level in group I, and at the minimum level in group II (reepithelization rate: group III > IV > I > II; $p < 0.05$).

In groups III and IV, the borders of the epidermis, dermis, and hypodermis showed normal morphological features, and the densities of connective tissue and collagen in the dermis layer were sufficient, whereas the density of collagen in the other groups was insufficient. Wound healing was characterized by a decrease in the number of neutrophils and new vascularization (Figure 6). The ABS-dopped wound dressing accelerated healing, whereas the non-dopped ABS wound dressing had a limited effect on wound healing (Figure 2). In addition, it was determined that the wound healing rate in the group that was administered local ABS to the injured area was slower than that in the control group.

Biochemical analysis

The level of oxidation (TOS) was the highest in the control group. ABS was found to reduce oxidation (Table 5). The application of wound dressing with the ABS additive caused a significant decrease in TOS values (Table 5). In parallel with these results, the level of antioxidants (TAS) increased in groups IV and II, but the highest increase was observed in group III ($p < 0.05$) (the OSI ranking: group III > IV > II > I).

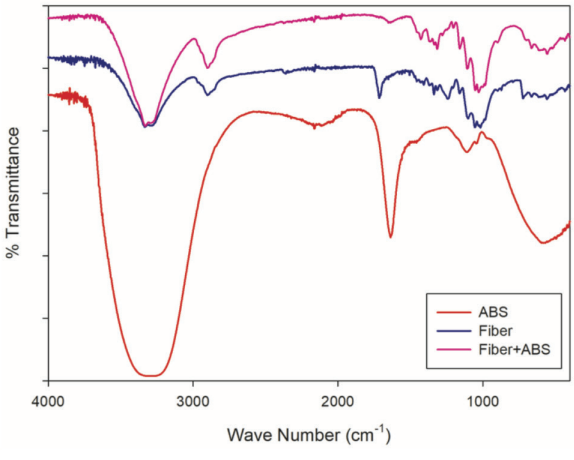

Figure 4. FTIR analysis chart

FTIR: Fourier transform infrared spectrophotometry

DISCUSSION

Injuries caused by traumas, surgical operations, and burns can lead to serious health problems, ranging from disability to death. Wound dressing is a practical process that allows the wound to heal in a short time under hygienic conditions.[38] If bleeding occurs in the injured area, wound dressings containing hemostatic additive agents may be preferred.[39] In this study, the effects of wound dressings containing nanofibers with doping with ABS, which is a hemostatic agent, on wound healing were evaluated in macroscopic, histopathological, and biochemical terms.

Hydrophilicity is a sought-after feature for wound dressing materials.[35,36,40-42] PVA and PVP are biocompatible polymers with biodegradability and non-toxic properties[9]. The addition of silver

Figure 5. Change in wound diameters in the groups determined on the first (A) and last (B) days of the study

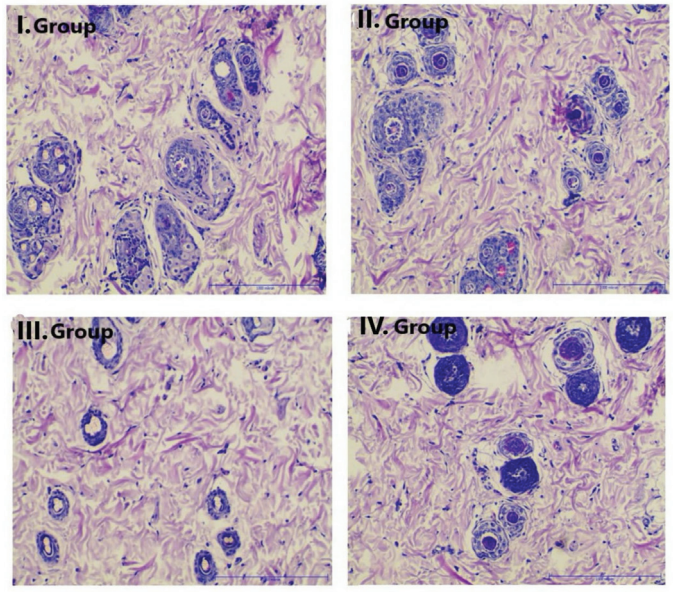

Figure 6. On the last day of the study, skin section samples belonging to different groups

(H-E staining, scale 100 µm x 40)

Table 5. Comparison of serum TAS, TOS, and OSI values between the groups

Groups/ Parameters	TAS (mmol Trolox Equiv/L) *Avg. ± SD	TOS (μmol H_2O_2 Equiv/L) *Avg. ± SD	OSI (Arbitrary Unit) *Avg. ± SD	p
Group I	1.01 ± 0.05[a]	13.21 ± 1.80[a]	1.31 ± 0.07a	0.000
Group II	1.50 ± 0.15[b]	13.00 ± 2.00[b]	0.87 ± 0.14b	
Group III	2.75 ± 0.01[c]	11.10 ± 2.18[c]	0.40 ± 0.13c	
Group IV	1.65 ± 0.20[b]	12.50 ± 1.25[b]	0.76 ± 0.13b	

*There are significant differences between different letters (a to c) in the same column ($p < 0.05$), Avg.: Average, SD: Standard deviation, TAS: Total antioxidant status, TOS: Total oxidant status, OSI: Oxidative stress index

nanoparticles to PVA and PVP had a notable effect on wound healing in New Zealand white rabbits.[14] It was determined that the wound dressing used in this study was sufficient to provide the permeability of fiber diameters. Moreover, no droplet or lump-like formation was observed on the surface. Because of these properties, it is thought that the substance produced in this study would be suitable for use and may be a preferred method in case of injuries.

During the recovery process, wound diameter was examined for reepithelialization and inflammation formation. In the measurements made on the last day of the study, the mean wound diameter in the ABS-dopped wound dressing group was much smaller than that in the control group, whereas the mean wound diameter in the local ABS-treated group was higher than that in the control group. This situation was interpreted as the ABS-dopped wound dressing being effective in healing, and the local ABS application slowed down healing.

There are many studies in the relevant literature investigating the effects of ABS on wound healing. It was reported that ABS is an agent that accelerates recovery and is effective in accelerating the wound healing process in periodontal treatment.[43] Similarly, ABS is effective in trauma-related soft tissue defects that cannot be repaired by primary closure.[44] ABS was observed to accelerate the healing process in bone defects created in the rat tibia.[45] It was shown that ABS applied to wounds on the back skin of rats accelerated healing.[46] According to a similar study, ABS speeds up wound healing in rats during the early period.[47] ABS has also been reported to be effective in healing full-thickness skin wounds in rats.[39] It was seen to provide healing even in second-degree burns.[4] In a similar study, ABS had a positive effect on wound healing in rats.[27] It was also stated that ABS has a positive effect on wound healing in diabetic rats.[48] In contrast with the aforementioned results, ABS was not found to be effective in preventing postoperative intra-abdominal adhesions, and its use could be harmful because it caused abdominal organ damage.[49] In the same study, it was stated that ABS did not prevent adhesions but increased them on a macroscopic level.

Our findings supported previous results, and the ABS-dopped dressings in this study were effective in reducing the wound size from 15x15 mm to 1x1 mm, thus contributing to healing. Although our results were similar to those of other studies in the literature in which the positive effects of ABS on wound healing have been stated,[26,27] they differed from some others showing that ABS is not effective alone, and it even slows healing. It was thought that the amount of ABS used in each study, the diameter of the wound that is created, and the age and sex of the animals may be different. The cycle occurring in females may have affected the results of our study by affecting the wound healing process and every other process in the body.

Reepithelialization is a stage of healing that occurs during the proliferation phase and is regulated by growth factors. Measuring the level of re-epitheliazation is a frequently used method for the histopathological evaluation of the healing process.[44,45] It was stated that the level of epithelialization in the tibia tissue of the rat group in which ABS was used in the treatment was higher than that in the control group.[44] ABS is effective in full-thickness wound healing by accelerating proliferation in the epithelial tissues of rats.[39] In a similar study, ABS, which was used for treating rat palatal mucosal injuries, increased the level of reepithelialization.[50] Another similar study revealed that ABS contributed to epithelialization in a full-thickness skin wound model in rats.[26] According to our results, the rate of re-epitheliazation was the highest in the ABS-dopped dressing group (III), and it was limited in the local ABS group (I) (Figure 5, Table 4). It was considered that brown scab formation, which was observed more prominently in the ABS-dopped dressing group than in the other groups, occurred because of reepithelialization and was caused by the formation of an encapsulated protein network on the wound area. Consistent with our results, scab formation was observed in the wound area in similar studies using ABS.[51-53]

Inflammation is a reaction developed by the body in cases of tissue damage, exposure to certain chemicals, and infectious diseases. This situation, in which the substances taking part in the immune system are directed to the damaged tissue, is an important parameter used in evaluating wound healing.[26] While inflammation is not observed in the normal healing process, its severity may increase in necrotic conditions.[53] In wound treatment, interventions that prevent inflammation are preferred. The use of ABS prevented inflammation and necrosis in experimentally created bone defects in the tibia of rats.[45] It has been reported that ABS does not cause inflammation in experimentally induced full-thickness skin wound healing in rats.[39] According to another study, ABS prevented inflammation by inhibiting collagen destruction during the recovery period.[53,54] ABS reduced inflammation in a wound model created in rats.[27] Likewise, it was reported that the use of ABS

in rats with colonic anastomosis-induced collagen formation and increased anastomosis.[55] In a study that was conducted to prevent postoperative intra-abdominal adhesions using ABS, an increase in inflammatory reactions to fibrosis was observed in the groups using ABS.[49] In the evaluation made with the available data, it was determined that inflammation did not occur in any animal in our study, and this situation was compatible with most other studies in the literature.

OSI is a measure of oxidative stress. Oxidative stress occurs because of the overproduction of reactive oxygen species or when antioxidant protection is insufficient.[56] It has been reported that increased OSI values in many conditions, such as diabetes, wounds, burns, and aging, can be reduced using the antioxidant properties of various herbal extracts.[17,57-67] Our results showed that ABS, which is an herbal product, is effective against oxidative stress that occurs during the wound healing process, in line with the literature. The use of only dressing and ABS alone corresponded to a reduction in the increased stress by 1.5 times ($p < 0.05$). It was determined that the ABS-dopped dressing increased the TAS levels by approximately twice, while reducing the OSI values by 1/3 compared with the control (Table 5).

CONCLUSION

The results showed that ABS alone did not contribute to wound healing, and the ABS-dopped wound dressing provided rapid and uneventful healing in the injured area. It was determined that local ABS application did not shorten the wound healing duration, and the ABS-dopped nanofiber dressing provided healing in the injured area in a much shorter time than the control group. Because it does not cause inflammation, ABS is a hemostatic agent with antiseptic and antimicrobial properties. Our results indicate that ABS-dopped dressings can be used safely, do not have any negative effects on wound healing, and can be an effective and safe product for use by shortening the healing process in skin wounds.

Ethics

Ethics Committee Approval: The study was initiated by obtaining the approval of the ethics committee of Selçuk University, Experimental Medicine Research and Application Center (decision date: 25.01.2019 and decision number: 2019-2).

Informed Consent: Not necessary.

Authorship Contributions

Concept: E.Ş., E.G., M.O.E., Design: E.Ş., E.G., Data Collection or Processing: E.Ş., E.G., Analysis or Interpretation: E.Ş., E.G., Literature Search: E.Ş., E.H., M.O.E., Writing: E.Ş., E.G., M.O.E.

Conflict of Interest: No competing interests declared.

Financial Disclosure: This research was supported within the scope of the project numbered 03-M-21, which was accepted by the Scientific Research Projects Commission of Karamanoğlu Mehmetbey University.

REFERENCES

1. Gupta A, Kowalczuk M, Heaselgrave W, Britland ST, Martin C, Radecka I. The production and application of hydrogels for wound management: A review. Eur Polym J. 2019;111:134-151.
2. Beyazit F, Beyazit Y, Tanoglu A, Haznedaroglu IC. Ankaferd hemostat (ABS) as a potential mucosal topical agent for the management of COVID-19 syndrome based on its PAR-1 inhibitory effect and oestrogen content. Med Hypotheses. 2020;143:110150.
3. Zeki ÖC, Nenni M, Çelebier M, Öncül S, Ercan A, Süslü İ, Haznedaroğlu İC. Antitumor activity of Ankaferd Blood Stopper® on MCF-7 breast cancer: A proteomic approach to ascertain the mechanism of the action. J Herb Med. 2021;28:100449.
4. Ozcan EC, Gul M, Dundar S, Bozoglan A, Karasu N, Bal A, Gunes N, Bingul MB. Effects of local application of the ankaferd blood stopper on osseointegration in three different surface titanium implants. J Oral Biol Craniofac Res. 2021;11:524-528.
5. Satar NY, Akkoc A, Oktay A, Topal A, Inan K. Evaluation of the hemostatic and histopathological effects of ankaferd blood stopper in experimental liver injury in rats. Blood Coagul Fibrinolysis. 2013;24:518-524.
6. Gül Satar N, Cangül İT, Topal A, Oktay A, İnan K, Akgül MB. Effects of Ankaferd Blood Stopper (ABS) and topical tripeptide copper complex (TCC) on wound healing in rats: an experimental study. Kafkas Univ Vet Fac. 2014;20:545-551.
7. Ambekar RS, Kandasubramanian B. Advancements in nanofibers for wound dressing: A review. Eur Polym J. 2019;117:304-336.
8. AlAbdulaal TH, Almoadi A, Yahia IS, Zahra HY, Alqahtani MS, Yousef ES, Hussein KI, Jalalah M, Harraz FA, Al-Assiri MS. High optical performance of Gd2O3-doped PVA/PVP composite films for electronic and laser CUT-OFF filters. Optik. 2022;268:169741.
9. Sanz Espinar G, Universidad Autónoma de Madrid (España). https://riull.ull.es/xmlui/bitstream/handle/915/30978/C_22_%282022%29_28.pdf?sequence=1&isAllowed=y.cedille.;undefined;513-519. Epub 2022
10. Dhivya S, Padma VV, Santhini E. Wound dressings-a review. Biomedicine (Taipei). 2015;5:22.
11. Li H, Williams GR, Wu J, Lv Y, Sun X, Wu H, Zhu LM. Thermosensitive nanofibers loaded with ciprofloxacin as antibacterial wound dressing materials. Int J Pharm. 2017;517:135-147.
12. Chen K, Hu H, Zeng Y, Pan H, Wang S, Zhang Y, Shi L, Tan G, Pan W, Liu H. Recent advances in electrospun nanofibers for wound dressing. Eur Polym J. 2022;178:111490.
13. Alharbi HF, Luqman M, Khalil KA, Elnakady YA, Abd-Elkader O, Rady AM, Alharthi NH, Karim MR. Fabrication of core-shell structured nanofibers of poly (lactic acid) and poly (vinyl alcohol) by coaxial electrospinning for tissue engineering. Eur Polym J. 2018;98:483-491.
14. Alipour R, Khorshidi A, Shojaei AF, Mashayekhi F, Moghaddam MJM. Skin wound healing acceleration by Ag nanoparticles embedded in PVA/PVP/Pectin/Mafenide acetate composite nanofibers. Polym Test. 2019;79:106022.
15. Geetha K, Sivasangari D, Kim H, Murugadoss G, Kathalingam A. Electrospun nanofibrous ZnO/PVA/PVP composite films for efficient antimicrobial face masks. Ceram Int. 2022;48:29197-29204.
16. Taş A, Köklü S, Beyazit Y, Karaca G, Astarcı HM, Akbal E, Koçak E, Topçu G, Haznedaroglu IC. Percutaneous ankaferd injection to *in vivo* liver tissue in comparison to ethanol in an experimental rat model. Clin Res Hepatol Gastroenterol. 2011;35:549-553.

17. Topal A, Satar NYG, Cangul IT, Oktay MA, Inan K, Cecen G, Akarsu EP, Can H. Ankaferd blood stopper accelerates deep second degree burn wound healing in rats. Acta Vet Brno. 2018;87:261-267.

18. Kurakula M, Koteswara Rao GSN. Moving polyvinyl pyrrolidone electrospun nanofibers and bioprinted scaffolds toward multidisciplinary biomedical applications. Eur Polym J. 2020;136:109919.

19. Bozkaya O, Arat E, Gün Gök Z, Yiğitoğlu M, Vargel I. Production and characterization of hybrid nanofiber wound dressing containing *Centella asiatica* coated silver nanoparticles by mutual electrospinning method. Eur Polym J. 2022;166:111023.

20. Kustiati U, Wihadmadyatami H, Kusindarta DL. Dataset of Phytochemical and secondary metabolite profiling of holy basil leaf (*Ocimum sanctum* Linn) ethanolic extract using spectrophotometry, thin layer chromatography, Fourier transform infrared spectroscopy, and nuclear magnetic resonance. Data Brief. 2022;40:107774.

21. Cross SE, Naylor IL, Coleman RA, Teo TC. An experimental model to investigate the dynamics of wound contraction. Br J Plast Surg. 1995;48:189-197.

22. Dorsett-Martin WA. Rat models of skin wound healing: a review. Wound Repair Regen. 2004;12:591-599.

23. Ramsey A, Bailey S, Pollock D. Diurnal differences in mitochondrial bioenergetics is lost in bmal1 knockout rats. FASEB J. 2022;36.

24. Imani A, Rajani SF, Rakhshan K, Faghihi M, Nemati M, Parsazadegan T. The role of nitric oxide on the antiarrhythmic effects of ketamine/xylazine in a rat model of acute cardiac ischemia-reperfusion. Curr Res Physiol. 2022;5:302-311.

25. Connell AR, Hookham MB, Fu D, Brazil DP, Lyons TJ, Yu JY. Comparisons of α2-adrenergic agents, medetomidine and xylazine, with pentobarbital for anesthesia: important pitfalls in diabetic and nondiabetic rats. J Ocul Pharmacol Ther. 2022;38:156-166.

26. Özbaysar Sezgin S, Saraç G, Şamdancı E, Şenol M. The effects of Ankaferd, a hemostatic agent, on wound healing. Turkderm - Turk Arch Dermatol Venereol. 2015;49:218-221.

27. Satar NY, Akkoc A, Oktay A, Topal A, Inan K. Evaluation of the hemostatic and histopathological effects of Ankaferd Blood Stopper in experimental liver injury in rats. Blood Coagul Fibrinolysis. 2013;24:518-524.

28. Gül M, Günay A. Effect of caffeic acid phenethyl ester and Ankaferd Blood Stopper® on palatal wound healing in the diabetic rats. SRM J Res Dent Sci. 2020;11:172-177.

29. Şensoy E, Öznurlu Y. Determination of the changes on the small intestine of pregnant mice by histological, enzyme histochemical, and immunohistochemical methods. Turk J Gastroenterol. 2019;30:917-924.

30. AL-Dahhan MAH, Al-Samawy ERM, Al-Kaisei BI, Jarad AS. Effect of synthetic colorants (Sunset yellow and Ponceau 4R) in some biochemical and histopathological parameters of albino rats. QJVMS. 2014;13:80-84.

31. Hassan MT, Mohamed HK, Hammad WA. Antihyperlipidemic activity of green coffee beans extract against Poloxamer407 toxicity in male albino rats. Egypt J Exp Biol (ZooL). 2020;16:65-72.

32. Elbanna K, Sarhan OM, Khider M, Elmogy M, Abulreesh HH, Shaaban MR. Microbiological, histological, and biochemical evidence for the adverse effects of food azo dyes on rats. J Food Drug Anal. 2017;25;667-680.

33. Alharbi N, Elobeid M, Virk P. Protective effect of quercetin treatment against cadmium-induced oxidative stress in a male rat model. Pakistan J Zool. 2019;51:2287-2296.

34. Erel O. A novel automated direct measurement method for total antioxidant capacity using a new generation, more stable ABTS radical cation. Clin Biochem. 2004;37:277-285.

35. Özgün E, Sayılan Özgün G, Eskiocak S, Yalçın O, Süer Gökmen S. Effect of L-carnitine on serum paraoxonase, arylesterase and lactonase activities and oxidative status in experimental colitis. Turk J Bioch. 2013;38:145-153.

36. Ovington LG. Advances in wound dressings. Clin Dermatol. 2007;25:33-38.

37. Sarip MN, Noor MFHM, Ahmad Z, Shuhaime N, Dahan RM, Arshad AN, Ismail WIWW. Conductivity study of polyvinyl alcohol/polyvinyl pyrrolidone (PVA/PVP)-KOH coatings system. AIP Conference Proceedings. 2018.

38. Wang Z, Rong F, Li Z, Li W, Kaur K, Wang Y. Tailoring gas-releasing nanoplatforms for wound treatment: An emerging approach. J Chem Eng. 2023;452:139297.

39. Yıldız Gülhan P, Güleç Balbay E, Çelik M, Annakkaya AN, Arbak P. Fatigue frequency and related factors in patients with sarcoidosis. Turk Thorac J. 2019;20(Suppl 1):244.

40. Akalin C, Kuru S, Barlas AM, Kismet K, Kaptanoglu B, Demir A, Astarci HM, Ustun H, Ertas E. Beneficial effects of Ankaferd Blood Stopper on dermal wound healing: an experimental study. Int Wound J. 2014;11;64-68.

41. Münch AS, Simon F, Merlitz H, Uhlmann P. Investigation of an oleophobic-hydrophilic polymer brush with switchable wettability for easy-to-clean coatings. Eur Polym J. 2022;180:111629.

42. Maalej H, Maalej A, Bayach A, Zykwinska A, Colliec-Jouault S, Sinquin C, Marchand L, Ktari N, Bardaa S, Ben Salah R, Chamkha M, Boufi S, Nasri M. A novel pectic polysaccharide-based hydrogel derived from okra (Abelmoschus esculentusL. Moench) for chronic diabetic wound healing. Eur Polym J. 2023;183:111763.

43. Erçetin S, Haznedaroğlu İC, Kurt M, Onal İK, Aktaş A, Kurt ÖK, Göker H, Özdemir O, Kirazlı S, Fırat HC. Safety and efficacy of ankaferd blood stopper in dental surgery. UHOD. 2010;20:1-5.

44. Demirel ME, Mohamed SM, Ali YB. Soft tissue infection and delayed wound healing due to neglected animal bite: A case report. J Contemp Med. 2018;8:280-281.

45. Işler SC, Demircan S, Cakarer S, Cebi Z, Keskin C, Soluk M, Yüzbaşioğlu E. Effects of folk medicinal plant extract Ankaferd Blood Stopper on early bone healing. J Appl Oral Sci. 2010;18:409-414.

46. Aktop S, Emekli-Alturfan E, Ozer C, Gonul O, Garip H, Yarat A, Goker K. Effects of Ankaferd Blood Stopper and Celox on the tissue factor activities of warfarin-treated rats. Clin Appl Thromb Hemost. 2014;20:16-21.

47. Aktaş A, Er N, Korkusuz P, Zeybek D, Onur M, Tan G, Özdemir O, Karaismailoğlu E, Karabulut E. Ankaferd-induced early soft tissue wound healing in an experimental rat model. Türkiye Klinikleri J Med Sci. 2013;33:1344-1353.

48. Bulut E, Baş B, Altunkaynak BZ, Bekçioğlu B, Erdem Koç G, Gönülol E, Önger ME, Kaplan S. Efficacy of Ankaferd Blood Stopper on bone healing in diabetic rats: a stereological and histopathological study. Biotech Histochem. 2014;89:535-543.

49. Arkan B, Yılmaz D, Gökdere Çinar H, Uzun R. Clinical decision-making levels of nursing students and affecting factors. Cyprus J Med Sci. 2022;7:738-744.

50. Gül M, Günay A, Tanik A. An evaluation of the effects of caffeic acid phenethyl ester and Ankaferd blood stopper on secondary wound healing of oral mucosal tissue. Turk J Med Sci. 2020;50:248-257.

51. Kandemir O, Buyukates M, Kandemir NO, Aktunc E, Gul AE, Gul S, Turan SA. Demonstration of the histopathological and immunohistochemical effects of a novel hemostatic agent, Ankaferd Blood Stopper, on vascular tissue in a rat aortic bleeding model. J Cardiothorac Surg. 2010;5:110.
52. Tokgöz H, Karakaya K, Hanci V, Abduşoğlu M, Erol B, Türksoy O, Akduman B, Mungan NA. Protective value of a folkloric medicinal plant extract against mortality and hemorrhage in a life-threatening renal trauma model. Urology. 2010;75:1515.
53. Karaca G, Aydin O, Pehlivanli F, Kocael A, Pekcici R, Duymus E, Akgedik S, Guler O. Effect of ankaferd blood stopper in experimental peritoneal adhesion model. Ann Surg Treat Res. 2016;90:213.
54. Aydın BK, Altan E, Acar MA, Erkoçak ÖF, Ugraş S. Effect of Ankaferd blood stopper® on tendon healing: an experimental study in a rat model of Achilles tendon injury. Jt Dis Relat Surg. 2015;26:31-37.
55. Ekici U, Ferhatoğlu MF, Çitgez B, Uludağ M. Effects of folk medicinal plant extract ankaferd blood stopper on healing of colon anastomosis: an experimental study in a rat model. Med Bull Şişli Etfal Hosp. 2019;53:154-159.
56. Çetin S, Usta A, Ekici P, Dede S, Yüksek V. Sarcoptes ovis ile Enfekte Koyunlarda Serum Protein Fraksiyon Profili. Atatürk University Journal of Veterinary Sciences. 2020;15:70-75.
57. Oxidative Stress in Neurodegenerative Diseases. Metal-based Neurodegeneration. 2013:75-109.
58. Shang M, Zhao J, Yang L, Lin L. Oxidative stress and antioxidant status in women with gestational diabetes mellitus diagnosed by IADPSG criteria. Diabetes Res Clin Pract. 2015;109;404-410.
59. Hailat N, Al-Kahil S, Alkofahi A, Lafi S, Al-Ani F, Al-Darraji A, Bataineh Z. Effects of *Nigella sativa* extracts on antibody response of rats vaccinated with *Brucella Vaccine* (Rev-1). Pharm Biol. 1998;36:217-221.
60. Ahmad S, Beg ZH. Evaluation of therapeutic effect of omega-6 linoleic acid and thymoquinone enriched extracts from *Nigella sativa* oil in the mitigation of lipidemic oxidative stress in rats. Nutrition. 2016;32;649-655.
61. Inci A, Sarı F, Sarıkaya M, Yılmaz U, Coban M, Gul S, Akın O, Şahinturk Y, Yılmaz N. Sp445increased oxidative stress in diabetic nephropathy and relationship to soluble klotho levels. Nephrol Dial Transplant.. 2017;32(Suppl 3):273.
62. Kumandaş A, Karslı B, Kürüm A, Çınar M, Elma E. Comparison of the effects of zinc-silver cream and Nigella sativa oil on wound healing and oxidative stress in the wound model in rats. Ankara Univ Vet Fak Derg. 2020;67:33-40.
63. Shedoeva A, Leavesley D, Upton Z, Fan C. Wound healing and the use of medicinal plants. Evidence-Based Complementary and Alternative Medicine. 2019;2019:1-30.
64. Abdulahad D. Investigation of the erythrocyte fragility, hematological and antioxidant effects of oleander (*Nerium oleander* L.) Flower ethanolic lyophilized extract in diabetic rats. KSU J. Agric Nat. 2020;23;1495-1502.
65. Saraç H, Durukan H, Demirbaş A. Nutrient Concentrations and antioxidant activity of *Achillea millefolium* L. (Yarrow), one of the important medicinal plants. Turkish JAF Sci Tech. 2021;9:590-594.
66. Sarıtaş Z, Korkmaz M, Demirel HH, Bülbül A, Sarıtaş TB, Görücü F, Koç Y. Wound healing effect of Anzer origin propolis specimens on rats' intestinal incision. Ankara Univ Vet Fak Derg. 2022;69;91-97.
67. Sahin NE, Oner Z, Oner S, Turan MK. A study on the correlation between spleen volume estimated via cavalieri principle on computed tomography images with basic hemogram and biochemical blood parameters. Anat Cell Biol. 2022;55;40-47.

Turk J Pharm Sci 2024;21(2):104-112
DOI: 10.4274/tjps.galenos.2023.14704

ORIGINAL ARTICLE

Antiseizure Activity of *Mitragyna inermis* in the Pentylenetetrazol-Induced Seizure Model in Mice: Involvement of Flavonoids and Alkaloids

Relwendé Justin OUÉDRAOGO[1,2*], Muhammad JAMAL[3], Lassina OUATTARA[1,2], Muhammad NADEEM-UL-HAQUE[3], Faisal KHAN[3], Shabana Usman SIMJEE[3], Georges Anicet OUÉDRAOGO[1,2], Farzana SHAHEEN[3]

[1]Nazi Boni University, Department of Biological Sciences, Life and Earth Sciences Training and Research Unit, Bobo-Dioulasso, Burkina Faso
[2]Nazi Boni University, Animal Health and Biotechnology Research and Teaching Laboratory, Bobo-Dioulasso, Burkina Faso
[3]Karachi University, Third World Center for Science and Technology, Hussain Ebrahim Jamal Research Institute of Chemistry, Karachi, Pakistan

ABSTRACT

Objective: This study aimed to investigate whether *Mitragyna inermis (Willd.)* Otto Kuntze organic and aqueous extracts are able to control seizures induced by pentylenetetrazol (PTZ) in mice based on flavonoid fingerprints and alkaloidal contents.

Materials and Methods: Ethanolic extract and decoction-derived fractions from roots, leaves, and stems were subjected to chromatographic fingerprinting using $AlCl_3$ and screening for their antiseizure effects using PTZ-induced acute seizure model. From the fractions that showed potent bioactivities, plausible antiseizure alkaloids were isolated using thin layer chromatography, and their structures were elucidated using ^{1}H NMR, 2D NMR, ^{13}C NMR, and FAB-HR (*+ve* or *–ve*).

Results: All fractions, with the exception of the dichloromethane and hexane fractions, revealed remarkable flavonoid fingerprints. An acute PTZ-induced seizure test revealed that ethanolic extract of stem bark [500 mg/kg body weight (bw)], ethyl acetate extract of stem bark (500 mg/kg bw), and aqueous extract of leaves (300 mg/kg bw) significantly delayed the occurrence of hind limb tonic extension (HLTE); however, a non-significant delay was observed in the onset of first myoclonic jerk compared with control animals. Isolation yielded four main alkaloids: that are, pteropodine (1), isopteropodine (2), mitraphylline (3) and corynoxeine (4). Corynoxeine is a new compound derived from *M. inermis*.

Conclusion: This study suggests that flavonoid fingerprints are tracers of *M. inermis* anticonvulsant ingredients. The stem bark ethanolic and ethyl acetate extracts and leaf aqueous extracts contain anticonvulsant bioactive principles that delay notifying the HLTE occurring in male naval medical research institute mice. Furthermore, alkaloidal contents also remain plausible bioactive anticonvulsant principles. All observations support the traditional use of *M. inermis* to manage epilepsy. However, further studies are needed to understand the effects of alkaloid fractions, flavonoids, and the isolated compounds as promising antiseizure agents derived from *M. inermis* in experimental animals.

Keywords: *Mitragyna inermis*, antiseptics, flavonoids, alkaloids, corynoxeine

INTRODUCTION

Epilepsy is neurological and seems to be systemic disorder (Yuen et al.[1]). Epilepsy presents as partial or generalized seizures along with psychiatric comorbidities (Banerjee et al.[2]). Furthermore, people suffering epilepsy are more represented in the middle and low-income countries due to the enormous treatment gaps. Social stigma, discrimination and misunderstanding are some prejudices to live with epilepsy (Moshé et al.[3]). In the recent development of various antiseizure drugs (AEDs), some prevents seizures by acting through multiple ways such as acting on sodium channels (valproic acid, phenytoin, carbamazepine), calcium channels (ethosuximide), α-amino-3-hydroxy-5-methyl-4-isoxazolepropionic acid receptors (parampanel), γ-aminobutyric acid (GABA) receptors (diazepam), or modulate the release of GABA (gabapentin,

*Correspondence: rjustino14@yahoo.com, Phone: +226 75386260, ORCID-ID: orcid.org/0000-0002-5036-2144
Received: 10.03.2023, Accepted: 13.05.2023

pregabalin or valproic acid) (Macdonald[4], Kobayashi et al.[5]). Unfortunately, some of them still exhibit adverse effects like hypersensitivity reactions, mood changes, hepatotoxicity and are also ineffective against drug-resistant seizures (Copmans et al.[6], Devinsky et al.[7]). Whereas, the primary goal of AED therapy is complete freedom from seizures without adverse side effects (Shorvon et al.[8]). So, the needs to develop new AEDs become imperative (Moshé et al.[3]). Pentylenetetrazol (PTZ) causes seizures on its administration by preventing inhibitory effects of GABA type A ($GABA_A$) receptor (Huang et al.[9]). Thus, this GABA receptor antagonist is widely used as a model for AED research. Natural sources like plants are suitable for development of various new drug candidates (Cragg et al.[10]).

Mitragyna inermis (Willd) Otto Kuntze (Rubiaceae) is a bushy tree or shrub (Arbonnier[11]). In Burkina Faso, its leaves, roots and stem barks are used in mental illness and epilepsy treatment (Arbonnier[11], Nacoulma[12]). Different modes of preparation such as maceration, infusion, decoction and leaching with various accessible solvents such as water, hydroalcoholic and acetonic solutions are used to obtain traditional medicines (Ouédraogo et al.[13]).

Moreover, previous studies were demonstrated anticonvulsant properties of leaf methanolic extract (300-1200 mg/kg) and stem bark ethanolic and aqueous extracts (62.5-500 mg/kg) (Timothy et al.[14], Atinga[15]). Those studies were reported on a moderate dose of convulsant agent (PTZ 60 mg/kg) and the anticonvulsant extract constituents were not specifically reported from this plant (Atinga et al.[15]). Therefore, these authors reported flavonoids, tannins, alkaloids, anthraquinone, glycosides, and terpenoids in these extracts. However, tube tests reported on these potent extracts are preliminary phytochemical screenings and can be confirmed or refuted by thin layer chromatography screenings (Ouédraogo et al.[13]). Also, extensive phytochemical report revealed that *M. inermis* contains polyphenols, triterpenoids, indole and oxindole alkaloids (Shellard and Sarpong[16,17], Toklo et al.[18], Ouédraogo et al.[19]). It has been reported that flavonoids and alkaloids or medicinal plant containing flavonoids and alkaloids interact with $GABA_A$ receptors leading to anticonvulsant activities (Copmans et al.[6], Jäger and Saaby[20], Zhu et al.[21]). Besides, several AEDs like diazepam, carbamazepine, lorazepam, midazolam, brivaracetam, piracetam, aniracetam, oxiracetam, pramiracetam, nefiracetam, nebracetam, fasoracetam and levetiracetam licensed or in clinical development have the common function like alkaloids (Shorvon et al.[8]). Nevertheless, the knowledge of the potential contribution of flavonoids and alkaloids patterns of *M. inermis* different part extracts on its therapeutic properties is unknown. In drug research based on traditional recipes, it is important to assay or highlight ubiquitous tracers of biological activity due to synergistic effects (Yuan et al.[22]). Indeed, flavonoids are generally followed in the standardization of raw materials from traditional medicine and chromatographic fingerprinting can be used in the quality control of medicinal plant materials (Ouédraogo et al.[13]).

This study aimed to investigate whether *M. inermis* organic and aqueous extracts are able to control seizures induced by PTZ in mice based on flavonoid fingerprints and alkaloidal contents.

MATERIALS AND METHODS

Phytochemical study

Plant materials and extract preparation

Based on a previous study, *M. inermis* parts (leaf, stem bark and root) samples were collected from Banfora, Dindérésso, and Boromo during September and November (Ouédraogo et al.[23]). A voucher specimen (UNB 939) is deposited in the Herbarium of University Nazi Boni. The collected samples were subjected to total phenolic compounds assays and antioxidant properties evaluation, which are sensitive to ecological factors (Ouédraogo et al.[23]). At the end of these analyses, three samples were categorized by plant part. Based on their phenolic contents and remarkable antioxidant potential, three samples by plant part were used to form composite samples *per* part, *i.e.* 40 + 40 + 40 = 120 g of stem bark, 40 + 40 + 40 = 120 g of root bark, and 30 + 30 + 30 = 90 g of leaves. The composite samples were used for different extractions, maintaining the ratio of plant matter. Different preparations have been made in relation to the traditional way of preparation and those reported from previous studies (Timothy et al.[14]; Ouédraogo et al.[19]).

Acetonic extraction

Ninety g of leaves, 120 g of root bark, and 120 g of stem bark were subjected to 10 fold 70% acetone (*v/w*) for 1 hour 30 min at 1500 rpm at 37 °C. Then, filtration and centrifugation at 3800 rpm/35 min/4 °C were carried out. The supernatant solvent were evaporated at 45 °C with rotary evaporator and stored at 4 °C until their use (Checkouri et al.[24]). This extraction yielded 32.74%, 13.76%, 22.87% from leaf, stem and root, respectively.

Aqueous decoction and fractionation

Five hundred g of each part of *M. inermis* was used for extraction. Thus, the extraction was performed with 10 fold distilled water (*v/w*) 100 °C/30 min (Ranilla et al.[25]). Filtrate pH was reduced to 3-4 and then subjected to fractionation successively with increasing polarity [hexane, dichloromethane (DCM), ethyl acetate to butanol]. The residual water and butanol were evaporated by freeze-drying and the other solvents at 45 °C using a rotary evaporator. This fractionation yielded 13.6%, 5.97%, and 4% for the leaf decoction, ethyl acetate, and butanol fractions, respectively. Also, 2% for the ethyl acetate fraction of stem bark and 3.10% for the ethyl acetate fraction of roots. Extracts and fractions were stored at 4 °C until use (Silva et al.[26]).

Ethanol extraction

Stem bark powder (120 g) was macerated for 24 hours with 1200 mL of ethanol (99%). Therefore, the raw material was macerated twice (the second with the recovered solvent). The solvent was then evaporated at 45 °C with a rotary evaporator (2% yield) and stored at 4 °C (Timothy et al.[14]).

Flavonoid fingerprinting, bioassay-guided fractionation, and alkaloids isolation

Extracts and fractions of each plant part were dissolved in methanol and applied on F254 silica plate. Then, elution was carried out over 8 cm with ethyl acetate: acetic acid: methanol: water (10:1.6:0.6:1.5) and the plates were viewed at ultraviolet (UV) 365 nm and after spraying with aluminum chloride (Ouédraogo et al.[19]). This first phytochemical screening is part of the confirmation of the presence of different subgroups of flavonoids reported as potential bioactive of traditional drugs. In addition, this screening allows the grouping of fractions according to the tracers that are flavonoids in a preliminary standardization guide. All extracts were subjected to anti-PTZ-induced seizures assays.

Furthermore, 20 g of the aqueous decoction of the leaves and 10 g of the ethanolic extract of the stem barks that exhibited potent antiseizure effects in PTZ-induced seizures were used for alkaloid treatments. Therefore, the extracts were treated with 10% acetic acid for 12 hours. At the end of the time, filtration was performed and the pH of the filtrate was adjusted to 10, followed by extraction with DCM three times. The DCM fraction was then concentrated in rotavapor and dissolved in 5% sulfuric acid, followed by extraction with hexane to remove non-alkaloids. The residual aqueous phase pH was increased to 10 using ammonia, followed by a new extraction with DCM. The last DCM fraction was concentrated in rotavapor, dissolved in methanol, and dried under the hood. Finally, DCM was used to recover the yellow-colored-soluble compounds. This process yielded 2.4% alkaloid fraction from the leaves and 7.8% alkaloid fraction from the stem bark. Similar spots were observed on both fractions after application on a precoated F254 silica plate and elution with DCM: acetone (9:1). Then, preparative thin layer chromatography (TLC) with the same system yielded four compounds: 1 (10 mg) and 2 (10 mg) from the leaves and 3 (6 mg) and 4 (5 mg) from the stem bark.

General methods

TLCs were performed on preheated Kieselgel 60 F254 (Merck) plates. Plates were developed using DCM-acetone and then UV 254 and 365 nm. The isolated compounds were subjected to ^{1}H NMR, 2D NMR, HMBC, HSQC, COSY and NOESY, ^{13}C NMR, and FAB-MS (*+ve* or *–ve*) analyses. Bruker Avance Neo NMR spectrometers operating at 400 and 600 MHz were used to run 1D and 2D NMR spectra, giving coupling constants (*J*) in Hz and chemical shifts (δ) in ppm relative to the residual CD_3OD signal with TopSpin.

Structure elucidation of pteropodine (1), isopteropodine (2), mitraphylline (3), and corynoxeine (4)

Elucidation was carried out by comparing ^{1}H NMR, 2D NMR, ^{13}C NMR, and FAB-HR (*+ve* or *–ve*) data with the reported data.

Pteropodine (1)

Amorphous white powder: FAB-HR (*+ve*): *m/z*= 369.1826 [M + H]$^{+}$; [M ($C_{21}H_{24}O_4N_2$) + H]= 369.1826. ^{1}H NMR (400 MHz, CD_3OD): δ = 8.53 (brs, NH), 2.34 (dd, *J*= 6.0, 2.4 Hz, H-3), 3.21 (dd, *J*= 8.2, 7.0 Hz, H-5a) 2.40 (t, *J*= 4.3 Hz, H-5b), 2.29 (dd, *J*= 3.2, 8.2 Hz, H-6a) 2.00 (ddd, *J*= 12.9, 7.9, 1.5 Hz, H-6b), 7.05 (td, *J*= 7.6, 1.1 Hz, H-9), 6.86 (d, *J*= 7.9 Hz, H-10), 7.19 (td, *J*= 7.7, 1.3 Hz, H-11), 7.27 (dd, *J*= 7.5, 1.2 Hz, H-12), 1.55 (d, *J*= 7.6 Hz, H-14a) 1.33 (dd, *J*= 3.7, 7.2 Hz, H-14b), 2.37 (dd, *J*= 3.3, 2.5 Hz, H-15), 7.50 (s, H-17); 4.47 (dq, *J*=12.4, 6.1 Hz, H-19), 1.59 (d, *J*= 4.6 Hz , H-20), 2.32 (d, *J*= 2.3 Hz, H-21a), 3.31 (H-21b), 3.57 (s, 3H, OCH_3), 1.39 (d, *J*= 6.1 Hz, CH_3). ^{13}C NMR (600 MHz, CD_3OD): δ = 183.36 (C-2), 75.31 (C-3), 55.91 (C-5), 34.98 (C-6), 57.76 (C-7), 134.60 (C-8), 123.79 (C-9), 110.57 (C-10), 129.19 (C-11), 124.18 (C-12), 142.78 (C-13), 30.84 (C-14), 32.31 (C-15), 110.57 (C-16), 156.83 (C-17), 73.72 (C-19), 39.29 (C-20), 54.27 (C-21), 51.67 (OCH_3), 169.66 (C=O), 18.95 (CH_3).

Infrared spectroscopy (IR) [potassium bromide (KBr)]: V_{max}= 3320.57, 2943.98, 2832.23, 668.42 cm^{-1}. UV/UV-visible (MeOH) A= 1.347 (218 nm) and 1.652 (247 nm).

Isopteropodine (2)

Amorphous white powder: FAB-HR (*+ve*): *m/z*= 369.1821 [M + H]$^{+}$; [M ($C_{21}H_{24}O_4N_2$) + H]= 369.1821. ^{1}H NMR (400 MHz, CD_3OD): δ = 8.54 (brs, NH), 2.42 (dd, *J*= 4.2, 2.8 Hz, H-3), 3.25 (td, *J*= 8.7, 2.7 Hz, H-5), 2.29 (ddd, *J*= 12.4, 9.6, 2.5 Hz, H-6b) 1.96 (dt, *J*= 13.0, 8.5 Hz, H-6b), 7.01 (td, *J*= 7.6, 1.1 Hz, H-9), 6.88 (d, *J*= 7.7 Hz, H-10), 7.18 (td, *J*= 7.7, 1.3 Hz, H-11), 7.27 (d, *J*= 6.7 Hz, H-12), 1.47 (dt, *J*= 13.1, 3.8 Hz, H-14a) 0.79 (q, *J*= 12.2 Hz, H-14b), 2.44 (dd, *J*= 8.2, 3.7 Hz, H-15), 7.42 (s, H-17), 4.32 (dq, *J*= 10.4, 6.2 Hz, H-19), 1.59 (ddd, *J*= 8.8, 7.7, 4.4, 3.6 Hz, H-20), 2.39 (dd, 3.6, 8.5 Hz, H-21), 3.36 (dd, *J*= 12.1, 2.1 Hz, H-21b), 3.58 (s, 3H, OCH_3), 1.40 (d, *J*= 6.24 Hz, CH_3). ^{13}C NMR (600 MHz, CD_3OD): δ = 183.17 (C-2), 72.77 (C-3), 55.10 (C-5), 35.36 (C-6), 58.51 (C-7), 135.09 (C-8), 123.43 (C-9), 110.83 (C-10), 128.98 (C-11), 125.47 (C-12), 142.35 (C-13), 31.41 (C-14), 31.92 (C-15), 110.97 (C-16), 156.50 (C-17), 73.64 (C-19), 39.36 (C-20), 54.50 (C-21), 51.56 (OCH_3), 169.40 (C=O), 18.78 (CH_3).

IR (KBr): V_{max}= 3320.43, 2944.11, 2832.23 cm^{-1}. UV/UV-Visible (MeOH) A= 0.790 (214 nm), 0.815 (244 nm).

Mitraphylline (3)

Amorphous white powder: FAB-HR (*+ve*): *m/z*= 369.1809 [M + H]$^{+}$; [M ($C_{21}H_{24}O_4N_2$) + H]= 369.1809. ^{1}H NMR (400 MHz, CD_3OD): δ = 8.50 (brs, NH), 2.45 (d, *J*= 2.5 Hz, H-3), 3.25 (d, *J*= 2.5 Hz, H-5a), 2.55 (d, *J*= 1.6 Hz, H-5b), 2.06 (ddd, *J*= 13.1, 8.1, 1.4 Hz, H-6a), 2.34 (dd, *J* = 4.6, 1.7 Hz, H-6b), 7.06 (td, *J*= 7.6, 1.0 Hz, H-9), 6.88 (d, *J*= 7.7 Hz, H-10), 7.21 (td, *J*= 7.7, 1.2 Hz, H-11), 7.29 (d, *J*= 7.6 Hz, H-12), 2.25 (dt, *J*= 3.1, 3.0 Hz, H-14a), 0.99 (q, *J*= 11.6 Hz, H-14b), 2.09 (d, *J*= 1.4 Hz, H-15), 7.44 (s, H-17), 4.42 (dd, *J*= 6.5, 3.5 Hz, H-19), 1.92 (dd, *J*= 4.6, 2.3 Hz, H-20), 3.11 (d, *J*= 7.3 Hz, H-21), 1.90 (s; H-21), 3.55 (s, 3H, OCH_3), 1.11 (d, *J*= 6.6 Hz, CH_3). ^{13}C NMR (600 MHz, CD_3OD): δ = 180.29 (C-2) , 75.56 (C-3), 54.97 (C-5), 35.48 (C-6), 57.07 (C-7), 134.71 (C-8), 123.73 (C-9), 110.56 (C-10), 129.23 (C-11), 124.14 (C-12), 143.17 (C-13), 30.72 (C-14), 31.56 (C-15), 108.17 (C-16), 155.63 (C-17), 75.43 (C-19), 42.91 (C-20), 54.92 (C-21), 51.39 (OCH_3), 168.91 (C=O), 15.08 (CH_3).

IR (KBr): V_{max}= 3323.82, 2943. 70, 2832.08, 1448.24, 1113.69 cm^{-1}. UV/UV-Visible (MeOH) A= 0.199 (230 nm), 0.303 (216 nm), 0.160 (243 nm), 0.104 (260 nm), 0.097 (267 nm).

Corynoxeine (4)

Amorphous white powder: FAB-HR (*+ve*): *m/z*= 383.1955 [M + H]$^+$; [M ($C_{22}H_{26}O_4N_2$) + H]= 383.1955. ^{1}H NMR (400 MHz, CD_3OD): δ = 8.55 (NH), 2.39 (d, *J*= 2.0 Hz, H-3), 2.45 (d, *J*= 9.1 Hz, H-5a), 3.28 (H-5b), 2.30 (m, H-6a), 2.00 (d, *J*= 11.9 Hz, H-6b), 7.02 (td, *J*= 7.6, 1.1 Hz, H-9), 6.87 (d, *J*= 7.7 Hz, H-10), 7.18 (td, *J*= 7.7, 1.3 Hz, H-11), 7.43 (d, *J*= 8.8 Hz, H-12), 1.88 (H-14), 2.50 (d, *J*= 3.3 Hz, H-15), 7.25 (s, H-17), 5.49 (m, H-18), 4.90 (d, *J*= 2.1 Hz, H-19), 2.84 (d, *J*= 11.0 Hz, H-20), 3.17 (dt, *J*= 11.0, 3.6 Hz, H-21a) 1.95 (m, H-21b), 3.55 (s, OCH_3), 3.72 (s, OCH_3). ^{13}C NMR (600 MHz, CD_3OD): δ = 180.26 (C-2), 73.88 (C-3), 55.02 (C-5), 36.06 (C-6), 58.12 -C-7), 135.0 (C-8), 123.45 (C-9), 110.72 (C-10), 128.86 (C-11), 125.94 (C-12), 142.3 (C-13), 24.17 (C-14), 73.37 (C-15), 112.56 (C-16), 161.48 (C-17), 140.87 (C-18), 115.97 (C-19), 43.6 (C-20), 60.05 (C-21), 51.29 (OCH_3), 61.85 (OCH_3), 170.31 (C=O).

IR (KBr): V_{max}= 3320.28, 2943.33, 2832.29, 1448.15, 1114.24 cm^{-1}. UV/UV-visible (MeOH) A= 0.987 (220 nm) and 1.058 (230 nm).

Compounds 1, 2, and 3 appeared as white amorphous powder with the respective molecular weights 368.1826, 368.1821 and 368.1809. All matched to the same calculated formula $C_{21}H_{24}O_4N_2$. In addition, the common fragment ions appeared at *m/z*= 339.3 [M-30]$^+$, 325.2 [M-44]$^+$, 291.2, 227.3, 164.1 [M-205]$^+$. Herein, they reveal similarity to pentacyclic oxindole alkaloids. On TLC with solvent system DCM: Acetone (9:1), these compounds showed different frontal reference high (1 > 2 > 3). All compounds (1, 2, 3) in ^{1}H NMR revealed presence of one methoxy group. That means, these compounds are the stereoisomers of pentacyclic oxindole alkaloids. Therefore, configuration assignment based on the chemical shift described by Beckett et al.[27] showed that compound 1 and compound 2 are on β configuration with C19, C20 but α configuration with C15. Also, compound 1 (δ*d*-CH_3= 1.39) and compound 2 (δ*d*-CH_3= 1.40) revealed *cis* D/E ring junction with three-proton doublet for the methyl (Beckett et al.[27]). Compound 3 three-proton doublet appeared at 1.11 ppm as D/E ring *trans* junction (Beckett et al.[27]). Correlation was observed between H-17 doublet and the proton H-15 *via* a long range in compounds 1, 2 and 3. However, according to asymmetric centers and their NMR spectra assignment by theoretical calculations of shielding constants of Paradowska et al.,[28] compound 1 (δC3 = 75.31) and compound 3 (δC3 = 75.56) appeared as *7R* alkaloids, but compound 2 (δC3 = 72.77) seemed like *7S* alkaloid. Also, compound 1 (δC20 = 39.29) and compound 2 (δC3 = 39.36) revealed to be *20S* alkaloid but *20R* alkaloid for compound 3 (δC3 = 42.91) (Paradowska et al.[28]). For that, compound 1 (*7R*, *20R*) *allo*-type isomer is identified to pteropodine (uncarine C), compound 2 (*7S*, *20R*) also *allo*-type isomer is identified to isopteropodine (uncarine E) and compound 3 (*7R*, *20R*) normal type isomer matched to mitraphylline (Paradowska et al.[28], Toure et al.[29], García Giménez[30], Salim and Ahmad[31]). Full ^{1}H and ^{13}C NMR signals assignment was made using HMBC, HSQC, COSY and NOESY correlation data. These compounds were previously reported from *M. inermis*.

Compound 4 appeared in molecular weight and formula 382.1955 and $C_{22}H_{26}O_4N_2$ respectively. Peaks at *m/z*= 339.2, 325.2 and 164.0 revealed the presence of olifinic and oxindole fragments. ^{1}H NMR revealed the presence of two methoxy groups at δH= 3.72, δC= 61.85 and δH= 3.55, δC= 51.29. Paradowska et al.[28] theoretical calculations of shielding constants were used for oxindole alkaloids asymmetric centers and NMR spectrum assignment. So, compound 4 (δC3 = 73.88; δC20 = 43.6) is (*7R, 20R*) alkaloid. The chemical shifts δC18 = 140.87, δH18 = 5.49 and δC19 = 115.97, δH19 = 4.90 are characteristic of the methylene group. It appeared to be a tetracyclic oxindol alkaloid. However, ^{1}H NMR, 2D NMR, ^{13}C NMR and FAB-HR compound **4** matched to those of rhyncophylline 18, 19 didehydro like corynoxeine reported from *M. speciosa* (Paradowska et al.[28], Flores-Bocanegra et al.[32]). Thus, in this study, we isolated new specific tetracyclic oxindole named corynoxeine from *M. inermis*.

Acute PTZ-induced seizure model in mice

All the procedures were performed according to the institutional animal care committee of the International Center for Chemical and Biological Sciences (ICCBS). The animal study protocol was submitted to the ICCBS/Karachi University Ethical Committee (date: 20.02.2019, approval number: 2019-006). Seventy-six male naval medical research institute (NMRI) mice with weights between 20 and 24 g were chosen for the experiment. Mice were sourced from ICCBS animal research facility. An experiment was conducted in the light of the daylight/darkness cycle at 25 ± 2 ˚C with appropriate moisture. Animals were brought into the experimental room 1 hour before the start of the experiment for the acclimatization and separated into control and test groups. 110 mg/kg body weight (bw) PTZ as convulsive dose was selected based on an acute crisis model. Mice were grouped together in batches of 7 mice for each dose and control. After acclimatization, the controls were treated with distilled water 10 mL/kg bw by intraperitoneal (*i.p.*). After 30 min, PTZ was injected into the animals, and the main stage of seizure development were observed. The extract ability to attenuate seizure threshold is indicated by absence of seizures at least 5 seconds (Atinga[15]). For the tests with the extracts and fractions of *M. inermis*, the 7 mice for each dose were subdivided into two sub-groups of 3 mice for the first test and 4 mice for the additional test. During the first phase, if no major capacity was observed to mitigate the effects of PTZ at a given dose, the additional test was not carried out. The following doses prepared in distilled water were considered based on data in the literature (Timothy et al.[14], Atinga[15]):

- Aqueous decoctate of leaves: 500, 300, and 150 mg/kg bw;
- Additional fractions acetone + ethyl acetate + butanol of leaves: 500 and 250 mg/kg;
- Stem bark ethanolic extract: 500 and 250 mg/kg bw;
- Additional stem bark ethyl acetate + acetone fractions: 500 and 250 mg/kg bw;
- Stem bark ethyl acetate fraction: 500 and 250 mg/kg bw;
- Stem bark acetone fraction: 500 and 250 mg/kg bw;
- Additional root bark ethyl acetate + acetone fractions: 500 and 300 mg/kg bw
- For the test groups, a suitable dose of the extract was injected intraperitoneally into the animals. After 30 min, a convulsive

dose of PTZ was administered, and the delay in the onset of first myoclonic jerk (FMJ) and hind limb tonic extension (HLTE) was observed and recorded for each animal. The flowchart of the entire study is presented in Figure 1.

Statistical analysis

Statistical analysis were performed by One-Way ANOVA followed by Dunnett's multiple comparison using Graph Pad Prism-8 Statistical Software Package at significance level set as $p < 0.05$.

RESULTS AND DISCUSSION

AED are more or less effective against generalized, myoclonic and absent tonic-colonial seizures (Macdonald[4]). Indeed, around 30% of patients do not respond to the currently available AEDs (Moshé et al.[3]). In traditional medicine, *M. inermis* is used to manage epilepsy. Unfortunately, there was no data on the required levels of herbal materials for therapeutic value. Chromatographic fingerprinting is used in the quality control of medicinal plant materials (Ouédraogo et al.[13]). This report focused first on flavonoid fingerprints as tracers of bioactive contain in various fractions of *M. inermis*. As a result, DCM and hexane fraction didn't show the remarkable flavonoid fingerprints (Figures 2-4). In the different parts, decoction, acetone, ethyl acetate and butanol fractions revealed various flavonoid fingerprints. Using flavonoid fingerprints, as fraction standardization, aqueous decoctate of leaves appeared atypical however, leaves ethyl acetate, butanol and acetone fractions appeared typical. Also, stem bark ethyl acetate and acetone fractions appeared typical, as well as root barks ethyl acetate and acetone fractions. Thus, for the same part, fractions may be combined for their similar flavonoid fingerprints. We noticed variability in flavonoids groups contain (Figures 2-4). Other studies reported the presence of flavonoids in *M. inermis* parts but still on content analyses (Nacoulma[12], Timothy et al.[14], Atinga[15], Ouédraogo et al.[33]).

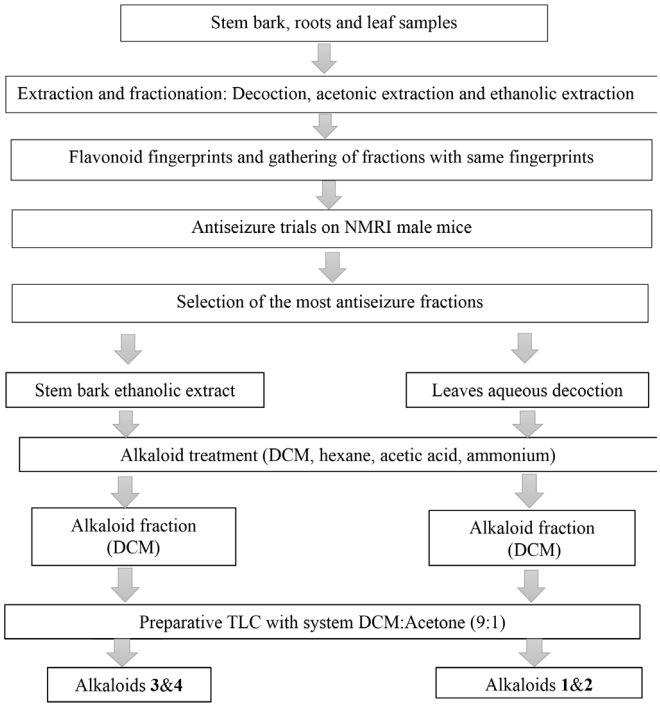

Figure 1. Flowchart of the entire study

NMRI: Naval medical research institute, DCM: Dichloromethane, TLC: Thin layer chromatography

Secondly, we conducted an investigation of *M. inermis* roots, leaves, and stem bark standardized fraction effects on acute PTZ-induced seizures in NMRI mice. All findings were presented in Table 1 and Figure 5. The preliminary study revealed that leaf decoction, stem bark ethyl acetate extract and ethanolic extract delayed the onset of PTZ-induced convulsions. In contrast, root fractions did not show antiseizure effects in the PTZ-induced seizure test in mice (Table 1). The using of

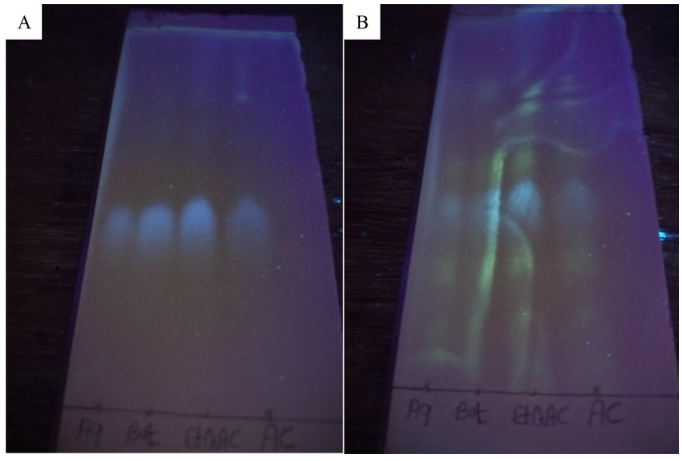

Figure 2. TLC of only leaves extract and fractions that contain flavonoids, A) UV light, B) AlCl3 spraying + UV light. Four additional yellow spots after spraying revealing flavonoids contain. But, EtOAc and Ac appeared as the same compound group contains

TLC: Thin layer chromatography, UV: Ultraviolet, Aq: Aqueous, But: Butanol, EtOAc: Ethyl acetate, Ac: Acetone fractions

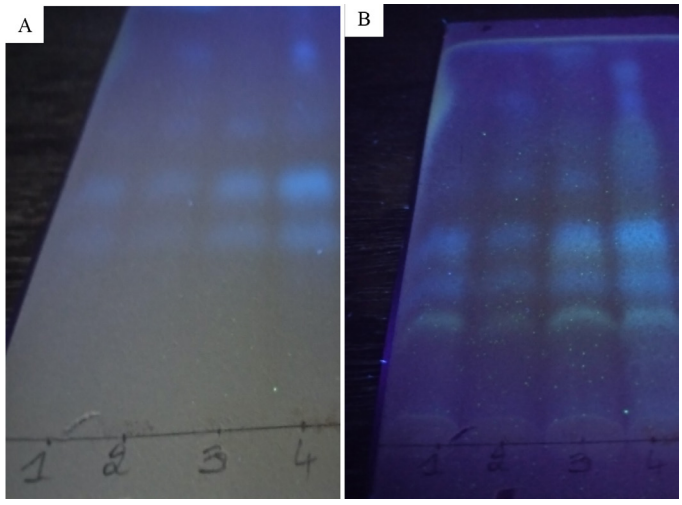

Figure 3. TLC of stem bark, A) UV light, B) AlCl3 spraying + UV light. 1) Hexane fraction, 2) DCM fraction, 3) EtOAc fraction, 4) AC. Three additional yellow spots after spraying revealing flavonoid contains. Most present in 3 and 4 that looked the same

TLC: Thin layer chromatography, UV: Ultraviolet, DCM: Dichloromethane, EtOAc: Ethyl acetate, Ac: Acetone fractions

M. inermis root in the management of epilepsy has not been reported in any ethnobotanical survey. This lack of antiseizure properties might justify its non-utility in traditional medicine. Herbal medicinal product must be manufactured from the indicated part of the plant and must be free of other parts of the same or other plants (Ouédraogo et al.[13]). The acetone stem bark fraction failed to demonstrated any effect, but the ethyl acetate stem bark fraction was found to be responsible of the combined antiseizure effects (Table 1). With the aim to confirm the abilities of *M. inermis*-derived fractions to reduce the seizures, more assays were carried out (Figure 5). PTZ 110 mg/kg bw showed FMJ at 49 ± 0.67 sec and HLT at 65.33 ± 4.22 sec in control group. So, ethyl acetate extract at 500 mg/kg bw, decoction at 300 mg/kg bw and ethanol extract at 500 mg/kg bw revealed the noticeable delay of HLTE occurs (more than 10 min). Moreover, no significant antiseizure effect was observed between stem bark ethanolic extract (500 mg/kg bw) and leaf decoction (300 mg/kg bw) ($p > 0.05$). In contrast, all the fractions failed to significantly delay the onset of first myoclonic seizures. These results suggested that *M. inermis* delay the seizures, specifically delayed HLTE occurred, but failed to show the abilities to delay first myoclonic seizures. The lack of abilities to delay the onset of FMJs suggests that *M. inermis* might require more time to exhibit antiseizures effects after the administration of the extract. However, the results observed in this study with the stem bark ethanolic extract are in agreement with the reported on temporary absence of seizures at 500 and 250 mg/kg bw (Timothy et al.[14]). Also, we reported that *M. inermis* leaves methanolic extract prevented seizures at the doses more than 600 mg/kg (Atinga[15]). But this latter study employed high doses of extracts. In traditional drug preparation methanol is subjected to usage limits (Ouédraogo et al.[13]). The high dose of PTZ used in this study to induced seizure may justify variability of anticonvulsant properties and lack of remarkable latency to FMJ occurred compared to the reported study (Timothy et al.[14], Atinga[15]). It has been reported that flavonoids or medicinal plant extracts containing flavonoids interact with $GABA_A$ receptors leading to anticonvulsant

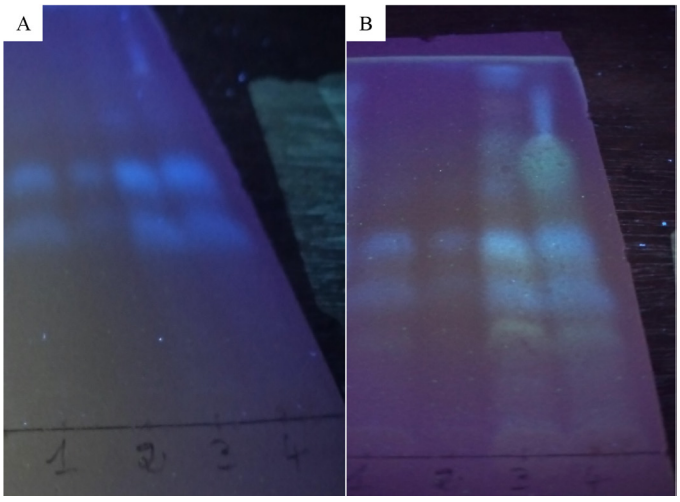

Figure 4. TLC of roots, A) UV light, B) $AlCl_3$ spraying + UV light. 1) Hexane fraction, 2) DCM fraction, 3) EtOAc fraction, 4) Ac. Three additional yellow spots after spraying revealing flavonoid content. Most present in 3 and 4 that appeared the same

TLC: Thin layer chromatography, UV: Ultraviolet, DCM: Dichloromethane, EtOAc: Ethyl acetate, Ac: Acetone fractions

Table 1. Screening of different parts extract and fraction of *M. inermis* for PTZ-induced seizures in mice

Parts	Extracts/fractions	Doses (mg/kg)	Delay in HLTE
Leaves	Decoction	500	++
		300	+++
		150	+
	Ethyl acetate + Butanol + Acetone	500	++
		250	+
Stem bark	Ethanol	500	++++
		250	+++
	Ethyl acetate + Acetone	500	+++
		250	++
	Ethyl acetate	500	+++
		250	+
	Acetone	500	-
		250	-
Roots	Ethyl acetate + Acetone	500	-
		300	-

Noticeable delay of HLTE was recorded by comparison with the group treated with distilled water as a control, n= 3. ++++: More than 10 min, +++: 5 to 10 min, ++: 2 to 5 min, +: less than 2 min, -: No activity, PTZ: Pentylenetetrazol, HLTE: Hind limb tonic extension

activities (Copmans et al.[6], Jäger and Saaby[20], Zhu et al.[21]). Indeed, the variability could arise from the difference of flavonoid fingerprints observed with leaves and stem bark leading to the variation of the HLTE delay. Moreover, it may be suggested that these active extracts might act as agonist of $GABA_A$ receptor, similar to the effects other AEDs that prevent seizures in PTZ-induced seizure test (Kobayashi et al.[5], Shorvon et al.[8],). So those derived fractions could be powerful sources of anticonvulsants. In addition, multiple studies reported lower toxicity of *M. inermis* different part-derived extracts in mice and rates (Timothy et al.[14], Monjanel-Mouterde et al.[34], Ouedraogo et al.[35]). Our latest research on these mixed fractions revealed that they are less hazardous to mouse fibroblast and human hepatocyte cell lines (Ouédraogo et al.[19]). Flavonoids could therefore be tracers to guarantee the quality and therapeutic value of *M. inermis* parts preparation in traditional use and the research of anticonvulsant phytomedicines.

A thorough phytochemical analysis was carried out on the most anticonvulsant extracts and stem bark ethanolic extract and leaf decostate. The fractionation revealed that the alkaloid fraction represented 2.4% of leaf decoction and 7.8% of stem bark ethanolic extract. Traore et al.[36] reported that alkaloid-rich fraction showed low toxicity on monocyte proliferation through inhibition of mammary cell protein production but no mutagenic or genotoxic activities. Subsequently, in order to know these fraction alkaloid ingredients, TLC on the derived alkaloid fractions offered the main oxindole alkaloids *viz* pteropodine, isopteropodine and mitraphylline. In addition, we isolated the new tetracyclic oxindol alkaloid, corynoxeine (Figure 6). Moreover, pteropodine and isopteropodine were reported for their lack of adverse effects on cell culture and DNA (Lee et al.[37], Aponte et al.[38], Ahmad and Salim[39]). Also, isopteropodine showed a neuroprotective effect without toxicity until 10^3 µM

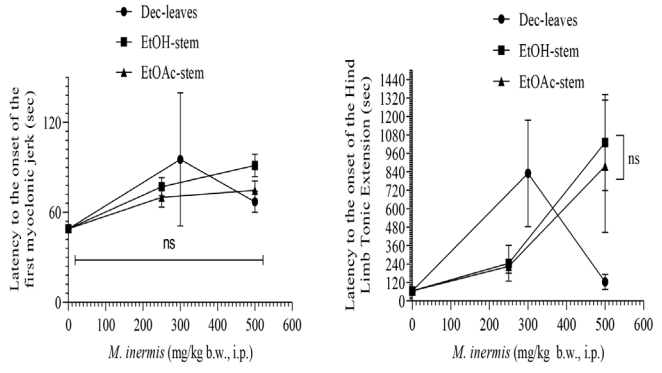

Figure 5. Anti-PTZ-induced seizures of some of the most active fractions. Onsets of FMJ and HLTE are expressed as mean ± SD, n= 7. The dose 0 mg/kg bw is the control (group treated with distilled water). No significant difference was observed between the FMJ onset of the control and treated groups. Compared with the control group, stem bark ethyl acetate and ethanol extract and leave decoction delayed noticeably HLTE ($p \leq 0.05$). Statistical analyses were performed by One-Way ANOVA with Dunnett's multiple comparison tests

Statistical significance levels: *$p \leq 0.05$, ns: Non-significant, Dec: Decoction, EtOH: Ethanol, EtOAc: Ethyl acetate, PTZ: Pentylenetetrazol, FMJ: First myoclonic jerk, HLTE: Hind limb tonic extension, SD: Standard deviation

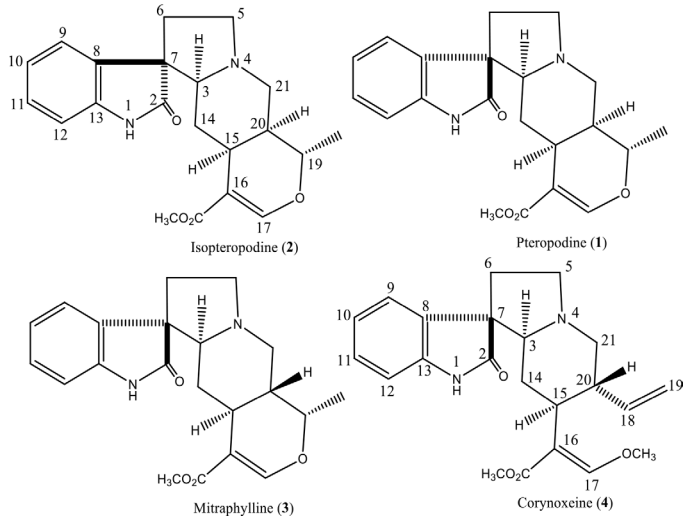

Figure 6. Structures of pteropodine (1), isopteropodine (2), mitraphylline (3), and corynoxeine

(Ahmad and Salim[39]). However, *M. inermis* alkaloid content was already reported (Shellard and Sarpong[16,17], Toure et al.[40]). Alkaloid extract and compounds of other *Mitragyna species* as well as *M. speciosa* are reported to exhibit benefit pharmacological effects on the brain, but require moderate doses (Nelsen et al.[41]). Indeed, alkaloid such as mitragynine interact with neurons by blocking calcium channel (Suhaimi et al.[42]). Therefore, neuronal Ca^{2+} channel-blocking effect abolish seizures (Kobayashi et al.[5]). Mitragynine is also reported in *M. inermis* leaf and stem bark (Shellard and Sarpong[16], Toure et al.[40]). However, indole alkaloids such as ibogaine similarly to pteropodine, isopteropodine and mitraphylline isolated in this study is reported to exhibit anticonvulsant activity by blocking *n*-methyl-D-aspartate (NMDA) receptors. Also, tetracyclic oxindole alkaloids such as rhynchophylline and isorhynchophylline present in *M. inermis* leave and stem bark have been reported with anticonvulsant activities by inhibiting NMDA (Zhu et al.[21]). Thus, the abilities of decoction and ethanolic extracts to exhibit acute antiseizure effects in PTZ-induced seizure test might be attributed to the alkaloid fractions with the plausible synergistic action of pteropodine, isopteropodine, corynoxeine and mitraphylline or due to flavonoid contains. Some AEDs such as phenytoin, carbamazepine and diazepam exhibit alkaloid functions (Kobayashi et al.[5]). However, the pro-seizure effect reported with the ingestion of *M. speciosa* alkaloids calls for having moderate look and use of *M. inermis* alkaloids for treating seizures.

CONCLUSION

This study suggests that flavonoid fingerprints are tracers of *M. inermis* anticonvulsant ingredients. Stem bark ethanolic and ethyl acetate extracts and leaf aqueous extracts contain anticonvulsant bioactive principles that delay HLTE in male NMRI mice. Furthermore, alkaloid contents also remain plausible bioactive anticonvulsant principles. All observations support the traditional use of *M. inermis* to manage epilepsy.

However, further studies might help understand the effects of alkaloid fractions, flavonoids, and the isolated compounds as promising antiseizure agents derived from *M. inermis* in experimental animals.

Acknowledgments

One of the authors would like to sincerely acknowledge The World Academy of Sciences-ICCBS/Karachi/Pakistan for providing research funding and analysis facilities through Sandwich Postgraduate Fellowship FR number 3240316605 to Relwendé Justin Ouédraogo.

Ethics

Ethics Committee Approval: The animal study protocol was submitted to the ICCBS/Karachi University Ethical Committee (date: 20.02.2019, approval number: 2019-006).

Informed Consent: Not necessary.

Authorship Contributions

Concept: R.J.O., L.O., S.U.S., F.S., Design: R.J.O., L.O., S.U.S., F.S., G.A.O., Data Collection or Processing: R.J.O., L.O., S.U.S., F.S., M.J., F.K., M.N.U.H., Analysis or Interpretation: R.J.O., L.O., S.U.S., F.S., M.J., F.K., Literature Search: R.J.O., L.O., S.U.S., F.S., M.J., F.K., Writing: R.J.O.

Conflict of Interest: No conflict of interest was declared by the authors.

Financial Disclosure: The authors declared that this study received no financial support.

REFERENCES

1. Yuen AWC, Keezer MR, Sander JW. Epilepsy is a neurological and a systemic disorder. Epilepsy Behav. 2018;78:57-61.
2. Banerjee PN, Filippi D, Allen Hauser W. The descriptive epidemiology of epilepsy-a review. Epilepsy Res. 2009;85:31-45.
3. Moshé SL, Perucca E, Ryvlin P, Tomson T. Epilepsy: new advances. Lancet. 2015;385:884-898.
4. Macdonald RL. Antiepileptic drug actions. Epilepsia. 1989;30 Suppl 1:S19-28.
5. Kobayashi K, Endoh F, Ohmori I, Akiyama T. Action of antiepileptic drugs on neurons. Brain Dev. 2020;42:2-5.
6. Copmans D, Orellana-Paucar AM, Steurs G, Zhang Y, Ny A, Foubert K, Exarchou V, Siekierska A, Kim Y, De Borggraeve W, Dehaen W, Pieters L, de Witte PAM. Methylated flavonoids as anti-seizure agents: Naringenin 4',7-dimethyl ether attenuates epileptic seizures in zebrafish and mouse models. Neurochem Int. 2018;112:124-133.
7. Devinsky O, Vezzani A, O'Brien TJ, Jette N, Scheffer IE, de Curtis M, Perucca P. Epilepsy. Nat Rev Dis Primers. 2018;4:18024.
8. Shorvon S, Perucca E, Engel J. The treatment of epilepsy. Third Edition, Blackwell Publishing Ltd. 2009:1075.
9. Huang RQ, Bell-Horner CL, Dibas MI, Covey DF, Drewe JA, Dillon GH. Pentylenetetrazole-induced inhibition of recombinant gamma-aminobutyric acid type A [GABA(A)] receptors: mechanism and site of action. J Pharmacol Exp Ther. 2001;298:986-995.
10. Cragg GM, Newman DJ, Snader KM. Natural products in drug discovery and development. J Nat Prod. 1997 ;60:52-60.
11. Arbonnier M. Arbres, arbustes et lianes des zones sèches d'Afrique de l'Ouest. 2002;2-87.
12. Nacoulma OG. Plantes médicinales et pratiques médicinales traditionnelles: cas du plateau central. Ph.D. Thesis, Universite de Ouagadougou. 1996;1-328.
13. Ouédraogo S, Yoda J, Traore TK, Nitiema M, Sombie BC, Diawara HZ, Yameogo JBG, Djande A, Belemnaba L, Kini FB, Ouédraogo S, Semde R. Production de matières premières et fabrication des médicaments à base de plantes médicinales. Int J Biol Chem Sci. 2021;15:750-772.
14. Timothy SY, Wazis CH, Helga BI, Maina A, Bomai HI. Anticonvulsant screening of the aqueous and ethanol extracts of *Mitragyna inermis* bark in pentylenetetrazole and strychnine induced seizures in albino rats. Int J Pharma Ther. 2014;5:358-363.
15. Atinga V. Evaluation of *Mitragyna inermis* (Wild) leaf extract as an anticonvulsant agent in pentylenetetrazole induced seizures in mice. Adv Biomed Pharm. 2015;2:205-210.
16. Shellard EJ, Sarpong K. The alkaloids of the leaves of *Mitragyna inermis* (Willd.) O. Kuntze. J Pharm Pharmacol. 1969;21:Suppl:113S+.
17. Shellard EJ, Sarpong K. The alkaloidal pattern in the leaves, stem-bark and root-bark of Mitragyna species from Ghana. J Pharm Pharmacol. 1970:Suppl:34S+.
18. Toklo PM, Eléonore YL, Amoussatou S, Fidèle MA, Géorcelin GA, Mathias AA, Sylvie HA, Joachim DG. Phytochemistry and pharmacological review of *Mitragyna inermis* (Willd.) Kuntze (*Rubiaceae*). J Pharmacogn Phytochem. 2020;9:22-30.
19. Ouédraogo RJ, Aleem U, Ouattara L, Nadeem-Ul-Haque M, Ouédraogo GA, Jahan H, Shaheen F. Inhibition of advanced glycation end-products by *Tamarindus indica* and *Mitragyna inermis* extracts and effects on human hepatocyte and fibroblast viability. Molecules. 2023;28:393.
20. Jäger AK, Saaby L. Flavonoids and the CNS. Molecules. 2011;16:1471-1485.
21. Zhu HL, Wan JB, Wang YT, Li BC, Xiang C, He J, Li P. Medicinal compounds with antiepileptic/anticonvulsant activities. Epilepsia. 2014;55:3-16.
22. Yuan H, Ma Q, Cui H, Liu G, Zhao X, Li W, Piao G. How Can synergism of traditional medicines benefit from network pharmacology? Molecules. 2017;22:1135.
23. Ouédraogo RJ, Ouattara L, Kabre P, Sanou Y, Somda MB, Ouoba P, Anicet G, Draogo Q. Season and ecotype effects on soluble phenolic compounds content and antioxidant potential of *Tamarindus indica* and *Mitragyna inermis*. J Pharm Pharmacol. 2022;10:143-156.
24. Checkouri E, Reignier F, Robert-Da Silva C, Meilhac O. Evaluation of polyphenol content and antioxidant capacity of aqueous extracts from eight medicinal plants from reunion island: protection against oxidative stress in red blood cells and preadipocytes. Antioxidants (Basel). 2020;9:959.
25. Ranilla LG, Kwon YI, Apostolidis E, Shetty K. Phenolic compounds, antioxidant activity and *in vitro* inhibitory potential against key enzymes relevant for hyperglycemia and hypertension of commonly used medicinal plants, herbs and spices in Latin America. Bioresour Technol. 2010;101:4676-4689.
26. Silva LMP, Alves JSF, da Silva Siqueira EM, de Souza Neto MA, Abreu LS, Tavares JF, Porto DL, de Santis Ferreira L, Demarque DP, Lopes NP, Aragão CFS, Zucolotto SM. Isolation and identification of the five novel flavonoids from genipa americana leaves. Molecules. 2018;23:2521.

27. Beckett AH, Shellard EJ, Phillipson JD, Lee CM. Alkaloids from *Mitragyna speciosa* (Korth). J Pharm Pharmacol. 1965;17:753-755.

28. Paradowska K, Wolniak M, Pisklak M, Gliński JA, Davey MH, Wawer I. (13)C, (15)N CPMAS NMR and GIAO DFT calculations of stereoisomeric oxindole alkaloids from Cat's Claw (*Uncaria tomentosa*). Solid State Nucl Magn Reson. 2008;34:202-209.

29. Toure H, Babadjamian A, Balansard G, Faure R, Houghton PJ. Complete ^{1}H and ^{13}C NMR chemical shift assignments for some pentacyclic oxindole alkaloids. Spectrosc Lett. 1992;25:293-300.

30. García Giménez D, García Prado E, Sáenz Rodríguez T, Fernández Arche A, De la Puerta R. Cytotoxic effect of the pentacyclic oxindole alkaloid mitraphylline isolated from *Uncaria tomentosa* bark on human Ewing's sarcoma and breast cancer cell lines. Planta Med. 2010;76:133-136.

31. Salim F, Ahmad R. Isopteropodic acid from Malaysian *Uncaria longiflora* var. pteropoda. World Appl Sci J. 2010;10:1333-1337.

32. Flores-Bocanegra L, Raja HA, Graf TN, Augustinović M, Wallace ED, Hematian S, Kellogg JJ, Todd DA, Cech NB, Oberlies NH. The Chemistry of Kratom [*Mitragyna speciosa*]: updated characterization data and methods to elucidate indole and oxindole alkaloids. J Nat Prod. 2020;83:2165-2177.

33. Ouédraogo RJ, Somda MB, Ouattara L, Kagambega W, Ouoba P, Ouédraogo GA. Evaluation of the antioxidant and α-amylase inhibitory activities of *Mitragyna inermis* (Willd) O. Kuntze and *Tamarindus indica* Linn. J Exp Biol Agric Sci. 2020;8:676-682.

34. Monjanel-Mouterde S, Traoré F, Gasquet M, Dodero F, Delmas F, Ikoli JF, Lorec AM, Chamlian V, Portugal H, Balansard G, Pisano P. Lack of toxicity of hydroethanolic extract from *Mitragyna inermis* (Willd.) O. Kuntze by gavage in the rat. J Ethnopharmacol. 2006;103:319-326.

35. Ouedraogo Y, Guissou IP, Nacoulma OG. Biological and toxicological study of aqueous root extract from *Mitragyna inermis* (Willd Oktze) *Rubiaceae*. Int J Pharmacol. 2007;3:80-85.

36. Traore F, Gasquet M, Laget M, Guiraud H, Di Giorgio C, Azas N, Doumbo O, Timon-David P. Toxicity and genotoxicity of antimalarial alkaloid rich extracts derived from *Mitragyna inermis* O. Kuntze and *Nauclea latifolia*. Phytother Res. 2000;14:608-611.

37. Lee JS, Yang MY, Yeo H, Kim J, Lee HS, Ahn JS. Uncarinic acids: phospholipase Cgamma1 inhibitors from hooks of *Uncaria rhynchophylla*. Bioorg Med Chem Lett. 1999;9:1429-1432.

38. Aponte JC, Vaisberg AJ, Rojas R, Sauvain M, Lewis WH, Lamas G, Sarasara C, Gilman RH, Hammond GB. A multipronged approach to the study of peruvian ethnomedicinal plants: a legacy of the ICBG-Peru Project. J Nat Prod. 2009;72:524-526.

39. Ahmad R, Salim F. Oxindole alkaloids of *Uncaria (Rubiaceae,* subfamily *Cinchonoideae*): a review on its structure, properties, and bioactivities. Stud Nat Prod Chem. 2015;45:485-525.

40. Toure H, Balansard G, Pauli AM, Scotto AM. Pharmacological investigation of alkaloids from leaves of *Mitragyna inermis* (*Rubiaceae*). J Ethnopharmacol. 1996;54:59-62.

41. Nelsen JL, Lapoint J, Hodgman MJ, Aldous KM. Seizure and coma following Kratom (*Mitragynina speciosa* Korth) exposure. J Med Toxicol. 2010;6:424-426.

42. Suhaimi FW, Yusoff NH, Hassan R, Mansor SM, Navaratnam V, Müller CP, Hassan Z. Neurobiology of Kratom and its main alkaloid mitragynine. Brain Res Bull. 2016;126:29-40.

Turk J Pharm Sci 2024;21(2):113-124
DOI: 10.4274/tjps.galenos.2023.46095

ORIGINAL ARTICLE

Electrochemical Properties of Fused Pyrimidine-Triazole Heterocyclic Molecules as Novel Drug Candidates

Fatma KURUL[1]*, Hüseyin İSTANBULLU[2], Hüseyin Oğuzhan KAYA[3], Arif Engin ÇETİN[4], Seda Nur TOPKAYA[3]

[1]Dokuz Eylül University, İzmir International Biomedicine and Genome Institute, İzmir, Türkiye
[2]İzmir Katip Çelebi University Faculty of Pharmacy, Department of Pharmaceutical Chemistry, İzmir, Türkiye
[3]İzmir Katip Çelebi University Faculty of Pharmacy, Department of Analytical Chemistry İzmir, Türkiye
[4]İzmir Biomedicine and Genome Center, İzmir, Türkiye

ABSTRACT

Objectives: Triazolopyrimidinones are compounds used in medicinal chemistry. In this study, three novel triazolopyrimidinone derivatives were synthesized as drug candidates: (5-(chloromethyl)-2-(4-methoxyphenyl)-[1,2,4]triazolo[1,5-a]pyrimidin-7(3H)-one) (S1-TP), 2-(4-methoxyphenyl)-5-(piperidinomethyl)-[1,2,4]triazolo[1,5-a]pyrimidin-7(3H)-one) (S2-TP), and 2-(4-methoxyphenyl)-5-(morpholinomethyl)-[1,2,4]triazolo[1,5-a] pyrimidin-7(3H)-one) (S3-TP). Their electrochemical properties were investigated for the first time using voltammetric techniques on carbon graphite electrodes. Moreover, stability tests for each drug candidate were performed on different days. After revealing the electrochemical properties of the drug candidates, their effect on double-stranded (ds) DNA was examined by measuring the oxidation currents of the guanine of dsDNA before and after the interaction.

Materials and Methods: An electrochemical setup that included a pencil graphite electrode as the working electrode, an Ag/AgCl reference electrode, and a platinum wire as the auxiliary electrode was used in this study. Experiments for optimum pH, scan rate, and concentration of drug candidates were conducted. The interaction between Ss-TP and dsDNA was evaluated using differential pulse voltammetry. The stability of each drug candidate was tested on various days.

Results: A comprehensive characterization of the S1-TP, S2-TP, and S3-TP compounds was performed for the first time. This study showed that the electrochemical oxidation of S1-TP and S2-TP was irreversible and diffusion-controlled. In addition, the transfer of electrons in S3-TP was controlled by adsorption. The interaction between Ss-TP and dsDNA resulted in notable changes in the peak potentialof dsDNA. The dsDNA peak potential shifted negatively after interaction with S1-TP, S2-TP, and S3-TP. Under optimum conditions, the detection limits for S1-TP, S2-TP, and S3-TP were 1.5 µg/mL, 1.0 µg/mL, and 2.0 µg/mL, respectively.

Conclusion: From our experimental data, we concluded that these molecules can be used as drug molecules because of their remarkable effects on DNA.

Keywords: Drug candidate, drug, DNA, drug-DNA interaction, triazolopyrimidinone, heterocyclic compounds

INTRODUCTION

Triazolopyrimidinones, a class of fuzed pyrimidinone-triazole heterocyclic ring systems, are considered to be privileged scaffolds in medicinal chemistry. A wide range of bioactivities of triazolopyrimidinone-bearing compounds has been reported as FABPs, ferrochelatase, and per-arnt-sim kinase inhibitors.[1,2] In addition, triazolopyrimidinones and triazolopyrimidines with purine bioisosteric analogs have been reported to have anticancer activity through various mechanisms.[3] Fandzloch et al.[4] reported that triazolopyrimidine ruthenium (II) complexes show anticancer activity on various cancer cell lines, and these complexes bind to the minor groove of DNA or intercalate it.

*Correspondence: sedanur6@gmail.com, Phone: +90 507 444 16 07, ORCID-ID: orcid.org/0000-0002-7816-3155
Received: 14.02.2023, Accepted: 13.05.2023

In another study, triazolopyrimidine copper (II) complexes and their DNA intercalating capacity were analyzed using absorption and fluorescence spectra.[5] The results suggested that the complexes were intercalated into DNA strands and damaged through metallonuclease activity. Harrison et al.[6] discovered a selective and highly soluble triazolopyrimidine derivative molecule as an NLRP3 inflammasome inhibitor using *an in silico* pharmacophore model, which could be used as an inhibitor for the treatment of inflammatory diseases.

Drugs and drug candidates can interact with DNA in several ways, and the interaction between them can be determined using various instrumental methods such as circular dichroism (CD), nuclear magnetic resonance (NMR), fourier transform infrared spectroscopy (FTIR), viscosity measurements, infrared spectroscopy (IR), mass spectrometry (MS), molecular docking, and electrochemical methods.[7-15] Morawska et al.[11] developed a voltammetric method to observe the electrochemical behavior of tenofovir and its interaction mechanism with ds/ssDNA and compared their method with spectrophotometric analyses, where the electrochemical method showed better analytical performance compared with spectrophotometry in terms of limit of detection (LOD) and linear range. In another study, the interaction mechanism of mitoxantrones and DNA molecules was studied using FTIR, ultraviolet-visible spectroscopy (VIS), and CD. According to spectroscopic results, mitoxantrone possibly binds to DNA from guanine (N7), thymine (O2), and cytosine (O2) locations.[16] Electrochemical methods are preferred because of their rapidness, high selectivity, low instrumentation cost, simple operation, and portability. They could reveal the chemical properties and potential toxic effects of drug candidates and determine the metabolic processes.[17]

The main interaction modes between the drug molecules and DNA can be simply classified as covalent and non-covalent binding. Among them, covalent binding with DNA is irreversible, inhibits the functions of DNA, and leads to cell death. In contrast, non-covalent binding is reversible, and they are subclassified as electrostatic, groove, and intercalative bindings. Electrostatic binding results from the interactions of positively charged ligands with the negatively charged DNA phosphate backbone structure. Groove binding is also sub-categorized as minor and major groove binding in which small ligands bind to the minor or major groove of DNA by van der Waals or hydrogen bonds. Small ligands can bind to DNA *via* unique binding sites, and this mode is called intercalation. In this mode, intercalators containing planar heterocycle groups could slide and stack between base pairs of DNA and stabilize the duplex without breaking the base pair or forming covalent bonds.

Our study is the first to analyze the electrochemical properties of novel triazolopyrimidine derivatives as purine analog chemical structures. First, we investigated the electrochemical properties of novel drug candidates, and then their interaction with dsDNA was analyzed using voltametric methods as differential pulse voltammetry (DPV) and cyclic voltammetry (CV). Experimental parameters, *e.g.*, pH, concentration of drug candidates, and scan rate, were examined to reveal the analytical properties of these novel drug candidates. Stability tests were performed under optimal storage conditions and within different days to observe the shelf life of the drug candidates.

MATERIALS AND METHODS

Materials

Salmon sperm DNA used in this experiment (Sigma Aldrich, purity ≥ 98%) was dissolved in deionized water to prepare stock solutions. 3-Amino-5-(methylthio)-4H-1,2,4-triazole (Merck, purity ≥ 97%) and chloroform (Alfa Aesar-Acros Organics, purity ≥ 99%) were used as received without further purification. The buffers were prepared using analytical grade chemicals from various companies such as Carlo Erba, Alfa Thermo Fisher Scientific, and Isolab. In the experiments, we used 0.5 M acetate (ACB, pH: 3.8, 4.8, 5.6) and 0.05 M phosphate (PBS, pH: 7.4) buffers containing 0.02 M NaCl and 0.05 M Tris-EDTA (TE, pH: 8.0) buffer.

Instrumentation

Analytical thin layer chromatography (TLC) was performed using Merck silica gel F-254 plates. Melting points were employed with Stuart SMP 30 (Staffordshire, ST15 OSA). NMR spectra were reported with a Varian AS 400 Mercury plus NMR (Varian Inc.) spectrometer at 400 MHz for ^{1}H and 100 MHz for ^{13}C using DMSO-*d6* as the solvent. The coupling constants (J) are presented in Hertz (Hz) without an internal standard. Splitting patterns were designated as follows: s (singlet); d (doublet); t (triplet); p (pentet); and m (multiplet). HR-MS was performed on Agilent 6200 Series TOF and 6500 Series Q-TOF LC/MS System with ESI (+) ionization. Microwave irradiation (MW) synthesis of the compounds was conducted on a Milestone MicroSYNTH (Milestone S.r.l.) microwave apparatus. A PalmSens4 handheld analyzer with PSTrace 5.8 software was used in electrochemical studies. Pencil graphite electrodes were employed as the working electrodes. To complete the three-electrode system, a platinum wire and an Ag/AgCl electrode were employed as auxiliary and reference electrodes, respectively.

Experimental

General synthesis of the drug candidates

The synthesis steps are shown in Figure 1.

Synthesis of the substituted triazole

5-(4-Metoxyphenyl)-3-amino-1,2,4-triazole was synthesized according to reference.[18] In the first step, aminoguanidine bicarbonate and 4-metoxybenzoyl chloride reacted. Later, the amide derivative was cyclized to yield 5-(4-metoxyphenyl)3-aminotriazole.

Synthesis of S_1-TP

5-(4-Metoxyphenyl)-3-amino-1,2,4-triazole (10 mmol) and ethyl 4-chloroacetoacetate (20 mmol) were mixed in 18 mL acetic acid (MW, 20 min, 180 °C). The formed solid was filtered, rinsed with acetic acid, and dried. These steps yielded S_1-TP (5-(chloromethyl)-2-(4-methoxyphenyl)-[1,2,4]triazolo[1,5-*a]* pyrimidin-7(*3H*)-one, which was used in the next steps without purification.

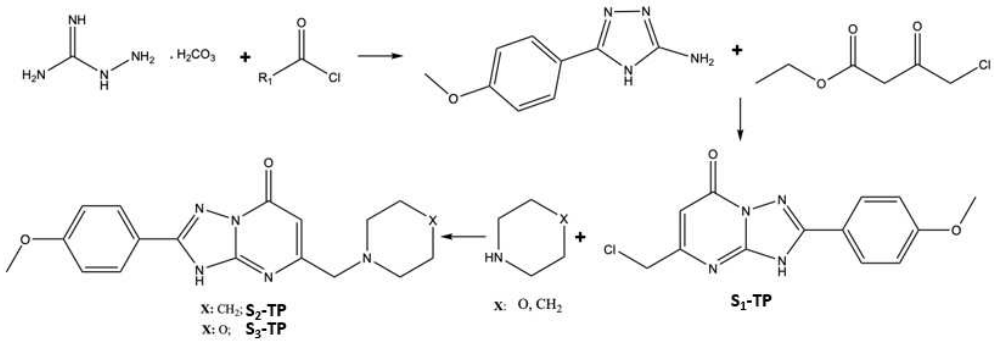

Figure 1. General synthesis scheme of the pyrimidinone-triazole derivatives: S_1-TP, S_2-TP, and S_3-TP
The characterization results are presented in the Supplementary Information (Supplementary Figures 1-6, Data Sheets 1-3)

Synthesis of S_2-TP and S_3-TP

In the last step of the synthesis, the nucleophilic substitution of the obtained S_1-TP with piperidine and morpholine yielded S_2-TP and S_3-TP. S_1-TP (1 mmol) and amine derivatives, namely, piperidine/morpholine (2 mmol), were stirred in 16 mL dimethylformamide (DMF) in the presence of 1.5 mmol caesium carbonate (Cs_2CO_3) using MW irradiation (150 W, 15-30 min, 95 °C). The excess Cs_2CO_3 was filtered, and the filtrate was concentrated under reduced pressure. This mixture was further purified by column chromatography over silica gel 60 (70-230 mesh American Standard Test Sieve Series, Merck) with chloroform: methanol (10:2), and the compounds were recrystallized from methanol or acetone. The crude yield was 40-45%.

S_2-TP: 2-(4-Methoxyphenyl)-5-(piperidinomethyl)-[1,2,4]triazolo[1,5-*a*]pyrimidin-7(*3H*)-one

S_3-TP: 2-(4-Methoxyphenyl)-5-(morpholinomethyl)-[1,2,4]triazolo[1,5-*a*]pyrimidin-7(*3H*)-one

Electrochemical investigation of drug candidates

+ 1.4 V potential for 30 s was applied to activate and clean the PGEs. 1000 µg/mL was prepared with TE buffer and diluted with ACB. 1000 µg/mL) were prepared in DMF and diluted with appropriate buffers. These solutions were then added to the electrochemical measuring cell. Activated PGEs were dipped in these solutions, and DPV measurements were performed.

Interaction

Solutions containing 50 µg/mL of dsDNA and 10 µg/mL of drug candidates were mixed in ACB (pH: 3.8 for S_1-TP/DNA, S_2-TP/DNA; and pH: 5.6 for S_3-TP/DNA). The solutions were then placed in a thermal shaker at 600 rpm and 45 °C for 30 min. Then, 100 µL of this interaction solution was added to the tubes. The PGEs were immersed in the interaction solutions for 30 min. Then, DPV measurements were performed.

Measurement

DPV and CV measurements were performed from + 0.4 and + 1.4 V at a scan rate of 100 mV/s with 0.5 s interval time. The experimental steps are illustrated in Figure 2.

RESULTS AND DISCUSSION

Synthesis of the compounds

Three novel drug candidates were synthesized follows:

5-(Chloromethyl)-2-(4-methoxyphenyl)-[1,2,4]triazolo[1,5-a]pyrimidin-7(3H)-one (S1-TP)

Yellow solid; yield, 52 %; *m.p.*, 113 °C; ^{1}H-NMR (DMSO-d_6, 400 MHz) δ 8.02 (d, *J*= 8.7 Hz, 2H), 7.07 (d, *J*= 8.8 Hz, 2H), 6.16 (s, 1H), 4.66 (s, 2H), 3.81 (s, 3H) ppm; ^{13}C-NMR (DMSO-d_6, 100 MHz) δ 161.6, 156.1, 151.8, 128.7, 114.8, 100.4, 55.8ppm; $C_{13}H_{11}ClN_4O_2$ HRMS *m/z*: 290.0552 (Calcd for 290.05705)

2-(4-Methoxyphenyl)-5-(piperidinomethyl)-[1,2,4]triazolo[1,5-a]pyrimidin-7(3H)-one (S2-TP)

Yellow solid; yield, 30 %; *m.p.*, 128 °C; ^{1}H-NMR (DMSO-d_6, 400 MHz) δ 8.01 (d, *J*= 8.7 Hz, 2H), 6.99 (d, *J*= 8.8 Hz, 2H), 5.63 (s, 1H), 3.79 (s, 3H), 3.30 (s, 2H), 3.23 (s, 2H), 2.34-2.42 (m, 2H), 1.50 (p, *J*= 5.5 Hz, 4H), 1.34-1.43 (m, 2H) ppm; ^{13}C-NMR (DMSO-d_6, 100 MHz) δ 162.39, 160.28, 159.72, 158.74, 128.12, 125.96, 114.21, 94.35, 65.34, 55.59, 54.70, 26.19, 24.47 ppm; $C_{18}H_{21}N_5O_2$ HRMS *m/z*: 339.16979 (Calcd for 339.16952).

2-(4-Methoxyphenyl)-5-(morpholinomethyl)-[1,2,4]triazolo[1,5-a]pyrimidin-7(3H)-one (S3-TP)

Yellow solid; yield, 35 %; *m.p.*, 103 °C; ^{1}H-NMR (DMSO-d_6, 400 MHz) δ 8.02 (d, *J*= 8.9 Hz, 2H), 6.99 (d, *J*= 8.9 Hz, 2H), 5.66 (s,

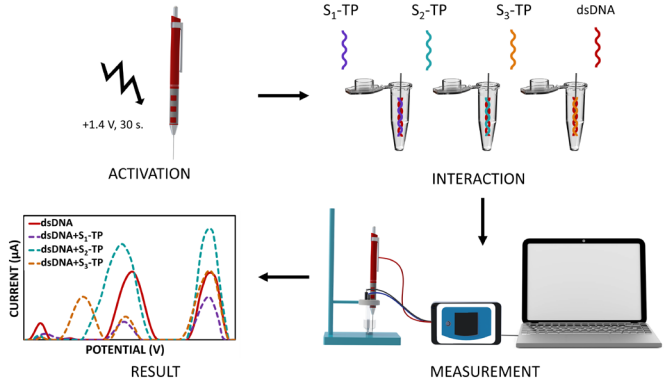

Figure 2. Experimental steps: activation of PGE with ACB, interaction of dsDNA with S_1-TP, S_2-TP, and S_3-TP, and DPV measurements
DPV: Differential pulse voltammetry, dsDNA: Double-stranded DNA

1H), 3.79 (s, 3H), 3.53-3.65 (m, 4H), 3.28 (s, 2H), 2.37-2.47 (m, 4H) ppm; ^{13}C-NMR (DMSO-d_6, 100 MHz) δ 161.27, 160.51, 160.34, 159.55, 158.65, 128.16, 125.82, 114.23, 94.76, 66.76, 64.72, 55.59, 53.91 ppm; $C_{17}H_{19}N_5O_3$ HRMS *m/z*: 341.14814 (Calcd for 341.14879).

The designed compounds were synthesized in three steps (Figure 1). The structures of the final compounds were determined by spectral analyses the spectroscopic data confirmed the proposed structures. In the ^{1}H NMR spectra, the hydrogen atom of the heterocyclic ring was observed as a singlet signal between δ 5.63-6.16 ppm. The methylene protons, attached to the heterocyclic ring at 5 positions, were observed as singlets with two proton integrals between δ 4.66-3.28 ppm. The proton signals of the benzene ring and cyclic amines were identified in the expected chemical shifts with expected divisions. The observed carbon signals in the ^{13}C NMR of the compounds were in accordance with those of the target compounds. The amide carbon signal was observed between δ 161-162 ppm in ^{13}C NMR spectrums.

The purity of the compounds was determined using HRMS spectra. The HRMS data were in accordance with the molecular formula and a found value within 0.003 *m/z* unit of the calculated value of a parent-derived ion. S_2-TP and S_3-TP were introduced earlier in the literature,[19] while the full spectral characterization of these compounds was introduced in this article.

Electrochemical properties of the drug candidates

In this section, the electrochemical behaviors of the drug candidates were analyzed using DPV. Because pH is important for the metabolism of drug molecules, the effect of pH on the oxidation signals of drug candidates was examined, and the obtained results are shown in Figure 3.

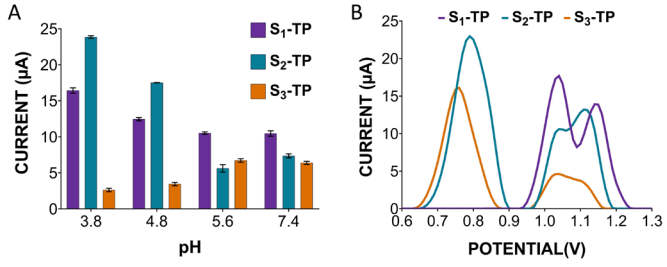

Figure 3. (A) Effect of pH on peak currents. Bar graphs: drug candidates at different pH values, 3.8 to 7.4, (B) DPV voltammogram of S_1-TP, S_2-TP, and S_3-TP prepared in ACB (pH: 3.8 for S_1-TP and S_2-TP, and pH: 5.6 for S_3-TP
DPV: Differential pulse voltammetry

For the pH study in DPV, drug candidates were prepared using buffers with pH ranging from 3.8 to 7.4. As shown in Figure 3A, S_1-TP and S_2-TP produced stable responses, and the highest currents were obtained at pH 3.8. S_3-TP showed the highest electrochemical signal at pH 5.6. Thus, pH 5.6 was chosen as the dilution buffer for S_3-TP (Figure 3A).

At pH 3.8, the oxidation peak potentials of S_1-TP were detected at 1.03 V and 1.15 V. Because it is more stable and higher, the signal obtained at 1.03 V was chosen as the main oxidation signal for further studies. At pH 3.8, S_2-TP produced two oxidation signals at 0.79 V and 1.11 V. At pH 5.6, the oxidation peak potentials of S_3-TP were observed at 0.76 V and 1.04 V (Figure 3B). All oxidation signals shifted to lower potentials with pH. These shifts in the peak potentials of drugs demonstrate that protons participate in the oxidation process of drugs.[20]

As shown in Figure 3B, all the drug candidates have oxidation capacity. The triazolopyrimidinone structure could form triazolopyrimidine by H atom shifting and tautomerization. Several factors could contribute to the stability between the two tautomers, *e.g.*, substitution, aromaticity, hydrogen bonding, and solvation. The redox mechanism of these novel agents on graphite electrode surfaces could involve the oxidation of the phenol groups of the compounds. Heteroatoms in the substituted amines might also contribute to the oxidation potency of the compounds, *e.g.*, they could change the oxidation potency. Considering the phenolic tautomerization of the heteroaromatic ring and the amine substitution, the title compound could possess oxidative properties.

In the second part of our study, DPV measurements were performed at different concentrations of drug candidates at 100 mV/s to determine the analytical concentration ranges for the drug candidates (Figure 4).

The formulas for calculating the LOD and limit of quantification (LOQ) depend on the specific method used, but generally, the LOD is calculated as 3 times the standard deviation of the response (ss) divided by the slope of the calibration curve (m), while the LOQ is calculated as 10 times the standard deviation of the response divided by the slope of the calibration curve'.

LOD = 3 s/m

LOQ = 10 s/m

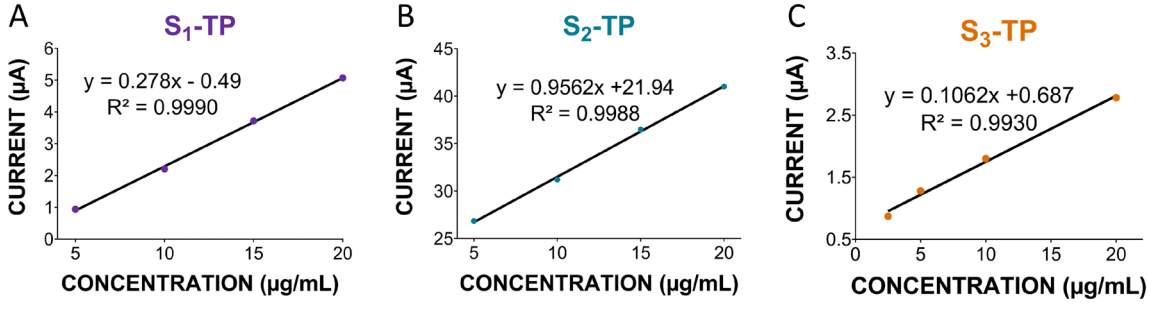

Figure 4. Calibration graphs for (A) S_1-TP, (B) S_2-TP, and (C) S_3-TP obtained from drug concentration *vs.* current peak data

LOD and LOQ were determined from Figure 4. For S_1-TP and S_2-TP, LOD and LOQ were calculated from the concentrations 5, 10, 15, and 20 µg/mL. For S_3-TP, LOD and LOQ were calculated from the concentrations 2.5, 5, 10, and 20 µg/mL. LOD and LOQ for S_1-TP are 1.5 µg/mL and 5.0 µg/mL, respectively (Figure 4A). The LOD and LOQ for S_2-TP are 1.0 µg/mL and 3.4 µg/mL, respectively (Figure 4B). The LOD and LOQ for S_3-TP are 2.0 µg/mL and 6.8 µg/mL, respectively (Figure 4C). The correlation coefficients were 0.9990, 0.9988, and 0.9930 for S_1-TP, S_2-TP, and S_3-TP, respectively.

The effects of scan rate (V) on peak current (I_p) were studied using a CV between 25 and 150 mV/s, as shown in Figure 5.

As shown in Figure 5A, the anodic peak current (Ip_a) has a linear relationship with the scan rate (v):

S_1-TP: Ip_a (µA) = 0.374v + 17.666 (R^2= 0.9990) (Equation 1)

S_2-TP: Ip_a (µA) = 0.1316v + 6.2628 (R^2= 0.9880) (Equation 2)

S_3-TP: (µA) = 0.2254v + 2.2687 (R^2= 0.9980) (Equation 3)

As shown in Figure 5B, the peak current (Ip_a) also has a linear relationship with the root of the scan rate ($v^{1/2}$):

S_1-TP: Ip_a (µA) = 203.97$v^{(1/2)}$ – 7.7443 (R^2=0.9928) (Equation 4)

S_2-TP: Ip_a (µA) = 72.771$v^{(1/2)}$ – 2.9923 (R^2=0.9977) (Equation 5)

S_3-TP: Ip_a (µA) = 122.95$v^{(1/2)}$ – 13.05 (R^2=0.9920) (Equation 6)

In Figure 5C, log(Ip_a) and log(v) linear relationship is presented within the scan rate range between 25 and 150 mV/s:

S_1-TP: *log* Ip_a = 0.5716 *log* v + 2.3213 (R^2=0.9937) *(Equation 7)*

S_2-TP: *log* Ip_a = 0.5996 *log* v + 1.899 (R^2= 0.9987) *(Equation 8)*

S_3-TP: *log* Ip_a = 0.8568 *log* v + 2.2551 (R^2= 0.9978) *(Equation 9)*

According to the literature, these slope values are close to the theoretical value, *e.g.*, 0.5, indicating diffusion-controlled processes, whereas for the theoretical value 1, the process is adsorption-controlled.[21] The slopes of Equations 7 and 8 were determined to be 0.5716 and 0.5996, respectively, which indicates that electrochemical oxidation of S_1-TP and S_2-TP are diffusion-controlled processes. According to Equation 9, the slope is 0.8568, which proves that the electrode process was adsorption controlled for S_3-TP.

Interaction

The intrinsic electroactivity of adenine and guanine bases is generally used as an indicator of drug-DNA interactions. In the next step of our study, we studied the interaction of drug candidates with dsDNA. 100 µg/mL were prepared with TE buffer (pH: 8.0).

The stock drug solutions were prepared with DMF and diluted with ACB (pH: 3.8 for S_1-TP and S_2-TP, and pH: 5.6 for S_3-TP). The final concentrations of dsDNA and Ss-TP were 50 µg/mL and 10 µg/mL, respectively. All solutions were placed in a thermal shaker, where stirring was applied at 600 rpm and 45 °C for 30 min. Then, 100 µL of the solution was transferred into tubes, and the electrodes were immersed in these tubes for 30 min. Oxidation signals were measured with DPV in the range between 0 and 1.4 V at a scan rate of 50 mV/s in the absence and presence of drug candidate molecules. Analytical signals associated with the guanine bases of DNA were obtained at ~1.0 V *vs.* Ag/AgCl.

In Figure 6A, two distinct oxidation signals associated with dsDNA in ACB (pH: 3.8) were obtained at + 0.92 V and + 1.17

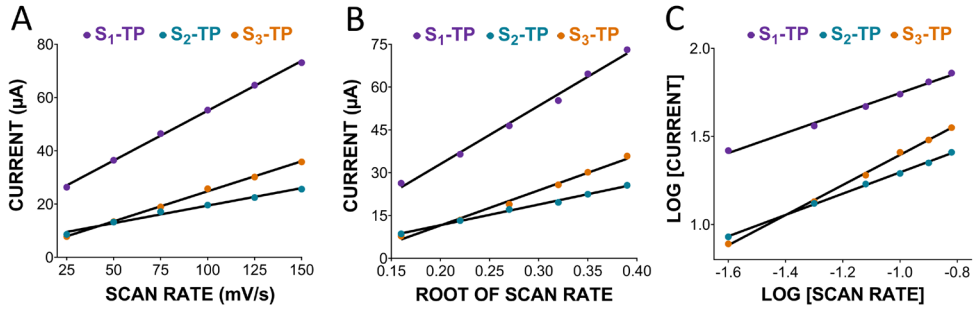

Figure 5. Effect of (A) scan rate and (B) scan rate root on peak current, and (C) scan rate on the log of peak current

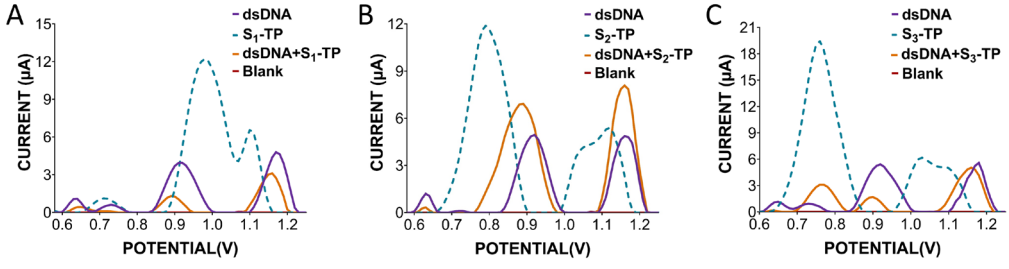

Figure 6. Differential pulse voltammograms of the guanine oxidation currents of dsDNA after interaction with (A) S_1-TP, (B) S_2-TP, and (C) S_3-TP. The experimental steps were as follows: PGE pretreatment: 1.4 V for 30 s, interaction: 100 µg/mL of dsDNA and 20 µg/mL of drug candidates, stirring: 600 rpm at 45 °C for 30 min, adsorption: 30 min, and DPV measurement within a range between 0 and + 1.4 V at 50 mV/s in ACB

dsDNA: Double-stranded DNA, DPV: Differential pulse voltammetry

V. After interaction with S_1-TP, the peak potential of dsDNA shifted to + 0.89 V and + 1.16 V, respectively. On the other hand, after interaction with S_2-TP, one of the peak potentials of dsDNA shifted negatively from + 0.92 V to + 0.89 V. Oxidation signals of dsDNA in ACB (pH: 5.6) were obtained at + 0.92 V and + 1.18 V. In the presence of S_3-TP, the peak potentials of dsDNA slightly shifted toward smaller values, *e.g.*, + 0.90 V and + 1.16 V (Figure 6C). dsDNA oxidation potentials shifted negatively after interacting with S_1-TP, S_2-TP, and S_3-TP. Here, positive or negative shifts in peak potential can reveal the interaction mechanism between the drug candidate and dsDNA. Positive peak potential shifts are associated with intercalative binding, whereas negative peak potential shifts are associated with electrostatic binding.[22] Bilge et al.[23] reported the interaction mechanism between ibrutinib (IBR) and dsDNA using electrochemical and molecular docking techniques. Voltametric studies have indicated that the peak potential of IBR shifts toward less positive potentials because of electrostatic interaction.[23] In our study, the shift in the peak potential toward negative could be attributed to the irreversible electrode process.[24] The reason for this shift could be explained by the electrostatic binding between Ss-TP and dsDNA.

In Figure 6A, the peak currents of dsDNA were found as 3.95 µA and 4.79 µA with the relative standard deviation (RSD) 5.45%, 3.76% which decreased to 1.30 µA and 3.11 µA after the interaction with RSD 3.12%, 4.87% (n= 5). In Figure 6B, the peak currents of dsDNA were found as 4.94 µA and 4.86 µA with RSD 1.68% and 4.54%, respectively, which increased, *e.g.*, 6.92 µA with RSD 3.95% and 7.62% and 8.08 µA with RSD 1.49% and 5.23%, due to the binding of S_2-TP to dsDNA, changing the dsDNA structure. Figure 6C demonstrates that S_3-TP caused a significant change in the oxidation currents of dsDNA. Here, the peak currents of dsDNA are as 5.42 µA with RSD 2.97% and 5.58 µA with RSD 7. 66%, while after interaction, we determined three peaks at 3.07 µA with RSD 5.22%, 1.66 µA with RSD 9.13%, and 5.03 µA with RSD 4.68%.

Stability

Stability is one of the most important factors related to the efficacy of drug candidates. To evaluate the stability of the drug candidates, we performed DPV (Figure 7). Stock solutions of drug candidates were freshly prepared and stored in the dark at room temperature (25 °C). Stock solutions of drug candidates measured within 0, 5, 7, 14, and 30 days. Here, S_1-TP and S_3-TP exhibited good stability for 30 days of storage without significant percentage changes in current values, *e.g.*, we observed a slight reduction in the percentage of current for S_1-TP between days 0 and 30. At the end of day 30, the percentage of the current values for S_1-TP was determined to be 91%. A noticeable change in the percentage current of S_2-TP was observed on day 30, *i.e.*, 48%. In contrast, minute changes in the current values of S_2-TP were observed between days 7 and 30, *e.g.*, the current value of S_3-TP decreased to 86% at day 30. These results proved that the stock solutions of drugs were stable for 30 days, except S_2-TP, which could be very advantageous for long-term use by retaining their pharmaceutical properties.

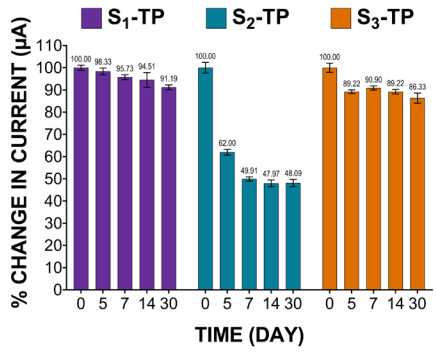

Figure 7. Change in current for S_1-TP, S_2-TP, and S_3-TP examined at 25 °C on different days, *e.g.*, 0, 5, 7, 14, and 30. The percentage current values of drug candidates were 91%, 48%, and 86% by the end of 30 days, respectively

CONCLUSION

In conclusion, in this article, we for the first time studied the full characterization of S_1-TP, S_2-TP, and S_3-TP compounds. Importantly, S_1-TP is reported for the first time in the literature, whereas S_2-TP and S_3-TP compounds were reported in the literature only for their screening activity against FABPs (Patent no; WO 2010/056630 A1). We have introduced the synthetic pathway and full spectral characterization data of these compounds to the literature. Our study focused on the electrochemical behaviors of Ss-TP and their interactions with dsDNA using DPV and CV. We showed that the interaction of Ss-TP-dsDNA resulted in significant changes in the dsDNA peak potential. The dsDNA peak potential shifted negatively after interaction with S_1-TP, S_2-TP, and S_3-TP. The shift of the dsDNA peak potential reveals the interaction of Ss-TP with DNA supporting the binding in between. Moreover, the shift in the peak potential of dsDNA toward more positive values indicates that the DNA-drug interaction mechanism is intercalation, whereas the shift toward more negative values indicates that the DNA-drug interaction mechanism is an electrostatic mode. Our study also showed that the electrochemical oxidation processes of S_1-TP and S_2-TP were irreversible and controlled by diffusion. In addition, the electron transfer process was an adsorption-controlled process for S_3-TP. We believe our study can provide critical information for understanding the DNA-drug interaction, which could be very advantageous for analyzing new drug compounds and their potential effects on target biomolecules.

Ethics

Ethics Committee Approval: This study does not require any ethical permission.

Informed Consent: Not necessary.

Authorship Contributions

Concept: H.O.K., H.İ., S.N.T., Design: F.K, H.O.K., H.İ., S.N.T., Data Collection or Processing: F.K., H.O.K., H.İ., A.E.Ç., S.N.T, Analysis or Interpretation: F.K., H.O.K., H.İ., A.E.Ç., S.N.T., Literature Search: F.K., H.O.K., H.İ., A.E.Ç., S.N.T., Writing: F.K., H.O.K., H.İ., A.E.Ç., S.N.T.

Conflict of Interest: No conflict of interest was declared by the authors.

Financial Disclosure: The authors declared that this study received no financial support.

REFERENCES

1. Aggarwal R, Sumran G. An insight on medicinal attributes of 1,2,4-triazoles. Eur J Med Chem. 2020;205:112652.
2. Janganati V, Ponder J, Balasubramaniam M, Bhat-Nakshatri P, Bar EE, Nakshatri H, Jordan CT, Crooks PA. MMB triazole analogs are potent NF-κB inhibitors and anti-cancer agents against both hematological and solid tumor cells. Eur J Med Chem. 2018;157:562-581.
3. Huo JL, Wang S, Yuan XH, Yu B, Zhao W, Liu HM. Discovery of [1,2,4] triazolo[1,5-a]pyrimidines derivatives as potential anticancer agents. Eur J Med Chem. 2021;211:113108.
4. Fandzloch M, Jędrzejewski T, Dobrzańska L, Esteban-Parra GM, Wiśniewska J, Paneth A, Paneth P, Sitkowski J. New organometallic ruthenium(ii) complexes with purine analogs-a wide perspective on their biological application. Dalton Trans. 2021;50:5557-5573.
5. Ruta LL, Farcasanu IC, Bacalum M, Răileanu M, Rostas AM, Daniliuc C, Chifiriuc MC, Măruțescu L, Popa M, Badea M, Iorgulescu EE, Olar R. Biological activity of triazolopyrimidine copper(ii) complexes modulated by an auxiliary N-N-Chelating heterocycle ligands. Molecules. 2021;26:6772.
6. Harrison D, Bock MG, Doedens JR, Gabel CA, Holloway MK, Lewis A, Scanlon J, Sharpe A, Simpson ID, Smolak P, Wishart G, Watt AP. Discovery and optimization of triazolopyrimidinone derivatives as selective NLRP3 inflammasome inhibitors. ACS Med Chem Lett. 2022;13:1321-1328.
7. Beniaminov AD, Chashchina GV, Livshits MA, Kechko OI, Mitkevich VA, Mamaeva OK, Tevyashova AN, Shtil AA, Shchyolkina AK, Kaluzhny DN. Discrimination between G/C binding sites by olivomycin a is determined by kinetics of the drug-DNA interaction. Int J Mol Sci. 2020;21:5299.
8. Erol A, Akpınar F, Muti M. Electrochemical determination of anticancer drug bendamustine and its interaction with double strand DNA in the absence and presence of quercetin. Colloids Surf B Biointerfaces. 2021;205:111884.
9. Ijäs H, Shen B, Heuer-Jungemann A, Keller A, Kostiainen MA, Liedl T, Ihalainen JA, Linko V. Unraveling the interaction between doxorubicin and DNA origami nanostructures for customizable chemotherapeutic drug release. Nucleic Acids Res. 2021;49:3048-3062.
10. Kozieł SA, Lesiów MK, Wojtala D, Dyguda-Kazimierowicz E, Bieńko D, Komarnicka UK. Interaction between DNA, albumin and apo-transferrin and iridium(III) complexes with phosphines derived from fluoroquinolones as a potent anticancer drug. Pharmaceuticals (Basel). 2021;14:685.
11. Morawska K, Popławski T, Ciesielski W, Smarzewska S. Electrochemical and spectroscopic studies of the interaction of antiviral drug tenofovir with single and double stranded DNA. Bioelectrochemistry. 2018;123:227-232.
12. Nimal R, Nur Unal D, Erkmen C, Bozal-Palabiyik B, Siddiq M, Eren G, Shah A, Uslu B. Development of the electrochemical, spectroscopic and molecular docking approaches toward the investigation of interaction between DNA and anti-leukemic drug azacytidine. Bioelectrochemistry. 2022;146:108135.
13. Ponkarpagam S, Vennila KN, Elango KP. Molecular spectroscopic and molecular simulation studies on the interaction of oral contraceptive drug ormeloxifene with CT-DNA. Spectrochim Acta A Mol Biomol Spectrosc. 2022;278:121351.
14. Shahabadi N, Abbasi AR, Moshtkob A, Hadidi S. Design, synthesis and DNA interaction studies of new fluorescent platinum complex containing anti-HIV drug didanosine. J Biomol Struct Dyn. 2020;38:2837-2848.
15. Wang W, Zhang Y, Liu D, Zhang H, Wang X, Zhou Y. Prediction of DNA-binding protein-drug-binding sites using residue interaction networks and sequence feature. Front Bioeng Biotechnol. 2022;10:822392.
16. Agarwal S, Jangir DK, Mehrotra R. Spectroscopic studies of the effects of anticancer drug mitoxantrone interaction with calf-thymus DNA. J Photochem Photobiol B. 2013;120:177-182.
17. Diculescu VC, Chiorcea-Paquim AM, Oliveira-Brett AM. Applications of a DNA-electrochemical biosensor. TrAC Trends Anal Chem. 2016;79:23-36.
18. Istanbullu H, Bayraktar G, Ozturk I, Coban G, Saylam M. Design, synthesis and bioactivity studies of novel triazolopyrimidinone compounds. J Res Pharm. 2022;26:231-242.
19. Lengyel E, Nieman K, Kenny H. Methods for treating ovarian cancer by inhibiting fatty acid binding proteins. 2014.
20. Deng P, Xu Z, Kuang Y. Electrochemically reduced graphene oxide modified acetylene black paste electrode for the sensitive determination of bisphenol A. J Electroanal Chem. 2013;707:7-14.
21. Jakóbczyk P, Dettlaff A, Skowierzak G, Ossowski T, Ryl J, Bogdanowicz R. Enhanced stability of electrochemical performance of few-layer black phosphorus electrodes by noncovalent adsorption of 1,4-diamine-9,10-anthraquinone. Electrochim Acta. 2022;416:140290.
22. S Sirajuddin M, Ali S, Badshah A. Drug-DNA interactions and their study by UV-Visible, fluorescence spectroscopies and cyclic voltametry. J Photochem Photobiol B. 2013;124:1-19.
23. Bilge S, Dogan-Topal B, Taskin Tok T, Atici EB, Sınağ A, Ozkan SA. Investigation of the interaction between anticancer drug ibrutinib and double-stranded DNA by electrochemical and molecular docking techniques. Microchem J. 2022;180:107622.
24. Radi A, El Ries MA, Kandil S. Electrochemical study of the interaction of levofloxacin with DNA. Anal Chim Acta. 2003;495:61-67.

SUPPLEMENTARY INFORMATION

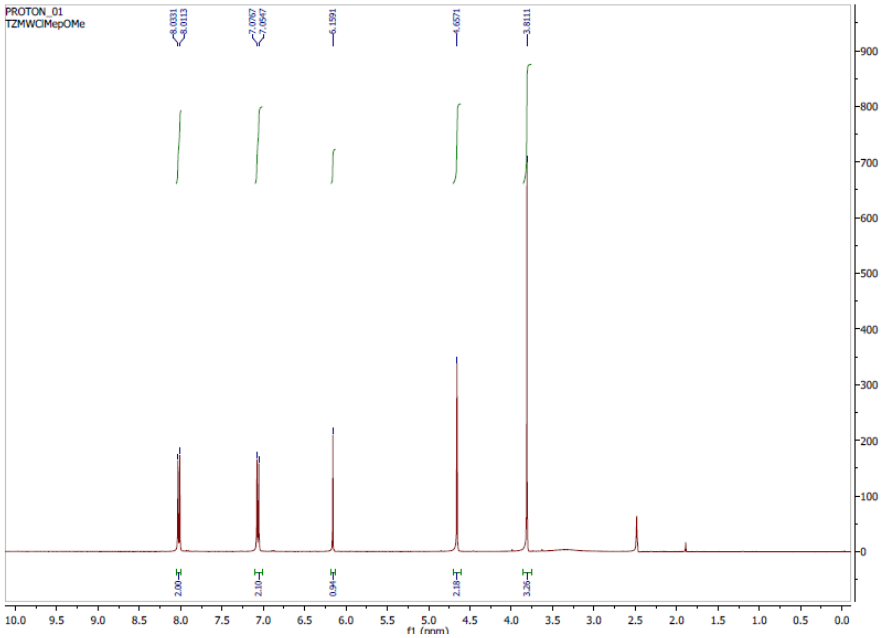

Supplementary Figure 1. ^{1}H NMR spectrum of S_1-TP.

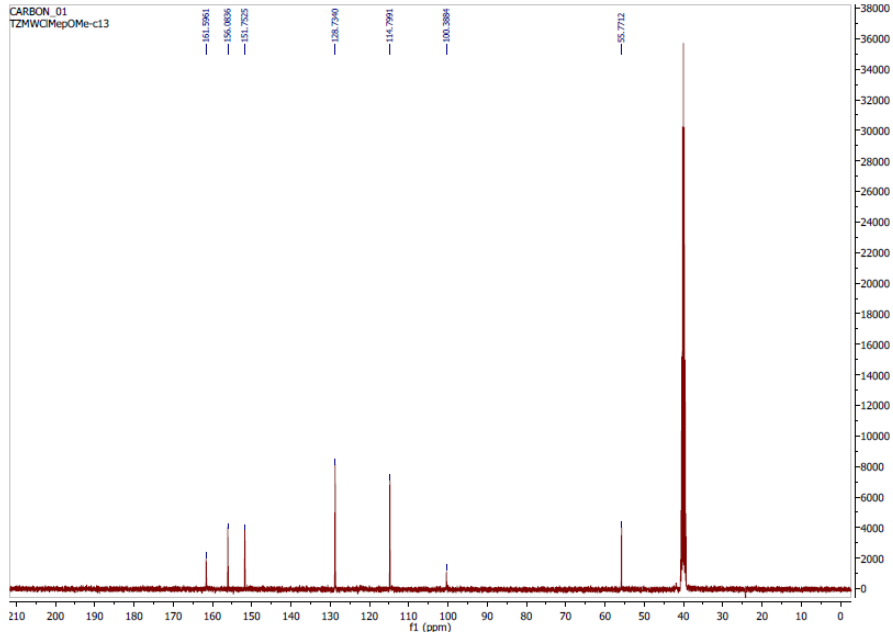

Supplementary Figure 2. ^{13}C NMR spectrum of S_1

User Spectra

Fragmentor Voltage	Collision Energy	Ionization Mode
90	0	ESI

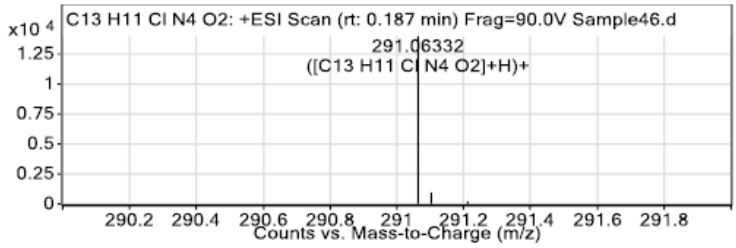

Peak List

m/z	z	Abund	Formula	Ion
291.06332	1	13984.74	C13 H11 Cl N4 O2	(M+H)+
313.04364	1	22951.55		
315.04157	1	6561.68		
329.01804	1	7036.92		
603.10071	1	101639.05		
604.10314	1	28659.66		
605.09877	1	67451.13		
606.09997	1	16867.94		
607.09646	1	11783.25		
619.07417	1	9988.45		

Formula Calculator Element Limits

Element	Min	Max
C	3	13
H	0	11
N	0	4
O	0	2
Cl	0	1

Formula Calculator Results

Formula	Best	Mass	Tgt Mass	Diff (ppm)	Ion Species	Score
C13 H11 Cl N4 O2	DOĞRU	290.05552	290.05705	5.29	C13 H12 Cl N4 O2	80.21

Data Sheet 1. HRMS data of S_1-TP

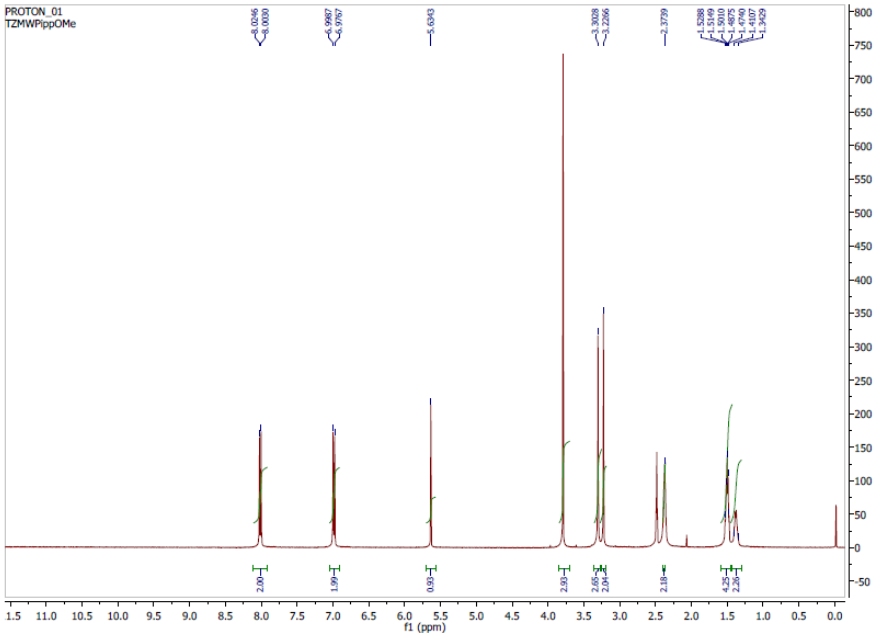

Supplementary Figure 3. ^{1}H NMR spectrum of S_2-TP

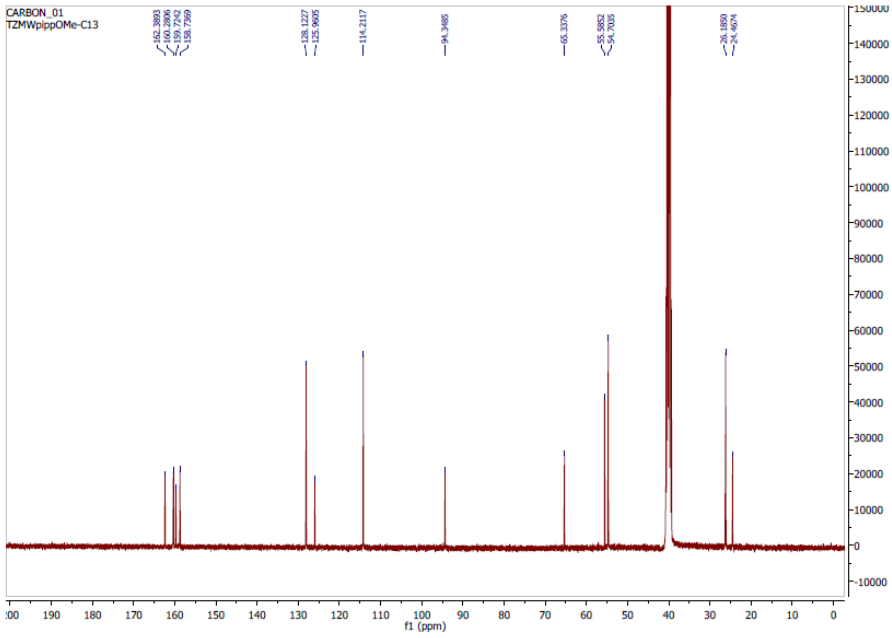

Supplementary Figure 4. ^{13}C NMR spectrum of S_2

User Spectra

Fragmentor Voltage	Collision Energy	Ionization Mode
90	0	ESI

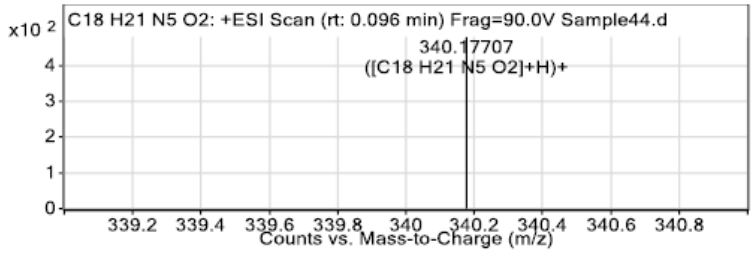

Peak List

m/z	z	Abund
100.01216		716
101.00172		758.46
102.12696		2935.24
125.98556		819.45
130.15831		1208.29
167.01174		868.47
185.11372	1	2942.39
362.15579	1	2343.85
378.1331		684.14
406.32531	1	1478.49

Formula Calculator Element Limits

Element	Min	Max
C	3	18
H	0	21
N	0	5
O	0	2

Formula Calculator Results

Formula	Best	Mass	Tgt Mass	Diff (ppm)	Ion Species	Score
C18 H21 N5 O2	DOGRU	339.16979	339.16952	-0.8	C18 H22 N5 O2	47.39

Data Sheet 2. HRMS data of S_2-TP

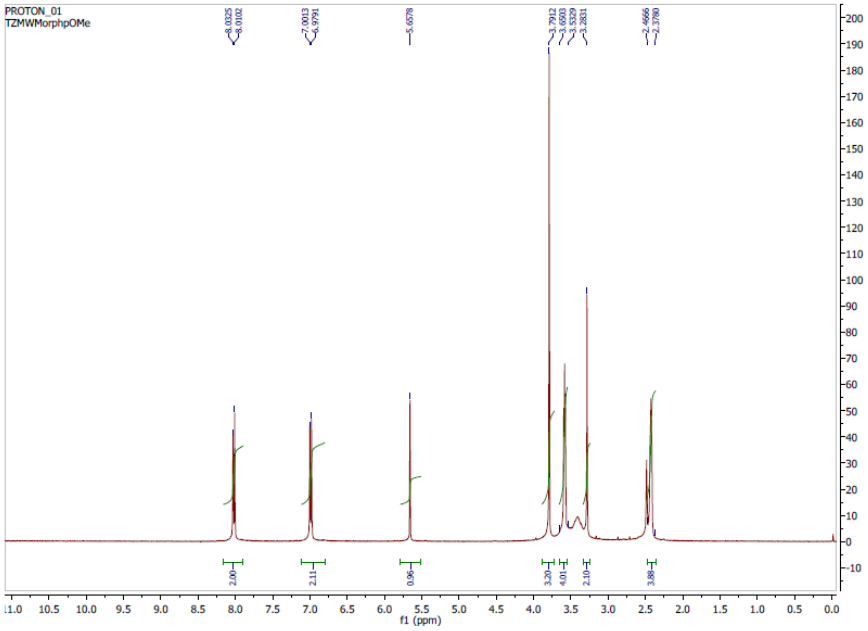

Supplementary Figure 5. ^{1}H NMR spectrum of S_3-TP

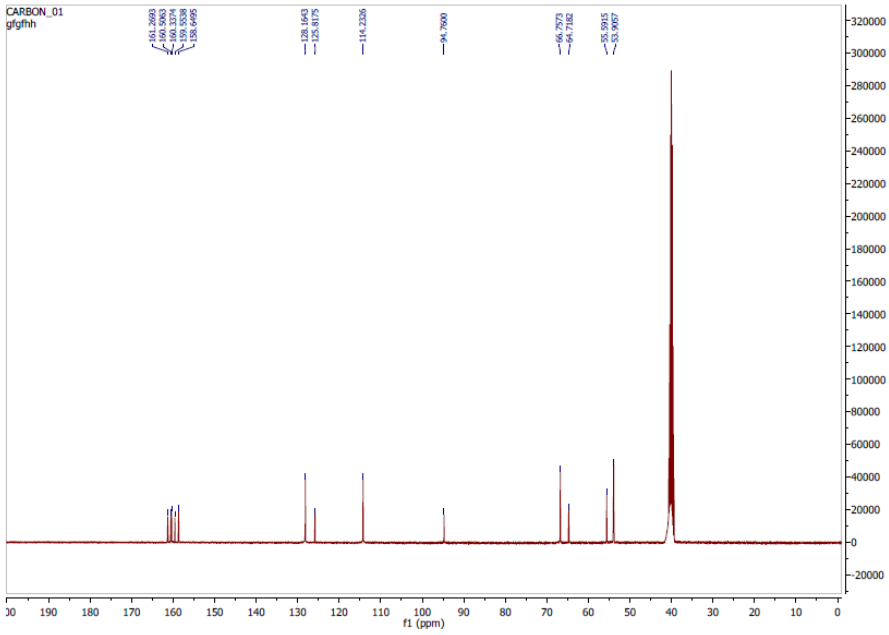

Supplementary Figure 6. ^{13}C NMR spectrum of S_3-TP

User Spectra

Fragmentor Voltage	Collision Energy	Ionization Mode
90	0	ESI

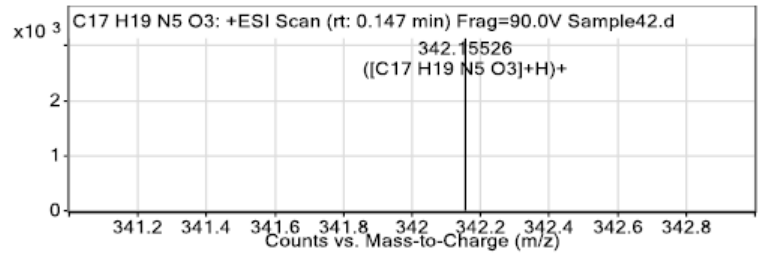

Peak List

m/z	z	Abund	Formula	Ion
132.90359		4762.14		
210.91546		1435.13		
342.15526	1	3130.95	C17 H19 N5 O3	(M+H)+
474.05149	1	16621.97		
474.10335		1299.25		
475.05505	1	2978.97		
547.10823	1	1285		
605.94806	1	4872.07		
683.30168	1	1764.2		
815.19928	1	3132.83		

Formula Calculator Element Limits

Element	Min	Max
C	3	17
H	0	19
N	0	5
O	0	3

Formula Calculator Results

Formula	Best	Mass	Tgt Mass	Diff (ppm)	Ion Species	Score
C17 H19 N5 O3	DOĞRU	341.14814	341.14879	1.89	C17 H20 N5 O3	83.48

Data Sheet 3. HRMS data of S_3-TP

Turk J Pharm Sci 2024;21(2):125-132
DOI: 10.4274/tjps.galenos.2023.87522

ORIGINAL ARTICLE

Developed and Validated for the Estimation of Bupropion and Dextromethorphan in a Fixed Dose Combination of the Tablet

Raghunatha Reddy CHAVVA

Sri Krishnadevaraya University, Department of Chemistry, Ananthapuramu, India

ABSTRACT

Objectives: The aim of this study was to develop a simple, accurate, and precise method for the estimation of bupropion and dextromethorphan in a fixed-dose combination of tablets and robust high-performance liquid chromatography for assay analysis of such a fixed combination.

Materials and Methods: Chromatographic analysis was performed and separations were achieved on a Denali C18 150 × 4.6 mm, 5 micron using a mobile phase composition of *ortho-phosphoric* acid and acetonitrile in the ratio of 600:400 (*v/v*), flow rate of 1.0 mL/min, injection volume is 10 µL and run time of 6 min in isocratic elution. Ultraviolet (UV) detection was performed at a wavelength of 221 nm. The temperature was maintained at 30 ˚C. Well-resolved peaks were observed with a high number of theoretical plates, lower tailing factor, and reproducible relative retention time. The method was validated, and all validation parameters were found to be within the acceptance limits.

Results: A simple, accurate, and precise method has been developed for estimating bupropion and dextromethorphan in a fixed dose combination of tablets. The optimized method included the following parameters: column temperature of 30 ˚C, 40% acetonitrile as the mobile phase, and flow rate of 1.0 mL/min. Retention times were 2.25 min and 3.12 min for bupropion and dextromethorphan, respectively. The method was found to be linear in the range of 17.5-105 µg/mL [for $R^2 < 0.999$) and 7.5-45 µg/mL (for $R^2 > 0.999$] for bupropion and dextromethorphan, respectively. Both active pharmaceutical ingredients dissolved more than 90% within 5 min.

Conclusion: The current study describes a new, simple, reliable, and economical elution reversed-phase high performance liquid chromatography method for estimating bupropion and dextromethorphan in a fixed combination tablet dosage form. The forced degradation studies were conducted using several degradation conditions such as acidic, alkali, oxidation, thermal, UV, and neutral conditions; the proposed method was effectively employed from the resolution of sample peaks. To the best of our knowledge, no such detailed and stability-indicating method has been reported for a fixed tablet dosage form.

Keywords: Bupropion, dextromethorphan, stress degradation, RP-HPLC method development and validation

INTRODUCTION

AUVELITY is a combination of dextromethorphan hydrobromide, an uncompetitive *n*-methyl-D-aspartate (NMDA) receptor antagonist and sigma-1 receptor agonist, and bupropion hydrochloride, an aminoketone and CYP450 2D6 inhibitor.[1]

Dextromethorphan is an uncompetitive antagonist of the NMDA receptor (an ionotropic glutamate receptor) and a sigma-1 receptor agonist. The mechanism of action of dextromethorphan for treating major depressive disorder (MDD) is unclear. The mechanism of action of bupropion for treating MDD is also unclear; however, it may be related to noradrenergic and/or dopaminergic mechanisms. Bupropion increases the plasma levels of dextromethorphan by competitively inhibiting cytochrome P450 2D6, which catalyzes a major biotransformation pathway for dextromethorphan. Bupropion is a relatively weak inhibitor of the neuronal reuptake of norepinephrine and dopamine and does not inhibit monoamine oxidase or the reuptake of serotonin.[1]

*Correspondence: raghunathareddy.chavva@gmail.com, Phone: +91 9948908588, ORCID-ID: orcid.org/0000-0003-4287-0971
Received: 09.04.2023, Accepted: 18.05.2023

Bupropion hydrochloride

Bupropion hydrochloride is an antidepressant of the aminoketone class. It is chemically unrelated to tricyclic, tetracyclic, selective serotonin reuptake inhibitors, or other known antidepressant agents. Its structure closely resembles that of diethylpropion; it is related to phenylethylamines and acts as a nicotinic acetylcholine receptor antagonist.[2-6]

Dextromethorphan hydrobromide

Dextromethorphan hydrobromide is an oral non-narcotic antitussive drug widely used in practical medicine. It was very well absorbed by the digestive system and did not bind to plasma proteins. A combination of pseudophedrine hydrochloride, chlorpheniramine maleate, and acetaminophen is used in pharmaceutical preparations to reduce symptoms usually associated with the common cold.[7-10]

Individual high-performance liquid chromatography (HPLC) methods reported for each drug were inappropriate for simultaneous determination because of interferences due to corresponding chromatographic peaks. However, these procedures require the use of more than one column, mobile phase, or flow rate, which can be time-consuming and uneconomical. Recently, a method has been reported for the simultaneous estimation of bupropion and dextromethorphan. However, the chromatogram revealed that the bupropion peak was eluted in the void volume where the interference was observed with the blank peak, and the placebo chromatogram was not recorded to identify the interference at bupropion and dextromethorphan. The reported method showed degradation of more than 10% for bupropion and dextromethorphan in acid, base, and peroxide, but degradation chromatograms were not shown.[11] The main aim of this method is to determine and validate bupropion and dextromethorphan in a fixed combination of tablet dosage forms based on the International Conference on Harmonization (ICH) guidelines.[12] This method was developed for use as a reproducible procedure for the quantitative analysis of drug samples. The designed method can be considered advisable for developing a precise, accurate, and simple reversed-phase high performance liquid chromatography (RP-HPLC) method.

The chemical name for bupropion is (±)-1-(3chlorophenyl)-2-[(1,1-dimethylethyl) amino]-1-propranone hydrochloride. The molecular formula is $C_{13}H_{18}ClNO•HCl$ and the molecular weight is 276.2 g/mol. The chemical structure of bupropion is shown in Figure 1.

The chemical name for dextromethorphan is (9S,13S,14S)-3-methoxy-17-methylmorphinan hydrobromide. The molecular formula is $C_{18}H_{26}BrNO$ and the molecular weight is 352.3 g/mol. The chemical structure of dextromethorphan is shown in Figure 2.

MATERIALS AND METHODS

Chemicals, reagents, and instruments

Bupropion, dextromethorphan, *ortho-phosphoric* acid (H_3PO_4), acetonitrile, and Milli-Q water. Denali C18 150 × 4.6 mm, 5-micron column, HPLC instrument equipped with ultraviolet-visible spectrophotometer and photo diode array (PDA) detector.

Chromatographic conditions

Flow rate: 1.0 mL, injection volume: 10 µL, detector: 221 nm, column temperature: 30 ˚C, column: Denali C18 150 × 4.6 mm, 5 m, and run time: 6 min.

Mobile phase and solution preparation

Preparation of the buffer

One milliliter of *ortho-phosphoric* acid solution was diluted to 1000 mL with Milli-Q water.

Preparation of the mobile phase

Mix 600 mL of buffer and 400 mL of acetonitrile and sonicate to degas.

Preparation of the diluent

Mix 500 mL of water and 500 mL of acetonitrile and sonicate to degas.

Standard preparation

As much as 35 mg of bupropion and 15 mg of dextromethorphan were accurately weighed and transferred according to working standards into a 50 mL clean, dry volumetric flask; 10 mL of diluent was added and sonicated for 10 min, and the final volume was made up to the mark with diluent (700 µg/mL bupropion and 300 µg/mL of dextromethorphan).

From the above stock solution, 1 mL was taken into a 10 mL volumetric flask and made up to the mark with diluent (70 µg/mL bupropion and 30 µg/mL of dextromethorphan).

Sample preparation

An equivalent weight of 70 mg of bupropion fixed dose combination tablet powder was accurately weighed and transferred into a 100 mL volumetric flask; 75 mL of diluent was added and sonicated for 25 min. The volume was made up to the mark with diluent and filtered using a Milli-Q filter (700

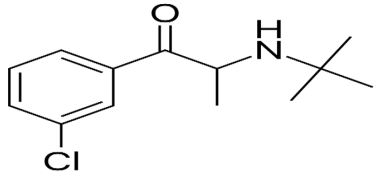

Figure 1. Chemical structure of bupropion

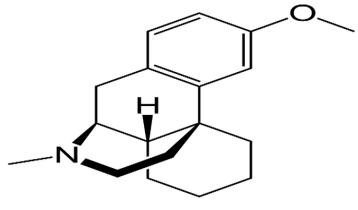

Figure 2. Chemical structure of dextromethorphan

µg/mL bupropion and 300 µg/mL of dextromethorphan). Then, 1 mL of filtered sample stock solution was transferred to a 10 mL volumetric flask and made up to the mark with diluent (70 µg/mL bupropion and 30 µg/mL of dextromethorphan).

Degradation studies

Oxidation

From a stock solution of 700 µg/mL bupropion and 300 µg/mL dextromethorphan, 1 mL was pipetted and 1 mL of 20% hydrogen peroxide (H_2O_2) was added separately. The resultant solution was maintained for 60 min at 30 ˚C. For the HPLC study, the resultant solution was diluted to obtain 70 µg/mL of bupropion and 30 µg/mL of dextromethorphan, then 10 µL injection volume was injected into the system, and the chromatogram was recorded to assess the stability of the sample.

Acid degradation studies

From a stock solution of 700 µg/mL bupropion and 300 µg/mL dextromethorphan, 1 mL was pipetted and 1 mL of 2 N hydrochloric acid was added separately. The resultant solution was refluxed for 30 min at 60 ˚C. The acid was then neutralized with an equivalent volume of sodium hydroxide solution. For the HPLC study, the resultant solution was diluted to obtain 70 µg/mL of bupropion and 30 µg/mL of dextromethorphan, then 10 µL injection volume was injected into the system, and the chromatogram was recorded to assess the stability of the sample.

Alkali degradation studies

From a stock solution of 700 µg/mL bupropion and 300 µg/mL dextromethorphan, 1 mL was pipetted and 1 mL of 2 N sodium hydroxide solution was added separately. The resultant solution was refluxed for 30 min at 60 ˚C. Next, the base was neutralized with an equivalent volume of hydrochloric acid solution. For the HPLC study, the resultant solution was diluted to obtain 70 µg/mL of bupropion and 30 µg/mL of dextromethorphan, then 10 µL injection volume was injected into the system, and the chromatogram was recorded to assess the stability of the sample.

Thermal degradation studies

The solution was exposed to heat at 105 ˚C for 6 h, and then 1 mL of the stock exposed solution of 700 µg/mL bupropion and 300 µg/mL dextromethorphan was pipetted. For the HPLC study, the resultant solution was diluted to obtain 70 µg/mL of bupropion and 30 µg/mL of dextromethorphan, then 10 µL injection volume was injected into the system, and the chromatogram was recorded to assess the stability of the sample.

Photostability studies

The solution was exposed to UV light at 1.2 million lux hours and 200 watt hour/m^2 for four days, and then 1 mL of stock exposed solution of 700 µg/mL bupropion and 300 µg/mL dextromethorphan was pipetted. For the HPLC study, the resultant solution was diluted to obtain 70 µg/mL of bupropion and 30 µg/mL of dextromethorphan, then 10 µL injection volume was injected into the system, and the chromatogram was recorded to assess the stability of the sample.

Neutral degradation studies

From the stock solution of 700 µg/mL bupropion and 300 µg/mL dextromethorphan, 1 mL of the solution was pipetted and 1 mL of water was added separately. The solution was refluxed for 6 h at 60 ˚C. For the HPLC study, the resultant solution was diluted to obtain 70 µg/mL of bupropion and 30 µg/mL of dextromethorphan, then 10 µL injection volume was injected into the system, and the chromatogram was recorded to assess the stability of the sample.

RESULTS

A simple, accurate, and precise method has been developed for estimating bupropion and dextromethorphan in a fixed dose combination of tablets. The optimized method included the following parameters: column temperature of 30 ˚C, 40% acetonitrile as the mobile phase, and flow rate of 1.0 mL/min. Retention times were 2.25 min and 3.12 min for bupropion and dextromethorphan, respectively.

DISCUSSION

With the progress of the ICH guidelines, the determination of a stability-indicating method has developed to be clearer and obligatory. The guidelines are necessary for handling forced degradation studies under different conditions, such as acid, base, photolytic, oxidation, heat, and neutral. Hence, the necessity of separation of several components through the study of stability samples is evident. HPLC has gained a reputation in stability studies due to its specificity, sensitivity, and high-resolution capacity. The work planned in this research was conducted to study the chromatographic actions of the samples of stress degradation of bupropion and dextromethorphan in the tablet dosage formulation. To the best of our knowledge, and motivated us to develop an RP-HPLC-PDA stability indicating test in which the degradation products were resolved from the integral drugs.

Method development

Initially, the analytical method was developed using *ortho-phosphoric* acid solution and acetonitrile in a ratio of 1:1, but the resultant chromatogram observed closed eluted peaks. The resultant chromatogram is shown in Figure 3.

Finally, the method was optimized with critical quality attributes such as standard preparation, sampling preparation, column,

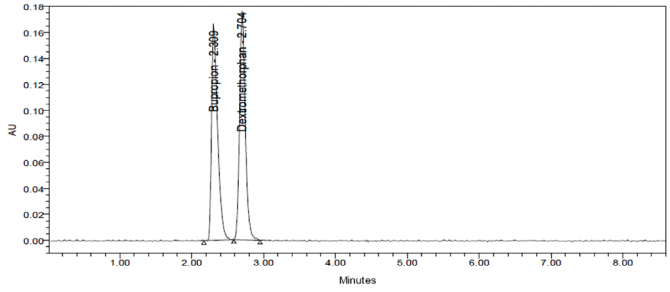

Figure 3. Standard chromatogram of bupropion and dextromethorphan
AU: Absorbance units

detector, resolution of peaks, and instrument. The optimized standard solution containing 70 µg/mL of bupropion and 30 µg/mL of dextromethorphan was used to validate the parameters. The resulting chromatograms are shown in Figures 4 and 5.

Method validation

The method was validated as *per* the ICH guidelines. The different validation parameters were performed as follows: linearity, precision, accuracy, specificity, limit of detection (LOD), limit of quantitation (LOQ), robustness, degradation studies, and stability-indicating capability.

System suitability test

System suitability was evaluated using freshly prepared standard solutions. Five replicate injections of standard solution were injected into the HPLC system, and the obtained areas, retention time, tailing factor, theoretical plates, and relative standard deviation % (RSD) were calculated. System suitability results are tabulated in Tables 1 and 2. % RSD values were within the limit of not more than 2%.

Specificity

Specificity tests were performed on freshly prepared blanks and placebos of bupropion and dextromethorphan tablets. The resultant chromatograms indicated that no interference was observed from blank and placebo at retention time of bupropion and dextromethorphan in the optimized method conditions. The resulting chromatograms are depicted in Figures 6 and 7.

Linearity

The linearity parameter was evaluated using standard drug solutions by preparing six different concentrations. Linearity levels were 25%, 50%, 75%, 100%, 125%, and 150%. All six linearity solutions were injected into the HPLC system, and the correlation coefficient values against drug concentrations versus peak areas were calculated. The results are presented in Table 3, and related graphs are depicted in Figures 8 and 9. The correlation coefficient values were within the limit of 0.999.

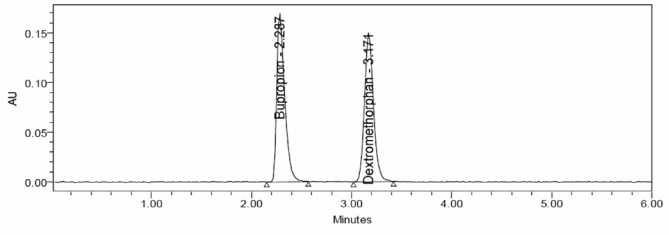

Figure 4. Standard chromatogram of bupropion and dextromethorphan
AU: Absorbance units

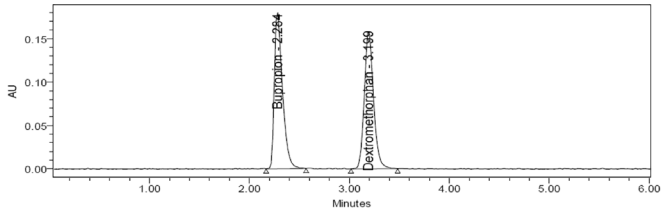

Figure 5. Sample chromatogram of bupropion and dextromethorphan
AU: Absorbance units

Precision

Precision was performed by preparing six replicate sample preparations from a homogeneous sample. Six replicate solutions were obtained as *per* the test procedure mentioned in the Materials and Methods section. % of RSD results were calculated for the areas and % assay. The obtained results are tabulated in Table 4. Precision results were found satisfactory, and the % RSD values were below 2%.

Intermediate precision

Intermediate precision was performed by preparing six replicate sample preparations from a homogeneous sample using different analysts, columns, and laboratories. Six replicate solutions were obtained as *per* the test procedure mentioned in the Materials and Methods section. % of RSD results were calculated for the areas and % assay. The obtained results are tabulated in Table 5. Intermediate precision results were found satisfactory, and the % RSD values were below 2%.

Table 1. System suitability results for bupropion

Injections	Retention time (min)	Area	USP plate count	USP tailing factor
1	2.265	939582	3409	1.63
2	2.284	941657	3650	1.50
3	2.287	944326	3791	1.47
4	2.290	946091	3827	1.46
5	2.291	948170	3946	1.47
Mean	2.283	943965	3724.6	1.506
SD	0.0106	3423.1	205.6	0.0709
% RSD	0.5	0.4	5.5	4.7

USP: United States Pharmacopeia, SD: Standard deviation, RSD: Relative standard deviation

Table 2. System suitability results for dextromethorphan

Injections	Retention time (min)	Area	USP plate count	USP tailing factor
1	3.138	763039	6037	1.14
2	3.142	765036	6148	1.16
3	3.150	763327	6085	1.16
4	3.165	767346	6141	1.15
5	3.171	755921	6194	1.15
Mean	3.153	762934	6121	1.152
SD	0.0143	4278.8	60.848	0.0084
% RSD	0.5	0.6	1.0	0.7

USP: United States Pharmacopeia, SD: Standard deviation, RSD: Relative standard deviation

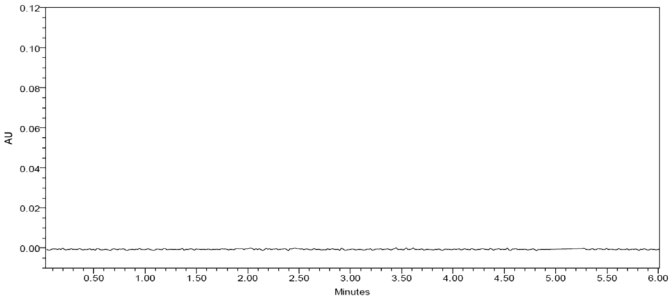

Figure 6. Blank chromatogram of bupropion and dextromethorphan
AU: Absorbance units

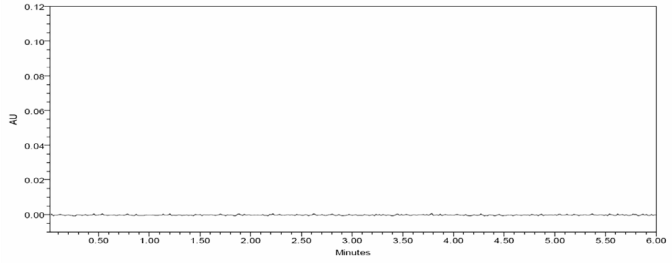

Figure 7. Placebo chromatogram of bupropion and dextromethorphan
AU: Absorbance units

Table 3. Linearity concentration

Linearity level	Bupropion		Dextromethorphan	
	Concentration (µg/mL)	Peak area	Concentration (µg/mL)	Peak area
25%	17.5	233642	7.5	189050
50%	35.0	477356	15.0	386094
75%	52.5	715373	22.5	573548
100%	70.0	946633	30.0	787591
125%	87.5	1178712	37.5	965859
150%	105.0	1413042	45.0	1145652
Correlation coefficient	0.999		0.999	

Accuracy

The accuracy of the method was determined at three concentration levels by performing recovery studies. The recovery studies were carried out by different concentrations of both drugs added to the placebo from 50%, 100%, and 150%. Recovery and percentage RSD were calculated. The obtained results are tabulated in Tables 6 and 7, and related graphs are depicted in Figures 10 and 11. % of recovery results were between 97 % and 103 %.

Robustness

The robustness of the method was evaluated by changing the flow rate, organic, and temperature. A system suitability test was conducted to check the variations, and the results were found to be satisfactory. The results are reported in Table 8.

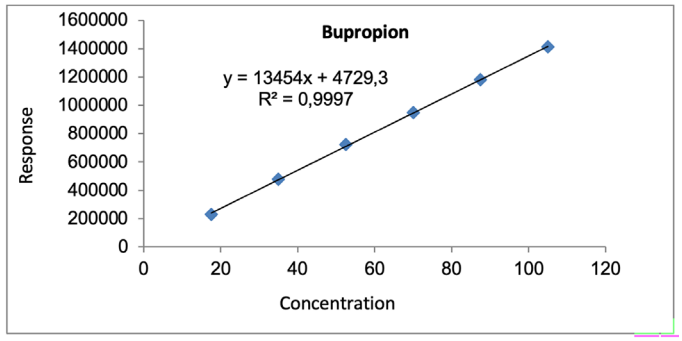

Figure 8. Linearity graph for bupropion
AU: Absorbance units

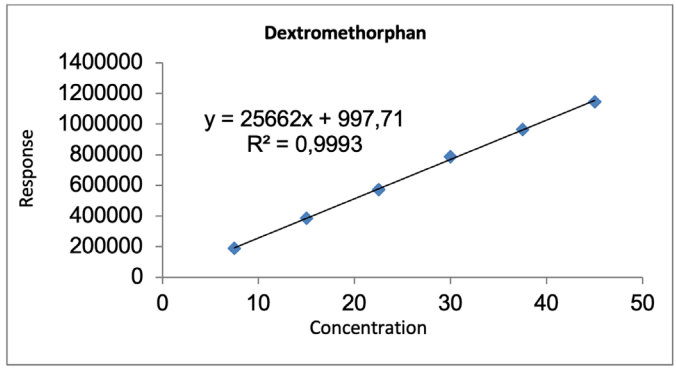

Figure 9. Linearity graph for dextromethorphan
AU: Absorbance units

Table 4. Precision results

S. no.	Bupropion		Dextromethorphan	
	Area	% Assay	Area	% Assay
1	946549	100.08	763992	99.96
2	946327	100.06	769671	100.70
3	947135	100.14	766504	100.29
4	942561	99.66	769536	100.68
5	950484	100.50	763402	99.88
6	949639	100.41	767899	100.47
Mean	947116	100.14	766834	100.33
SD	2807.2	0.30	2699.9	0.35
% RSD	0.3	0.3	0.4	0.4

SD: Standard deviation, RSD: Relative standard deviation, S. no.: Sample number

LOD and LOQ

LOD is the lowest concentration of analyte in a sample that can be identified but not quantified. LOQ is defined as the lowest concentration of analyte in a sample that can be estimated with tolerable precision, accuracy, and reliability by a specified method under affirmed experimental conditions. The LODs were found to be 0.15 µg/mL and 0.06 µg/mL for bupropion and dextromethorphan, respectively. The LOQs were found to be 2.91 µg/mL and 0.18 µg/mL for bupropion and dextromethorphan, respectively.

Degradation studies

Degradation studies involving acid, base, peroxide, thermal, UV, and neutral conditions were evaluated. Furthermore, all stress degradation results are tabulated in Tables 9 and 10, and the resultant chromatograms are shown in Figures 12 to 17.

Statistical analysis

The accuracy of the method was determined at three concentration levels by performing recovery studies. The recovery studies were carried out by different concentrations of both drugs added to the placebo from 50%, 100%, and 150%. The related graphs are depicted in Figures 10 and 11. % of recovery results were between 97% and 103%. The LODs were found to be 0.15 µg/mL and 0.06 µg/mL for bupropion and dextromethorphan, respectively. The LOQs were found to be 2.91 µg/mL and 0.18 µg/mL for bupropion and dextromethorphan, respectively.

Table 5. Intermediate precision results

S. no.	Bupropion		Dextromethorphan	
	Area	% Assay	Area	% Assay
1	945886	100.01	761882	99.68
2	939324	99.32	766487	100.29
3	939052	99.29	759040	99.31
4	945600	99.98	763144	99.85
5	939091	99.29	759107	99.32
6	946842	100.11	762823	99.81
Mean	942633	99.67	762081	99.71
SD	3832.0	0.41	2800.9	0.37
% RSD	0.4	0.4	0.4	0.4

SD: Standard deviation, RSD: Relative standard deviation, S. no.: Sample number

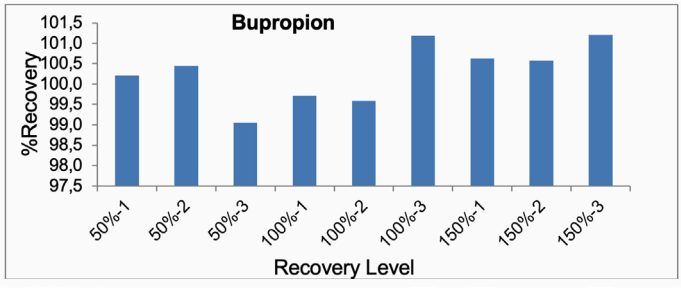

Figure 10. %recovery graph for bupropion

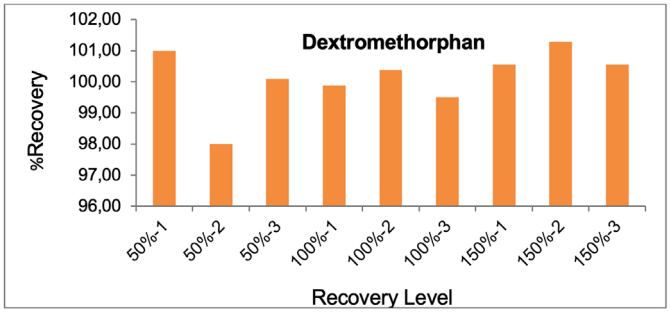

Figure 11. %recovery graph for dextromethorphan

Table 6. Accuracy results for bupropion

S. no.	Recovery level	% Assay	Average	SD	% RSD
1	50%-1	100.2			
2	50%-2	100.4	99.9	0.7462	0.7
3	50%-3	99.1			
4	100%-1	99.7			
5	100%-2	99.6	100.2	0.8907	0.9
6	100%-3	101.2			
7	150%-1	100.6			
8	150%-2	100.6	100.8	0.3504	0.3
9	150%-3	101.2			

SD: Standard deviation, RSD: Relative standard deviation, S. no.: Sample number

Table 7. Accuracy results for dextromethorphan

S. no.	Recovery level	% Assay	Average	SD	% RSD
1	50%-1	100.99			
2	50%-2	98.00	99.7	1.5357	1.5
3	50%-3	100.09			
4	100%-1	99.88			
5	100%-2	100.36	99.9	0.4321	0.4
6	100%-3	99.50			
7	150%-1	100.55			
8	150%-2	101.28	100.8	0.4211	0.4
9	150%-3	100.55			

SD: Standard deviation, RSD: Relative standard deviation, S. no.: Sample number

Table 8. Robustness results

S. no.	Condition	Bupropion	Dextromethorphan	Resolution between both peaks
		% RSD	% RSD	
1	Optimized condition	0.4	0.5	5.4
2	Low flow rate (0.9 mL/min)	0.6	0.8	6.1
3	High flow rate (1.1 mL/min)	0.3	0.7	5.9
4	Low column temperature (25 °C)	0.7	1.0	7.2
5	High column temperature (35 °C)	0.7	0.6	5.7
6	Low organicvolume (+4 mL)	0.8	0.8	7.5
7	High organicvolume (-4 mL)	0.4	0.7	5.2

S. no.: Sample number, RSD: Relative standard deviation

Table 9. Degradation results for bupropion

Stress condition	% Amount remaining	% Amount degraded	Peak purity	
			Purity angle	Purity threshold
Acid	94.40	5.60	0.635	0.745
Base	95.29	4.71	0.555	0.732
Oxidation	95.50	4.50	0.944	1.090
Thermal	97.60	2.40	0.725	0.917
UV	98.67	1.33	0.538	0.726
Neutral	99.60	0.40	0.552	0.753

UV: Ultraviolet

Table 10. Degradation results for dextromethorphan

Stress condition	% Amount remaining	% Amount degraded	Peak purity	
			Purity angle	Purity threshold
Acid	94.38	5.62	1.270	1.525
Base	95.87	4.13	1.201	1.523
Oxidation	95.65	4.35	1.730	2.167
Thermal	97.58	2.42	1.915	2.304
UV	98.52	1.48	1.175	1.459
Neutral	99.01	0.99	1.187	1.498

UV: Ultraviolet

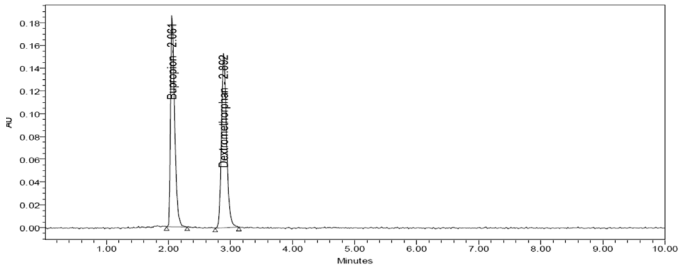

Figure 12. Acid degradation chromatogram
AU: Absorbance units

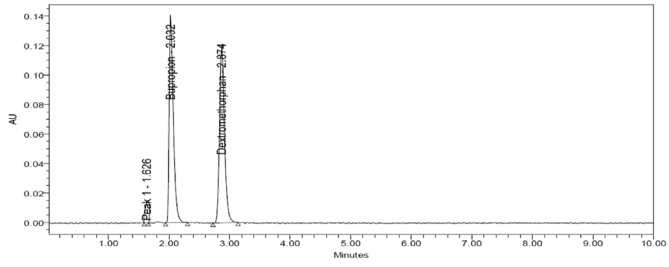

Figure 13. Base degradation chromatogram
AU: Absorbance units

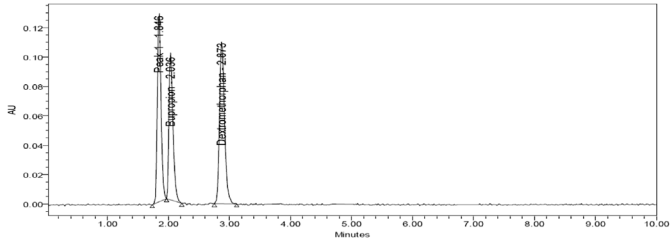

Figure 14. Oxidation degradation chromatogram
AU: Absorbance units

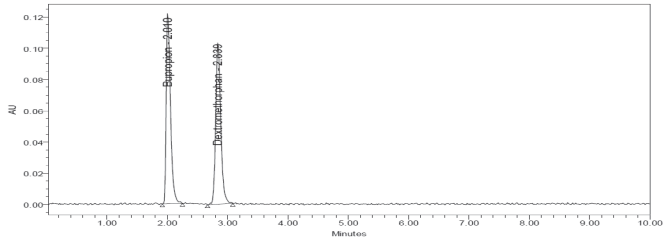

Figure 15: Thermal degradation chromatogram
AU: Absorbance units

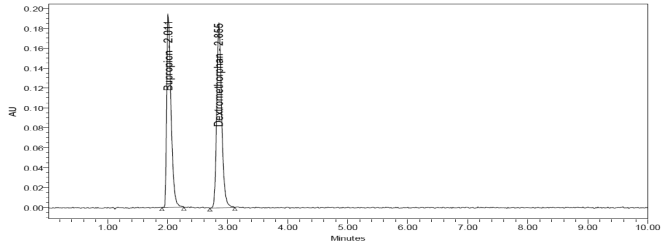

Figure 16: UV degradation chromatogram
AU: Absorbance units

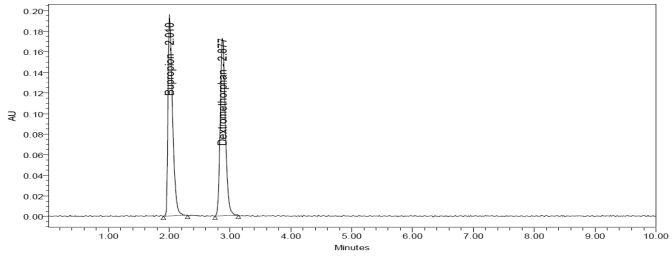

Figure 17: Water degradation chromatogram
AU: Absorbance units

CONCLUSION

The current study describes a new, simple, reliable, and economical elution RP-HPLC method for estimating bupropion and dextromethorphan in a fixed combination tablet dosage form. The forced degradation studies were conducted using several degradation conditions such as acidic, alkali, oxidation, thermal, UV, and neutral conditions; the proposed method was effectively employed from the resolution of sample peaks. To the best of our knowledge, no such detailed and stability-indicating method has been reported for a fixed tablet dosage form. The developed method was completed using a PDA as a tool for peak integrity and purity confirmation. Therefore, the proposed method can be used for the quantification of bupropion and dextromethorphan in a fixed tablet dosage form. Finally, this method was carefully validated; as a result, it can be suggested for routine analysis testing in a quality control laboratory.

Acknowledgement

The author thanks the Sri Krishnadevaraya University, Department of Chemistry, Ananthapuramu, India, for their support.

Ethics

Ethics Committee Approval: There is no requirement for ethical approval.

Informed Consent: Not necessary.

Conflict of Interest: No conflict of interest was declared by the authors.

Financial Disclosure: The authors declared that this study received no financial support.

REFERENCES

1. FDA Registration. Available from: https://www.accessdata.fda.gov/drugsatfda_docs/label/2022/215430Orig1s000Correctedlbl.pdf
2. Loboz KK, Gross AS, Ray J, McLachlan AJ. HPLC assay for bupropion and its major metabolites in human plasma. J Chromatogr B Analyt Technol Biomed Life Sci. 2005;823:115-121.
3. Slemmer JE, Martin BR, Damaj MI. Bupropion is a nicotinic antagonist. J Pharmacol Exp Ther. 2000;295:321-327.
4. Meiling Q, Peng W, Yingshu G, Junling G, Ruonong F. Development and validation of an HPLC method for the determination of bupropion hydrochloride in tablets. J Chin Pharm Sci. 2002;11:16.
5. Skarydova L, Tomanova R, Havlikova L, Stambergova H, Solich P, Wsol V. Deeper insight into the reducing biotransformation of bupropion in the human liver. Drug Metab Pharmacokinet. 2013;29:177-184.
6. Cooper TB, Suckow RF, Glassman A. Determination of bupropion and its major basic metabolites in plasma by liquid chromatography with dual-wavelength ultraviolet detection. J Pharm Sci. 1984;73:1104-1107.
7. Heydari R. A New HPLC Method for the simultaneous determination of acetaminophen, phenylephrine, dextromethorphan and chlorpheniramine in pharmaceutical formulations. Anal Lett. 2008;41:965-976.
8. Lin SY, Chen CH, Ho HO, Chen HH, Sheu MT. Simultaneous analysis of dextromethorphan and its three metabolites in human plasma using an improved HPLC method with fluorometric detection. J Chromatogr B Analyt Technol Biomed Life Sci. 2007;859:141-146.
9. Bendriss EK, Markoglou N, Wainer IW. High-performance liquid chromatography assay for simultaneous determination of dextromethorphan and its main metabolites in urine and in microsomal preparations. J Chromatogr B Biomed Sci Appl. 2001;754:209-215.
10. Bitar Y. Separation and assay of three anti-cough drugs pseudoephedrine, dextromethorphan and chlorpheniramine in pharmaceutical forms by using single RP-HPLC Method. Res J Pharm Technol. 2020;13:831-839.
11. Kumar PS. Rambabu K. Development and validation of a method for simultaneous estimation of bupropion and dextromethorphan using reverse phase high performance liquid chromatography in active pharmaceutical ingredient form. J Pharm Res Int. 2022;34:10-19.
12. International Conference on Harmonization (ICH); Validation of analytical procedures: Methodology, Q2B (CPMP/ICH/281/95), 1995. Available at: http://www.ich.org.

Turk J Pharm Sci 2024;21(2):133-140
DOI: 10.4274/tjps.galenos.2023.95690

ORIGINAL ARTICLE

Pharmaceutical Properties and Phytochemical Profile of Extract Derived from Purple Leaf *Graptophyllum pictum* (L.) Griff

Jepri Agung PRIYANTO[1]*, Muhammad Eka PRASTYA[2], Minarti MINARTI[2], Vera PERMATASARI[2]

[1]IPB University Faculty of Mathematics and Natural Sciences, Department of Biology, Division of Microbiology, West Java, Indonesia
[2]Research Center for Pharmaceutical Ingredients and Traditional Medicine, National Research and Innovation Agency (BRIN), Kawasan Sains dan Teknologi (KST), BJ Habibie (PUSPIPTEK) Serpong, South Tangerang, Banten, Indonesia

ABSTRACT

Objective: *Graptophyllum pictum* (L.) Griff is a medicinal shrub belonging to the Acanthaceae family and is traditionally used to treat various diseases. Therefore, this study aimed to evaluate the pharmaceutical properties and phytochemical profiles of the methanolic extract of *G. pictum*.

Materials and Methods: *G. pictum* leaves was extracted using methanol. Antioxidant, cytotoxic on Michigan Cancer Foundation-7 (MCF-7) and HepG2, antidiabetic, and antibacterial properties were evaluated *in vitro*. Chemical profile of the extract was identified through qualitative (for phytochemicals), quantitative (for phenolic and flavonoid content), and gas chromatography-mass spectrometry (GC-MS) analysis.

Results: The results showed that the extract had potent antioxidant activity against 2,2-azino-bis (3-ethylbenzothiazoline-6-sulphonic acid) and 2,2-diphenyl-1-picrylhydrazyl radicals with IC_{50} values of 49.00 ± 3.20 µg/mL and 70.18 ± 3.27 µg/mL, respectively. It also exhibited cytotoxic effects on human breast (MCF-7) and liver (HepG2) carcinoma cells with growth inhibition percentages of 74.29 ± 1.53% and 64.90 ± 1.94%, respectively. The antidiabetic assay showed that the extract had inhibitory effects on α-glucosidase activity with IC_{50} value 194.59 ± 15.59 µg/mL, indicating its potential to be developed as an antidiabetic agent. Furthermore, it had antibacterial properties against four test strains, and the highest activity was found against *Bacillus subtilis* American Type Culture Collection 19659, with minimum inhibitory concentration and minimum bactericidal concentration values of 625 µg/mL and 1250 µg/mL, respectively. Phytochemical tests indicated the presence of alkaloids, flavonoid and terpenoids in the extract, with total phenolic content and total flavonoid content of 41.17 ± 2.38 mg gallic acid equivalents/g and 26.52 ± 0.61 mg quercetin equivalent/g, respectively. GC-MS analysis revealed that it contained several active compounds, including eicosane, 2,4-Di-*tert*-butylphenol, hentriacontane, tetracosane, octacosane, sulfurous acid, 2-methylhexacosane, docosane, heneicosane, 1-propene-1,2,3-tricarboxylic acid, tributyl ester, and pentacosane.

Conclusion: The extract derived from *G. pictum* leaves was a potential source of therapeutic compounds, particularly for antioxidant, antidiabetic, anticancer, and antibacterial agents.

Keywords: Antioxidant, cytotoxic, flavonoids, phytochemical, phenols, α-glucosidase inhibitor

INTRODUCTION

Several plants have gained recognition for their potential as primary sources of medicine in drug discovery. These natural sources of herbal medicine offer an alternative to synthetic and modern drugs because of their lower potential to have side effects. An estimated 70.000 species have been studied for their therapeutic functions,[1] and more than 50% of commercially available drugs are derived from medicinal plants, which act as analgesics, anticancer agents, antidiabetics, and antioxidants.[2] Indonesia is a tropical country with the second largest potential for medicinal plants, following Brazil, with a minimum of 30.000 species spread across various regions.[3]

G. pictum Griff, locally known as daun ungu, daun wungu, and handeuleum, is an herbal shrub of the Acanthaceae family.

*Correspondence: jepriyanto@apps.ipb.ac.id, Phone: +62-251-8622833, ORCID-ID: orcid.org/0000-0003-2227-5040
Received: 14.02.2023, Accepted: 18.05.2023

The plant is native to New Guinea and has spread widely to various countries, including the United States, Mexico, Ghana, Bolivia, India, and Indonesia.[4,5] Furthermore, it has brownish-purple leaves due to its high anthocyanin, chlorophyll, and carotenoid content.[6] *G. pictum* leaf has long been used as a traditional drug to treat various diseases, including hemorrhoid, analgesic, antipyretic, menstrual problems, and wound healing.[7] Several studies have investigated the therapeutic values of *G. pictum* leaf, which have been shown to possess *in vitro* anti-inflammatory, antibacterial, and antioxidant.[8,5,9] *In vivo* studies also revealed that it can decrease blood glucose levels, as well as act as an antihemorrhoid, antioxidant, and anti-inflammatory agents.[10,11,12] These biological activities have been linked to its phytochemical content, namely phenols, flavonoids, tannins, alkaloids, saponins, terpenoids, and steroids.[8]

Although several studies have reported the biological properties and metabolite profiles of *G. pictum*, the use of different geographical plant origins, extraction techniques, and solvents can lead to varying chemical profiles and bioactivities.[13,14] The majority of reports on this species used plants growing in Thailand, India, as well as East and Central Java-Indonesia, but there is no information on the pharmaceutical values of those cultivated in Cirebon, West Java-Indonesia.[9,4,10] Therefore, this study aims to evaluate the chemical profile, as well as the antibacterial, antioxidant, antidiabetic, and cytotoxic properties of *G. pictum* leaf methanolic extract obtained from Cirebon, Indonesia.

MATERIALS AND METHODS

Plant materials and extraction

Fresh leaves of *G. pictum* were harvested from Cirebon, West Java, Indonesia, at the coordinates 6°36'15.7"S 108°21'23.0"E. The obtained leaves were then air-dried and crushed into powder for further procedures. Subsequently, 100 g of the powder was extracted in 1000 mL methanol (1:10, *w/v*) and shaken continuously in a rotary shaker (100 rpm) at room temperature for 24 h. The mixture was filtered using filter paper (Whatman no. 1), and the filtrate was collected, followed by evaporation at 40 °C using a rotary evaporator.[15]

Antioxidant assay

The free radical scavenging activity of the extract was measured using 2,2 diphenylpicrylhydrazyl (DPPH) and 2,2'-azino-bis(3-ethylbenzothiazoline-6-sulfonic acid) (ABTS) assay.[16] A total of 100 µL of 250 µM DPPH radical solution was added to 100 µL extract solutions, ranging from 2500 to 20 µg/mL. The reaction was allowed to proceed for 30 min at room temperature, and the absorbance was measured at 515 nm using a Thermo Scientific Varioskan Flash (Thermo Fischer), followed by the calculation of the percentage inhibition (%). For the ABTS assay, radicals were produced by reacting 7 mM ABTS solution with 2.45 mM potassium persulfate (1:1) and incubating for 12-14 h at room temperature in dark conditions. Furthermore, 170 µL of the radicals was mixed with 30 µL extract and incubated for 30 min, with the determination of absorbance at 734 nm. The inhibition of both assays was calculated using the formula: % = $[(A_1-A_2)/A_1] \times 100\%$. A_1 represents the absorbance of the DPPH/ABTS blank (without samples), and A_2 = the absorbance of the samples. The concentration of the sample required to scavenge 50% free radicals (IC_{50} value) was calculated from the plotted graph of radical scavenging activity against each extract concentration. In this study, ascorbic acid and quercetin were used as positive controls.

Cytotoxicity assay

This study used human breast adenocarcinoma Michigan Cancer Foundation-7 (MCF-7) and liver carcinoma HepG2 cell lines [American Type Culture Collection (ATCC); Rockville, MD, USA], which were obtained from the Laboratory of Biochemical and Natural Product Isolation, Research Centre for Pharmaceutical Ingredients and Traditional Medicine, KST BJ. Habibie, BRIN, Serpong, Banten, Indonesia. Cells were cultured in Dulbecco's Modified Eagle Medium high glucose medium (Sigma), which was supplemented with 10% fetal bovine serum and 1% antibiotics (penicillin/streptomycin) (Sigma) in a humidified atmosphere containing 5% CO_2 and 95% air at 37 °C. The cytotoxic assay was then performed by seeding MCF-7 and HepG2 cells on a 96-well microplate at a concentration of 1×10^4 cells *per* well, followed by incubation for 24 h to maximize attachment. Subsequently, the media were replaced with fresh samples containing 100 µg/mL of extract (diluted on DMSO) and incubated for 48 h. A total of 10 µL of 3- (4,5-dimethylthiazol-2-yl)-2,5-diphenyl-2H-tetrazolium bromide) stock solution (0.5 mg/mL) was added and incubated for 3 h at 37 °C, leading to the dissolution of the crystals in 99% DMSO. After the complete dissolution of formazan blue, cell proliferation was measured at 570 nm using a Thermo Scientific Varioskan Flash (Thermo Fischer). The inhibition percentage was then calculated using the formula: $[1- (Abs._{Sample}-Abs._{DMSO\ control})] \times 100\%$. DMSO at a final concentration of 0.05% and 100 µg/mL cisplatin (Sigma) were used as negative and positive controls, respectively.[17]

Antidiabetics assay

Antidiabetic activity was measured based on the method proposed by a previous study.[18] The extract was diluted in 99% DMSO to prepare various concentrations, ranging from 12.5 to 200 µg/mL, while quercetin was used as the positive control, ranging from 35 to 70 µg/mL. A total of 495 µL of 100 mM phosphate buffer with pH 7 and 250 µL substrate (20 mM, *p*-nitrophenyl-α-glucopyranoside) were added, and the mixture was incubated at 37°C for 5 min. Subsequently, 250 µL α-glucosidase (0.065 U/mL) was added to the mixture and incubated at 37 °C for 15 min. The reaction was stopped by supplementing 1 mL of 200 mM Na_2CO_3 in the sample. The release of *p*-nitrophenol from the α-linkage of glucopyranoside was then determined at 400 nm. The percentage of enzyme inhibition (%) was calculated using the following formula: $[(Abs._{control}-Abs._{sample})/Abs._{control}] \times 100\%$. The concentration of the sample required to inhibit 50% of α-glucosidase reaction (IC_{50}) was calculated from the plotted graph of the inhibition value of each extract concentration.

Antibacterial activity

A standard disk diffusion assay was performed based on a method proposed in a previous study.[19] The process was performed using four targeted bacterial ATCC strains, including *Escherichia coli* ATCC 8739, *Pseudomonas aeruginosa* ATCC 15442, *Bacillus subtilis* ATCC 19659, and *Staphylococcus aureus* ATCC 6538 (IPB University Faculty of Mathematics and Natural Sciences, Department of Biology, Collection of Laboratory of Microbiology). Furthermore, a suspension of bacterial inoculum with a concentration of 1.5% (*v/v*) was applied to Mueller Hinton Agar (MHA) (Himedia) plate medium and allowed to solidify. A total of 20 µL of extract diluted in 99% DMSO was added to sterile filter paper disks with a diameter of approximately 6 mm and placed on the surface of the inoculated agar plate. Antibacterial activity was then evaluated by measuring the diameter of inhibition zones surrounding the disks after incubation for 24 h at 37 °C. Tetracycline (200 µg/mL) and 1% DMSO were used as positive and negative controls, respectively.

Determination of minimum inhibitory concentration (MIC) and minimum bactericidal concentration (MBC)

The MIC of the *G. pictum* leaf extracts was determined using sterile 96-well plates.[19] The 96 wells of each row was filled with 100 µL of sterilized Mueller Hinton Broth. Furthermore, wells 1-8 of each row were then filled with 100 µL of a mixture of culture medium and plant extract, which were serially diluted to create a concentration sequence from 5000 to 35 µg/mL. Bacterial cultures were prepared in 0.85% NaCl and adjusted to McFarland standard 0.5 (equivalent to 1×10^8 colony-forming units/mL), after which 100 µL was added to each well. Tetracycline hydrochloride and 1% DMSO were used as positive and negative controls, respectively. The deep wells were incubated for 24 h at 37 °C, and the turbidity obtained was observed. MIC was determined as the concentration at which no visible cell growth was observed. To evaluate MBC, a portion of liquid (100 µL) from each well with no growth was taken and spread on MHA plate agar, followed by incubation at 37°C for 24 h. The lowest concentration that caused the absence of visible bacterial colonization after sub-culturing was taken as MBC.

Qualitative phytochemical analysis

Phytochemical analysis was performed to determine the presence or absence of some classes of compounds, including flavonoids, alkaloids, saponins, tannins, and terpenoids.[20] Furthermore, *G. pictum* extracts were mixed with an appropriate chemical reagent for each analysis. The mixtures obtained were then vortexed and qualitatively observed for the presence of the targeted compound class.

Determination of total phenolic and flavonoid content

The analysis of the total phenolic content (TPC) was carried out using the Folin Ciocalteu reagent based on the method used in a previous study.[21] A total of 0.5 mL of the extract (1 mg/mL) was mixed with 0.25 mL Folin Ciocalteu reagent and 3.5 mL distilled water. The solution was then kept at 28 °C for 5-8 min before adding 0.75 mL of 20% sodium carbonate solution. Subsequently, the absorbance was measured at 765 nm after incubation for 2 h at 28 °C. Gallic acid was used as the standard for the calibration curve in this study. The total flavonoid content (TFC) was measured using a colorimetric assay (Priyanto et al.,[15] 2022), and the results were expressed as mg gallic acid equivalents *per* gram of extract (mg GAE/g extract). A total of 500 µL extract (1 mg/mL) and 0.15 mL of 5% sodium nitrite were added to 2.45 mL of distilled water. After 3 min, 0.15 mL of 10% aluminum chloride was added, and the mixture was incubated for 8 min, followed by the addition of 2 mL of 1 M sodium hydroxide. The absorbance was then determined at 510 nm, and quercetin was used as a standard for the calibration curve. The TFC of the extract was expressed as mg quercetin equivalents *per* gram of extract (mg QE/g extract).

Gas chromatography-mass spectrometry (GC-MS) analysis

GC-MS analysis was performed using an Agilent 19091S-433: 93.92873 GC-MS. A total of 1 µL extract solution dissolved in *n*-hexane was injected into HP-5MS 5% phenyl methyl silox at 0 °C-325 °C (325 °C) measuring 30 m x 250 µm x 0.25 µm. The initial temperature of the oven was set at 40 °C and increased gradually over 30 min to 300 °C. Furthermore, helium was used as carrier gas at a flow rate of 1 mL/min. MSD Chem-Station Data Analysis software was then used to analyze the mass spectra and chromatograms of the GC-MS results.

Statistical analysis

The data obtained from antioxidant, cytotoxicity, antidiabetic, and antibacterial assays are presented as means ± standard deviation from triplicates. One-way analysis of variance was used to compare the mean values with 95% and 99% confidence levels. Further analysis was performed using the Tukey test, and p values < 0.05 were considered statistically significant.

RESULTS

Antioxidant activity

G. pictum leaf extract showed antioxidant activity with IC_{50} values of 49.00 ± 3.20 µg/mL and 70.18 ± 3.27 µg/mL against ABTS and DPPH, respectively. Furthermore, the extract was significantly ($p < 0.05$) less active than ascorbic acid as a positive control, which had IC_{50ABTS} and IC_{50DPPH} of 10.99 ± 2.66 µg/mL and 3.82 ± 0.59 µg/mL, respectively, as shown in Table 1.

Cytotoxic property

A total of 100 µg/mL of *G. pictum*-derived extract inhibited MCF-7 and HepG2 cell growth with inhibition percentages of 74.29 ± 1.53% and 64.90 ± 1.94%, respectively. At this concentration, there was a significant decrease in cellular density, indicating that the treatment affected cancer cell growth. Apoptotic cells of MCF-7 and HepG2 appeared during inverted microscope observation after 48 h of treatment with the extract, as shown in Figure 1. As a positive control, cisplastin (100 µg/mL) was also tested, and it exhibited cytotoxic properties on MCF-7 and HepPG2 cells with growth inhibition percentages of 86.28 ± 0.22% and 64.90 ± 1.94%, respectively.

Antidiabetic activity

G. pictum leaf extract exhibited antidiabetic activity, as indicated by the inhibition of α-glucosidase activity with an IC_{50} value of 194.59 ± 15.59 µg/mL, as shown in Table 2. The IC_{50} of the extract was higher than that of the positive control quercetin at 3.35 ± 0.01 µg/mL.

Antibacterial activity

The methanolic extract of *G. pictum* exhibited various antibacterial activities against *E. coli* ATCC 8739, *P. aeruginosa* strain ATCC 15442, *S. aureus* ATCC 6538, *and B. subtilis* strain ATCC 19659, as indicated by the different inhibition zone diameters, as shown in Table 3. Among the four target bacteria, the extract was most active on *the B. subtilis* ATCC 19659. The inhibition zone was also determined using tetracycline and DMSO as the positive and negative controls, respectively (Figure 2). The extract also had the lowest MIC of 625 µg/mL and an MBC of 1250 µg/mL against the *B. subtilis* strain ATCC 19659, as shown in Table 4.

Phytochemical profile

Alkaloids, flavonoids, and terpenoids were found in the *G. pictum* leaf-derived extract, but tannins and saponins were absent. The extract's TPC and TFC were 41.17 ± 2.38 mg GAE/g and 26.52 ± 0.61 mg QE/g, respectively.

Chemical profile of the G. pictum leaf extract

GC-MS analysis revealed that the compounds identified in *G. pictum* leaf extract included eicosane, 2,4-Di-*tert*-butylphenol, hentriacontane, tetracosane, octacosane, sulfurous acid, 2-methylhexacosane, docosane, heneicosane, 1-propene-1,2,3-tricarboxylic acid, tributyl ester, and pentacosane, as shown in Table 5.

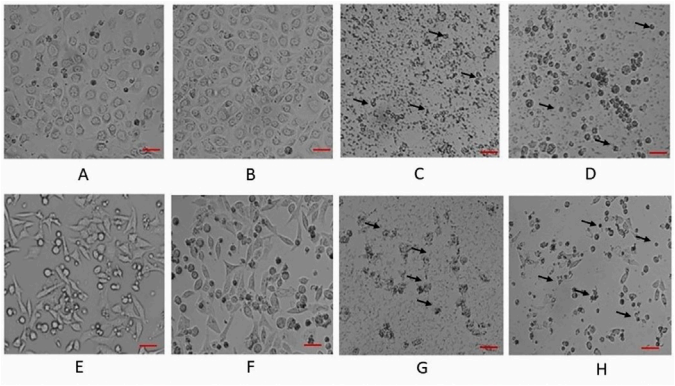

Figure 1. Cytotoxicity of *G. pictum* leaf extract on MCF-7 (A-D) and HepG2 cells (E-H); MCF-7 cell line on (A) DMEM medium; treatment with (B) 1% DMSO; (C) Cisplatin 100 µg/mL; (D) Extract 100 µg/mL; (E) HepG2 cell line on DMEM medium; treatment with (F) 1% DMSO; (G) Cisplatin 100 µg/mL; (H) Extract 100 µg/mL. The cell morphology and density were observed under an inverted microscope with magnification 100x. Bars represent 30 µm, and black arrows indicate apoptotic cells.

MCF-7: Michigan Cancer Foundation-7, DMEM: Dulbecco's Modified Eagle Medium

Table 1. Antioxidant activity of the extract derived from *G. pictum* leaves against DPPH and ABTS

Sample	Antioxidant activity (IC_{50} ± SD in µg/mL)	
	DPPH	ABTS
G. pictum leaf extract	70.18 ± 3.27[b]	49.00±3.20[b]
Ascorbic acid	3.82 ± 0.59[a]	10.99±2.66[a]

Values with the same superscript letter in the same column are not significantly different based on one-way ANOVA analysis followed by multiple Duncan test range ($p < 0.05$), DPPH: 2,2 diphenylpicrylhydrazyl, ABTS: 2,2-azino-bis(3-ethylbenzothiazoline-6-sulfonic acid), SD: Standard deviation, IC: Inhibitory concentration

Table 2. Antidiabetic activity of the *G. pictum* leaf extract

Samples	Antidiabetic activity (IC_{50}: Average µg/mL ± SD)
G. pictum leaf extract	194.59 ± 15.59[b]
Quercetin	3.35 ± 0.01[a]

Values with the same superscript letter in the same column are not significantly different based on one-way ANOVA analysis followed by multiple Duncan test range ($p < 0.05$), SD: Standard deviation, IC: Inhibitory concentration

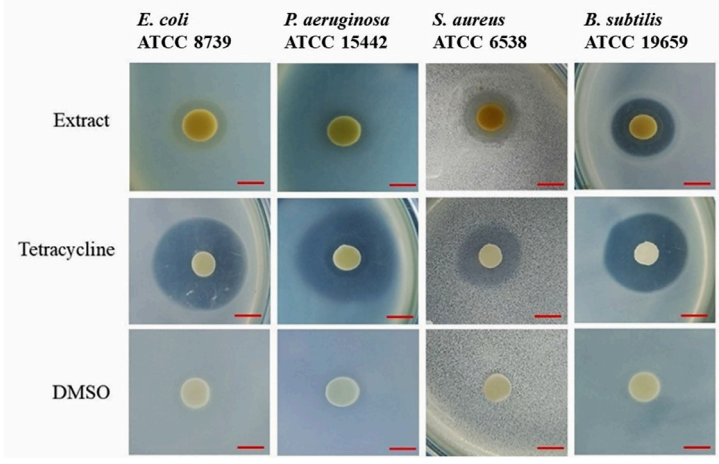

Figure 2. Antibacterial activity of *G. pictum* leaf extract (25 mg/mL) against the bacteria tested; 1% DMSO and tetracycline (200 µg/mL) were used as negative and positive controls, respectively. Bars represent 6 mm

Table 3. Antibacterial activity of *G. pictum* leaf extract by the disk diffusion method

Samples	Inhibition zone (mm ± SD)			
	E. coli ATCC 8739	*P. aeruginosa* ATCC 15442	*S. aureus* ATCC 6538	*B. subtilis* ATCC 19659
G. pictum leaf extract	8.5 ±1.4[b]	7.3 ± 0.4[b]	10.3 ± 0.2[b]	13.3 ± 0.4[b]
Tetracycline	22.3 ± 0.9[c]	22.7 ± 0.9[c]	13 ± 0.8[c]	22.3 ± 2.3[c]
DMSO	0 ± 0[a]	0 ± 0[a]	0 ± 0[a]	0 ± 0[a]

Extract and tetracycline were applied at concentrations of 25 and 200 µg/mL, respectively. Values with the same superscript letter in the same column are not significantly different based on one-way ANOVA analysis followed by multiple Duncan test range ($p < 0.05$), SD: Standard deviation, IC: Inhibitory concentration, ATCC: American Type Culture Collection

Table 4. MIC and MBC of *G. pictum* leaf extract

Samples	MIC/MBC values (µg/mL)			
	E. coli ATCC 8739	*P. aeruginosa* ATCC 15442	*S. aureus* ATCC 6538	*B. subtilis* ATCC 19659
G. pictum leaf extract	2500/ › 2500	2500/ › 2500	1250/2500	625/1250
Tetracycline	7.81/7.81	7.81/7.81	3.90/7.81	3.90/7.81

MIC: Minimum inhibitory concentration, MBC: Minimum bactericidal concentration, ATCC: American Type Culture Collection

Table 5. Chemical profile of exract from *G. pictum* leaves

Number	Proposed compound	Molecular formula	Chemical class	Retention time (min)	Similarity (%)	Bioactivity	References
1	Eicosane	$C_{20}H_{42}$	alkane	18.5011	72	Antifungal; antioxidant and wound healing	[22, 23]
2	2,4-Di-*tert*-butylphenol	$C_{14}H_{22}O$	phenol	18.9044	95	Antifungal, antioxidant, and cytotoxic on HeLa and MCF-7 cells; antibacterial	[24, 25, 26]
3	Hentriacontane	$C_{31}H_{64}$	alkane	19.0557	52	Anti-inflammatory	[27]
4	Tetracosane	$C_{24}H_{50}$	alkane	20.631	60	Cytotoxic on AGS, MDA-MB-231, HT-29 and NIH 3T3 cells; antioxidant	[28, 29]
5	Octacosane	$C_{28}H_{57}$	short chain hydrocarbon	20.9587	86	Cytotoxic on B16F10-Nex2 cells; antioxidant and wound healing	[30, 23]
6	Sulfurous acid	$C_{22}H_{46}O_3S$	mineral acid	21.299	49	Unknown	
7	2-Methylhexacosane	$C_{27}H_{56}$	fatty acid	22.4459	53	Unknown	
8	Docosane	$C_{22}H_{46}$	alkane	22.5971	58	Antimicrobial	[31]
9	Heneicosane	$C_{21}H_{44}$	alkane	25.1681	90	Antimicrobial	[32]
10	1-Propene-1,2,3-tricarboxylic acid	$C_{18}H_{30}O$	tricarboxylic acid	26.2646	68	Unknown	
12	Pentacosane	$C_{25}H_{52}$	alkane	26.9956	90	Volatile attractant	[33]

DISCUSSION

This study evaluated the pharmaceutical properties of *G. pictum* leaf extract, including its *in vitro* antioxidant, cytotoxic, antidiabetic, and antibacterial activities. The antioxidant activity of the sample was tested against DPPH and ABTS free radicals. Furthermore, free radicals cause oxidative stress, which facilitates pathological manifestations.[34] Antioxidants have been reported to inhibit these compounds and prevent the occurrence of diseases through scavenging activities or induction of defense mechanisms.[35] Two radicals were used in this study to determine the antioxidant activity of *G. pictum* leaf extract. The DPPH assay was used to assess the electron transfer reaction, whereas ABTS was used to evaluate the hydrogen transfer reaction.[36] The results showed that *G. pictum* leaf extract had stronger effects against ABTS than DPPH, as indicated by the IC_{50} value. Based on previous studies, the smaller the value obtained, the higher the effect. Furthermore, the antioxidant activity of natural extracts can be categorized on the basis of their IC_{50} value, namely solid (‹ 50 µg/mL), strong (50-100 µg/mL), moderate (101-150 µg/mL), and weak (› 150 µg/mL).[37] The methanolic extract of *G. pictum* leaf was shown to have strong effects against DPPH and ABTS free radicals. Scavenging capabilities are essential to avoid the damaging activities of these compounds in different illnesses.

Several studies have shown that antioxidant compounds play a vital role in cancer prevention and treatment.[38,39] In the current study, 100 µg/mL of *G. pictum* leaf extract inhibited the growth of MCF-7 and HepG2 cells, with inhibition percentages of 74.29 ± 1.53% and 64.90 ± 1.94%, respectively. Cell viability was also reduced after the extract was applied for 48 h. The treatment also caused apoptosis and morphological changes in the form of membrane disruption in the cells, as shown in Figure 1. This finding indicated that the extract can induce an apoptotic pathway in MCF-7 and HepG2 cells. A previous study also revealed that it exhibited cytotoxic properties against human colon cancer cell WiDr with an IC_{50} value of 195.61 µg/mL in the *n*-hexane fraction, but was not toxic to Verro cells.[40,41]

The α-glucosidase inhibitory effect of the extract was evaluated to determine its potency as an antidiabetic agent. The α-glucosidase enzyme was responsible for the hydrolysis

of oligosaccharides and disaccharides to glucose.[42] Therefore, blood glucose levels can be controlled by inhibiting its activity. In this study, the methanolic extract of *G. pictum* displayed an inhibitory effect towards α-glucosidase, with an IC_{50} value of 194.59 ± 15.59 µg/mL. These findings are consistent with previous studies, which showed that the *n*-hexane and ethyl acetate extracts derived from the plant showed inhibitory activity.[43]

The methanolic extract of *G. pictum* leaf showed antibacterial effects against four test bacteria, namely *E. coli* ATCC 8739, *P. aeruginosa* ATCC 15442, *B. subtilis* ATCC 19659, and *S. aureus* ATCC 6538. The results also showed that it was more active in the Gram-positive strains, namely *S. aureus* and *B. subtilis*, compared with the Gram-negative bacteria because of differences in cell membrane structure. Gram-negative bacteria are known to have three layers in their external cell structure, including the outer membrane, peptidoglycan layer, and inner membrane, whereas the outer membrane was absent in Gram-positive strains.[44] This absence caused increased sensitivity to antibacterial agents. These results agree with previous studies that showed that the extract had toxic effects on *Aggregatibacter actinomycetemcomittans*, *S. aureus*, *P. aeruginosa*, and *Streptococcus mutans*.[5,45,46,47]

This study also investigated the phytochemical constituents of the methanolic extract of *G. pictum* leaf, and the results showed that it contained alkaloids, flavonoid and terpenoids. Furthermore, these compounds are responsible for several biological activities in natural products such as plants.[48,49] This indicated that they played an essential role in the pharmaceutical properties of the extract, including its antioxidant, cytotoxic, antidiabetic, and antibacterial activities. TPC of the *G. pictum* extract was higher than TFC, namely 41.17 ± 2.38 mg GAE/g and 26.52 ± 0.61 mg QE/g. TFC obtained using methanol as a solvent was higher than that obtained using aqueous, butanol, ethyl acetate, and hexane with values of 2.02, 9.02, 22.45, and 28.21 mg QE/g, respectively. For TPC, higher values were recorded in the ethyl acetate (102.57 mg GAE/g) and butanolic (45.33 mg GAE/g) extracts compared with the methanolic extract with a value of 26.52 ± 0.61 mg QE/g.[12] Based on these results, the solvent used for extraction influenced the TPC and TFC.

The pharmaceutical properties, such as antioxidant, cytotoxic, antidiabetic, and antibacterial activities, of *G. pictum* leaf extract were promoted by the presence of biologically active compounds. GC-MS analysis showed that the extract contained 12 compounds with pharmaceutical activity, as shown in Table 5. Furthermore, it consisted of eicosane, 2,4-Di-*tert*-butylphenol, tetracosane, and octacosane, which were reported to have antioxidant activity and cytotoxic properties on some carcinoma cells.[22-24,29] 2,4-Di-*tert*-butylphenol has also been shown to have toxic effects on microorganisms.[24,26] The other constituent compounds included docosane and heneicosane, which had similar effects against microbes.[31,32] A previous study isolated pentacosane, a volatile attractant, from *G. pictum* leaf extract.[31] Only three compounds, namely sulfurous acid, 2-methylhexacosane, and 1-propene-1,2,3-tricarboxylic acid, have not been reported to have biological activity, but their presence can correlate with pharmaceutical properties.

CONCLUSION

This study showed the pharmaceutical properties of extract obtained from the leaves of *G. pictum*, including antioxidant, cytotoxic, antidiabetic, and antibacterial activities. Furthermore, the extract contained phytochemicals, such as alkaloids, flavonoid and terpenoids, which are believed to be responsible for its bioactivities. The total phenolic and flavonoid compounds in the sample were also determined. GC-MS analysis showed that it contained eicosane, 2,4-Di-*tert*-butylphenol, hentriacontane, tetracosane, octacosane, sulfurous acid, 2-methylhexacosane, docosane, heneicosane, 1-propene-1,2,3-tricarboxylic acid, tributyl ester, and pentacosane. These compounds contribute to the pharmaceutical activity of the extract. Based on these results, extracts from the leaves of *G. pictum* grown in Cirebon, West Java, Indonesia, are a potential source of therapeutic compounds that can be further studied.

Acknowledgement

We thank the Directorate of Research and Innovation, IPB University, and the Research Health Organization of National Research and Innovation Agency Indonesia for supporting this study.

Ethics

Ethics Committee Approval: This study does not require any ethical permission.

Informed Consent: Not necessary.

Authorship Contributions

Concept: J.A.P., M.E.P., Design: J.A.P., M.E.P., Data Collection or Processing: J.A.P., M.E.P., M.M., V.P., Analysis or Interpretation: J.A.P., M.E.P., Literature Search: J.A.P., Writing: J.A.P., M.E.P., M.M., V.P.

Conflict of Interest: No conflict of interest was declared by the authors.

Financial Disclosure: This work was partly funded by the the Directorate of Research and Innovation, IPB University through The National Collaborative Research Program 2023-2024 (grant number: 505/IT3.D10/PT.01.03/P/B/2023) awarded to Jepri Agung Priyanto, and the Research Health Organization of National Research and Innovation Agency, Indonesia through "Rumah Program Purwarupa Bahan Baku Obat Terapi Terarah 2024" (grant number: B-11155/III.9/TK.02.02/12/2023) awarded to Muhammad Eka Prastya.

REFERENCES

1. Veeresham C. Natural products derived from plants as a source of drugs. J Adv Pharm Technol Res. 2012;3:200-201.
2. Mollik M, Islam H. Diversity of natural bioactive compound in plant origin. Medicinal Plants (editor Kumar S). IntechOpen. 2022.

3. Decree of Minister of Health of the Republic of Indonesia Number: 381/ Menkes/SK/III/2007, March 27, 2007: National Policy of Traditional Medicine in 2007.
4. Singh P, Khosa RL, Mishra G, Jha KK. Pharmacognostical evaluation of aerial parts of *Graptophyllum pictum* (L.) Griff. (Syn: *Justicia picta* Linn.): A well-known folklore medicinal plant. Anc Sci Life. 2015;34:223-229.
5. Kusumaninsih T, Sidarningsih, Putra AA, Aljunaid M. Antibacterial differences effect between purple leaves (*Graptophyllum pictum* (L) Griff.) 70% and 96% ethanol extract against *Aggregatibacter actinomycetemcomittans* Bacteria. J Int Dental Med Res. 2021;14:519-524.
6. Rosmala A, Khumaida N, Sukma D. Alteration of leaf anatomy of handeuleum (*Graptophyllum pictum* L. Griff) due to gamma irradiation. J Biosci. 2016;23:138-142.
7. Makkiyah F, Rahmi EP, Revina R, Susantiningsih T, Setyaningsih Y. *Graptophyllum pictum* (L.) Griff. (Syn: *Justicia picta* Linn.) and its effectiveness: a well-known Indonesian plant. Pharmacog J. 2021;13:835-838.
8. Juniarti DE, Kusumaningsih T, Soetojo A, Hariyani N. Effect of purple leaf extract (*Graptophyllum pictum* (L.) Griff) on the number of macrophage cells in pulp perforation. Indian J For Med Toxicol. 2020;14:1846-1851.
9. Jiangseubchatveera N, Liawruangrath B, Liawruangrath S, Teerawutgulrag A, Santiarworn D, Korth J, Pyne SG. The chemical constituents and the cytotoxicity, antioxidant and antibacterial activities of the essential oil of *Graptophyllum pictum* (L.) Griff. J Essent Oil Bear Plants. 2015;18:11-17.
10. Leonoreza A, Excelinda T, Elnitiarta J, Heri-Nugroho HS, Hendrianingtyas M, Retnoningrum D. Effectiveness of *Graptophyllum pictum* (L.) Griff leaf extraction on blood glucose level in alloxan-induced Wistar rat. Food Res. 2022;4(Suppl 3):123-126.
11. Kusumawati I, Rullyansyah S, Rohmania, Rizka AF, Hestianah EP, Matsunami K. Histomorphometric study of ethanolic extract of *Graptophyllum pictum* (L.) Griff. leaves on croton oil-induced hemorrhoid mice: A Javanese traditional anti-hemorrhoid herb. J Ethnopharmacol. 2022;284:114765.
12. Azhar A, Riwanto I, Nugroho EA, Susilaningsih N, Prajoko YW, Budiono P, Prasetyo SA. Antioxidant and anti-inflammatory effect of *Graptophyllum pictum* (L.) Griff extract study on SOD and COX-2 serum of experimental hemorrhoids. Med Hosp J Clin Med. 2020;7:422-426.
13. El Menyiy N, Bakour M, El Ghouizi A, El Guendouz S, Lyoussi B. Influence of geographic origin and plant source on physicochemical properties, mineral content, and antioxidant and antibacterial activities of Moroccan Propolis. Int J Food Sci. 2021;2021:5570224.
14. Ngo TV, Scarlett CJ, Bowyer MC, Ngo PD, Vuong QV. Impact of different extraction solvents on bioactive compounds and antioxidant capacity from the root of *Salacia chinensis* L. J Food Qual. 2017;2017:1-8.
15. Priyanto JA, Prastya ME, Primahana G, Randy A, Utami DT. Paederia foetida Linn leaves-derived extract showed antioxidant and cytotoxic properties against breast carcinoma cell. HAYATI J Biosci. 2023;30:271-280.
16. Prastya ME, Astuti RI, Batubara I, Takagi H, Wahyudi AT. Natural extract and its fractions isolated from the marine bacterium *Pseudoalteromonas flavipulchra* STILL-33 have antioxidant and antiaging activities in *Schizosaccharomyces pombe*. FEMS Yeast Res. 2020;20:1-4.
17. Priyanto JA, Astuti RI, Nomura J, Wahyudi AT. Bioactive compounds from sponge-associated bacteria: anticancer activity and NRPS-PKS gene expression in different carbon sources. American J Biochem Biotechnol. 2017;13:148-156.
18. Dewi RT, Tachibana S, Fajriah S, Hanafi M. α-Glucosidase inhibitor compounds from *Aspergillus terreus* rcc1 and their antioxidant activity. Med Chem Res. 2015;24:737-743.
19. Priyanto JA, Prastya ME, Sinarawadi GS, Datu'salamah W, Avelina TY, Yanuar AIA, Azizah E, Tachrim ZP, Mozef T. The antibacterial and antibiofilm potential of *Paederia foetida* Linn. leaves extract. J Appl Pharm Sci. 2022;12:117-124.
20. Harbourne JB. Phytochemical methods: a guide to modern techniques of plants analysis, London; Chapman and Hall, 1983.
21. Prastya ME, Astuti RI, Batubara I, Wahyudi AT. Antioxidant, antiglycation and *in vivo* antiaging effects of metabolite extracts from marine sponge-associated bacteria. Indian J Pharm Sci. 2019;81:344-353.
22. Ahsan T, Chen J, Zhao X, Irfan M, Wu Y. Extraction and identification of bioactive compounds (eicosane and dibutyl phthalate) produced by *Streptomyces* strain KX852460 for the biological control of *Rhizoctonia solani* AG-3 strain KX852461 to control target spot disease in tobacco leaf. AMB Express. 2017;7:54.
23. Balachandran A, Choi SB, Beata MM, Małgorzata J, Froemming GRA, Lavilla CA Jr, Billacura MP, Siyumbwa SN, Okechukwu PN. Antioxidant, wound healing potential and *in silico* assessment of naringin, eicosane and octacosane. Molecules. 2023;28:1043.
24. Varsha KK, Devendra L, Shilpa G, Priya S, Pandey A, Nampoothiri KM. 2,4-Di-*tert*-butyl phenol as the antifungal, antioxidant bioactive purified from a newly isolated *Lactococcus* sp. Int J Food Microbiol. 2015;211:44-50.
25. Chawawisit K, Bhoopong P, Phupong W, Lertcanawanichakul M. 2, 4-Di-*tert*-butylphenol, the bioactive compound produced by *Streptomyces* sp. KB1. J Appl Pharm Sci. 2015;5:7-12.
26. Seenivasan A, Manikkam R, Kaari M, Sahu AK, Sais M, Dastager SG. 2,4-Di-*tert*-butylphenol (2,4-DTBP) purified from *Streptomyces* sp. KCA1 from *Phyllanthus niruri*: isolation, characterization, antibacterial and anticancer properties. J King Saud Univ Sci. 2022;34:102088.
27. Khajuria V, Gupta S, Sharma N, Kumar A, Lone NA, Khullar M, Dutt P, Sharma PR, Bhagat A, Ahmed Z. Anti-inflammatory potential of hentriacontane in LPS stimulated RAW 264.7 cells and mice model. Biomed Pharmacother. 2017;92:175-186.
28. Uddin SJ, Grice D, Tiralongo E. Evaluation of cytotoxic activity of patriscabratine, tetracosane and various flavonoids isolated from the Bangladeshi medicinal plant *Acrostichum aureum*. Pharm Biol. 2012;50:1276-1280.
29. Kalegari M, Miguel MD, Philippsen AF, Dias JDFG, Zanin SMW, de Lima CP, Miguel OG. Antibacterial, allelopathic and antioxidant activity of extracts and compounds from *Rourea induta* Planch. (Connaraceae). J Appl Pharm Sci. 2012;2:61-66.
30. Figueiredo CR, Matsuo AL, Pereira FV, Rabaça AN, Farias CF, Girola N, Massaoka MH, Azevedo RA, Scutti JA, Arruda DC, Silva LP, Rodrigues EG, Lago JH, Travassos LR, Silva RM. *Pyrostegia venusta* heptane extract containing saturated aliphatic hydrocarbons induces apoptosis on B16F10-Nex2 melanoma cells and displays antitumor activity *in vivo*. Pharmacogn Mag. 2014;10(Suppl 2):363-376.
31. Lammers A, Zweers H, Sandfeld T, Bilde T, Garbeva P, Schramm A, Lalk M. Antimicrobial Compounds in the Volatilome of Social Spider Communities. Front Microbiol. 2021;12:700693.
32. Vanitha V, Vijayakumar S, Nilavukkarasi M, Punitha VN, Vidhya E, Praseetha PK. Heneicosane-A novel microbicidal bioactive alkane identified from Plumbago zeylanica L. Ind Crops Prod. 2020;154:112748.

33. Sun X, Zhang X, Wu G, Li X, Liu F, Xin Z, Zhang J. n-Pentacosane Acts as both Contact and Volatile Pheromone in the tea Weevil, Myllocerinus aurolineatus. J Chem Ecol. 2017;43:557-562.

34. Sharma N. Free radicals, antioxidants and disease. Biol Med. 2014;6:1-6.

35. Hunyadi A. The mechanism(s) of action of antioxidants: From scavenging reactive oxygen/nitrogen species to redox signaling and the generation of bioactive secondary metabolites. Med Res Rev. 2019;39:2505-2533.

36. Liang N, Kitts DD. Antioxidant property of coffee components: assessment of methods that define mechanisms of action. Molecules. 2014;19:19180-19208.

37. Irawan C, Putri ID, Sukiman M, Utami A, Ismail, Putri RK, Lisandi A, Pratama AN. Antioxidant activity of DPPH, CUPRAC, and FRAP methods, as well as activity of alpha-glucosidase inhibiting enzymes from *Tinospora crispa* (L.) stem ultrasonic extract. Pharmacogn J. 2022;14:511-520.

38. Arsova-Sarafinovska Z, Dimovski AJ. Natural antioxidants in cancer prevention. Macedonian Pharmaceut Bul. 2013;59:3-14.

39. Avcil M. The importance of antioxidants in the treatment of cancer. Oxidants and Antioxidants in Medical Science. 2022;11:1.

40. Amin A, Gani AP, Murwanti R. (2020) Cytotoxic activities of (*Graptophyllum pictum* (L.) Griff) ethanolic extract and its fractions on human colon cancer cell WiDr. Trad Med J. 2000;25:29-33.

41. Jiangseubchatveera N, Liawruangrath S, Teerawutgulrag A, Santiarworn D, Pyne SG, Liawruangrath B. Phytochemical screening, phenolic and flavonoid contents, antioxidant and cytotoxic activities of *Graptophyllum pictum* (L.) Griff. Chiang Mai J Sci. 2017;44:193-202.

42. Zhang X, Li G, Wu D, Yu Y, Hu N, Wang H, Li X, Wu Y. Emerging strategies for the activity assay and inhibitor screening of alpha-glucosidase. Food Funct. 2020;11:66-82.

43. Nurcholis W, Artika IM, Seno DSH, Andrianto D, Aprianti A, Febrianti F, Inawati I, Ratu AP, Arendra A. Phytochemical analysis, α-glucosidase inhibition activity *in vitro* and enzyme kinetics of ethyl acetate and hexane extracts of *Graptophylum pictum* (L.) Griff. Cur Biochem. 2014;1:58-65.

44. Breijyeh Z, Jubeh B, Karaman R. Resistance of gram-negative bacteria to current antibacterial agents and approaches to resolve it. Molecules. 2020;25:1340.

45. Friska YD, Hujjatusnaini N, adah A, Amin AM. The potential of purple leaves ethanol extract (*Graptophyllum pictum* L.) against the growth of *Staphylococcus aureus* and *Candida albicans*. J Agronomi Tanaman Tropika. 2021;3:196-207.

46. Kanedi M, Widodo S, Fitri A, Handayani K, Setiawan WA. Antibacterial activity of leaf extract of caricature plant (*Graptophyllum pictum* L.) against *Staphylococcus aureus* and *Pseudomonas aeruginosa*. Int J Pharm Sci Res. 2021;6:1-3.

47. Juniarti DE, Kusumaningsih T, Juliastuti WS, Soetojo A, Wungsu ND. Phytochemical analysis and antibacterial activity of purple leaf extract [*Graptophyllum pictum* (L.) Griff] against *Streptococcus mutans*. Acta Med Philipp. 2021;55:802-806.

48. Xiao J. Phytochemicals in medicine and food. Phytochem Rev. 2015;14:317-320.

49. Saxena M, Saxena J, Nema R, Singh D, Gupta A. Phytochemistry of medicinal plants. J Pharmacog Phytochem. 2013;1:168-182.

Turk J Pharm Sci 2024;21(2):141-151
DOI: 10.4274/tjps.galenos.2023.15945

ORIGINAL ARTICLE

Flaxseed Mucilage/Hydroxypropyl Methylcellulose and Sodium Alginate/Polyvinyl Alcohol Composite Bilayer Film as a Promising Drug Carrier for Periodontal Treatment

Ujjwala Yadav KANDEKAR[1]*, Chaitrali Raghunath GORE[1], Neha Manish MUNOT[1], Ashlesha Pravin PANDIT[1], Kishanchand Radheshyam KHANDELWAL[2], Neha Pradip PATIL[1], Pravin Digambar CHAUDHARI[3]

[1]JSPM's Rajarshi Shahu College of Pharmacy and Research, Department of Pharmaceutics, Pune, India
[2]JSPM's Rajarshi Shahu College of Pharmacy and Research, Department of Pharmacognosy, Pune, India
[3]PES Modern College of Pharmacy, Department of Pharmaceutics, Pune, India

ABSTRACT

Objectives: The present study focused on the formulation of mucoadhesive bilayer composite films for the treatment of periodontitis and evaluation of their physicochemical properties.

Materials and Methods: The solvent casting technique was used to prepare films. The primary layer (D) was prepared with flaxseed and hydroxypropyl methylcellulose composite to sustain the release of doxycycline hyclate. The second layer (S) comprised sodium alginate and polyvinyl alcohol composite for faster release of clove oil. Both layers were combined to generate the bilayer film (B). All formulations were characterized further to obtain an optimized formulation.

Results: Attenuated total reflection-Fourier transform infrared radiation results showed intactness of drug and clove oil in the presence of excipients. The pH of the films was compatible with the periodontal cavity and the thickness was suitable for inserting into the cavity. The immediate release layer showed faster disintegration and swelling. The content of clove oil was above 80%. The rate of swelling of the primary layer was slow and drug content complied with the United States Pharmacopoeia. Scanning electron microscope analysis revealed intact, non-porous and smooth films. Films exhibited better mechanical strength and bioadhesiveness. Clove oil was released from the immediate release layer within 10 min, and doxycycline hyclate release was retarded to a minimum of up to 8 h in the primary layer as well as the bilayer. Formulation also had a significant effect on both *Escherichia coli* and *Staphylococcus aureus*.

Conclusion: In the current study, bilayers were successfully prepared and characterized. The optimized formulation can be effectively used for the treatment of periodontitis.

Keywords: Periodontitis, flax seed mucilage, HPMC, sodium alginate, polyvinyl alcohol, doxycycline hyclate, clove oil

INTRODUCTION

Periodontal diseases have gained considerable attention as they are a widely spread chronic disease around the world. Around 20 to 50% population around the globe is suffering from periodontal diseases and tooth loss.[1] It is mainly caused by bacterial attack on tissues that support and surround teeth. The space between the tooth and gingiva is referred to as the periodontal pocket, and disease of the periodontal pocket is known as periodontitis. Periodontitis is a complex inflammation caused by periodontal microorganisms that destroy periodontal tissue. Predominantly gram-negative, microaerophilic, anaerobic bacteria colonize as biofilms in the subgingival

*Correspondence: ujja2303@gmail.com, Phone: +91 9822920236, ORCID-ID: orcid.org/0000-0003-3520-9675
Received: 01.03.2023, Accepted: 06.06.2023

area, altering connective tissue and bone metabolism, leading to periodontal damage. The severity of disease also depends on the host's immune response to bacterial challenges and environmental factors (smoking, chewing tobacco).[2]

Mechanical methods are available to control periodontal infection, but procedures to clean periodontal pockets are tedious due to limited accessibility in the area. Investigations were conducted to slow progression or improve periodontal status by systemic administration of antibiotics. A class of tetracycline antibiotics has been studied for the treatment of periodontitis.[3] Doxycycline hyclate from this class exerts anti-inflammatory and antibacterial effects. The United States Food and Drug Administration (USFDA) authorized doxycycline hyclate 20 mg capsule as an addition to root planning and scaling for periodontitis treatment. It presents an anti-inflammatory effect as an anti-collagenase agent and suppresses the activity of matrix metalloproteinases that are responsible for the destruction of periodontal tissues.[4] In addition, it stimulates the formation of bone tissue by instigating the inhibition of bone resorption and osteoblasts. Local administration of antibiotics reduces pocket depth, and a better effect was achieved by the use of doxycycline hyclate.[5] Owing to its antimicrobial and non-antimicrobial properties, doxycycline hyclate was selected as the first model drug in a bilayer film. Clove oil was permitted by USFDA in dentistry as a natural analgesic and antiseptic.[6] Eugenol suppresses the expression of cyclooxygenase II enzyme and cytokines, thus showing an anti-inflammatory effect.[7] It is also reported to exhibit antibacterial potential in both negative and gram-positive bacteria.[8] The antimicrobial activity of eugenol on some bacteria was due to the induction of cell lysis *via* the leakage of lipids and proteins in the cell membrane.[9]

Flax seed was reported to contain protein and a mixture of various carbohydrates, mainly rhamnose, galactose, glucose, and arabinose. Acidic polysaccharide galacturonic acid, pectin-like polymers, rhamnogalacturonan, and arabinoxylans were also reported. It is also composed of 3 to 9% of water-soluble heteropolysaccharides of total seed content, which is of low molecular weight and possesses a Newtonian flow pattern even at high concentrations. It exhibits shear thinning flow above 1% concentration. Flax seed mucilage has numerous applications in food and pharmaceuticals. It possesses excellent rheological characteristics and water holding capacity.[10] Hence, found application as a thickening agent, emulsifying agent, drug release retardant and mucoadhesive agent, *etc*.[11] hydroxypropyl methylcellulose (HPMC) has also been explored as a mucoadhesive and sustained release polymer. HPMC is a hydrophilic polymer that fits to a group of hydroxyethyl ethers. It is soluble in both organic and aqueous solvents and forms transparent, flexible films in aqueous solution. Low toxicity biodegradability and biocompatibility are key properties of HPMCs, and its application in pharmaceutical and biomedical fieldsis explored. Several researchers have combined HPMC with other polymers and lipids to form composites with enhanced characteristics. Sustained release and mucoadhesive properties of HPMC have also been reported by scientists.[12] Polysaccharide of alginic acid: sodium alginate is made up of α-l-guluronic (G) and β-d-mannuronic (M) acid units. It is an integral element of the cell wall of brown algae and a few bacteria. It is widely available, inexpensive, and biodegradable in nature. It can form transparent, water-insoluble, thermoirreversible gels by crosslinking with di- and trivalent ions and hence has wide application in pharmaceuticals. Sodium alginate has been extensively explored as a film former and drug carrier, but it is always used in combination with another polymer to form a film.[13] Polyvinyl alcohol (PVA) is a synthetic polymer produced by complete or partial hydrolysis of polyvinyl acetate. It is a biodegradable, biocompatible, tasteless, odorless, and translucent granular powder soluble in water. It has been studied for several pharmaceutical applications.[14] It can be blended with natural materials to enhance mechanical strength. It undergoes rapid swelling and dissolution in water. It exhibits excellent film-forming ability and has been studied by researchers for various targeted applications.[15]

Taking note of the above data, the current research work aimed to prepare composite films to treat periodontitis. The composite was prepared in two layers. The first layer was aimed at the sustained release of doxycycline hyclate and comprised flaxseed and HPMC. The second layer was made to release clove oil immediately and comprised sodium alginate and PVA composite. Films were evaluated and explored as carriers of doxycycline hyclate and clove oil.

MATERIALS AND METHODS

Materials

Flaxseeds were purchased from a domestic market in Pune, Maharashtra, India. Doxycycline hyclate was purchased from Swapnaroop Drug Agency, Aurangabad, India. Clove oil was purchased from Aaria Bio-Lifesciences Research, India. HPMC was purchased from Loba Chemie, India. Sodium alginate was purchased from Thermosil Fine Chemical Industries, Pune, India. PVA was acquired from Research-Lab Fine Chemical Industries, India. All other reagents used were of analytical grade.

Extraction of flaxseed mucilage

Flaxseeds were purchased from a local store and cleaned. Flaxseeds (30 g) drenched in 900 mL of distilled water at a ratio of 1:30. To obtain a mucilage solution, soaked flaxseed was stirred at 1000 rpm at 80 °C to 100 °C for at least 3 h using a hot plate magnetic stirrer. The supernatant solution was then kept for normalizing to ambient conditions (27 °C). The mixture was placed into centrifuge test tubes and rotated at 3900 rpm for 15 min to separate the mucilage solution from flaxseed. Flaxseed was subsequently filtered with cheesecloth to obtain reaming mucilage attached to the flaxseed coat. Ethanol was added to the filtered extract to precipitate the mucilage. The precipitated mucilage was isolated and dehydrated for 5 h in a hot air oven at 50 °C. The yield of the dried mass was quantified, phytochemical screening was performed, and the mass was stored in a desiccator.[16]

Preparation of the double-layer film

Preparation of the primary flaxseed mucilage drug-loaded film layer (D)

The primary layer was prepared by solubilizing 0.1 g flaxseed mucilage polymer and 0.1 g HPMC in 15 mL distilled water for 1 hour at 60-70 °C with continual stirring. Doxycycline hyclate was solubilized in 5 mL of purified water and slowly mixed into the polymeric composition while constantly stirring. Glycerin was added as a plasticizer, and the polymeric composition was cast in a petri-plate. The petri plate was then placed in a hot air oven (Biotechniques, India) for 24 h at 40 °C (Figure 1). Film was enveloped in aluminum foil and kept in a desiccator.[17]

Preparation of the secondary clove oil-loaded film (S)

A second polymeric layer was formulated by solubilizing sodium alginate and PVA in 10 mL of purified water with uninterrupted stirring. Glycerin was incorporated as a plasticizer in the polymeric composition. Clove oil was dissolved in 3 mL of ethanol using 0.2% *w/v* tween 80. The resulting solution was loaded dropwise in a polymeric composition of sodium alginate and PVA and sonicated to eliminate entrapped air. The solution was finally spread evenly in a petri dish and dehydrated in an oven for 24 h at 40 °C. The film was enveloped in aluminum foil and kept in a desiccator (Figure 2).[18]

Preparation of the bilayer film (B)

The primary layer was dried thoroughly and 0.5% *w/v* of a freshly prepared calcium chloride solution was sprinkled over it. A polymeric mixture of sodium alginate and PVA-containing clove oil was cast over the primary layer. The bilayer film was further dried in a hot air oven and peeled off (Figure 3). The film was enveloped in aluminum foil and kept in desiccator (Table 1, 2).[19]

Evaluation of the films

Surface pH determination

Agar plates expressed in phosphate buffer (pH 6.8) were allowed to hydrate for 2 h on agar plates. A pH meter (Mettler Toledo, India) was positioned in contact with the hydrated patch, and the pH of the surface was checked. The average of three measurements was recorded.[20]

Attenuated total reflectance-Fourier transform infrared radiation (ATR-FTIR)

ATR accessory, Tensor 37 FTIR equipment (Bruker, Germany) spectra of pure drug, physical mixture of drug and excipient, and optimum formulation were recorded. By averaging 10 scans at a resolution of 4 cm^{-1}, single spectra in the wavelength range of 4000 to 400 cm^{-1} were obtained.[21]

Thickness and weight

Three films selected with a surface area of 9 × 9 mm^2 were used for the measurement of thickness at 10 different points. The thickness of the films was estimated using a digital vernier caliper (Mitutoyo, Japan). The average weight was calculated by weighing 9 × 9 mm^2 films on an analytical balance (Shimadzu, Japan). Both these readings were recorded in triplicate, and the mean was estimated.[22]

Drug content

Primary film equivalent to a surface area of 1 cm^2 was miscibilized in 10 mL phosphate buffer (pH 6.8) and transferred

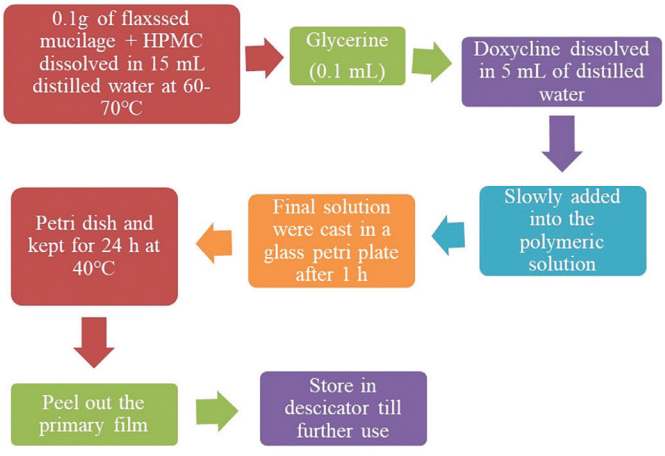

Figure 1. Schematic representation of the preparation of the primary layer

HPMC: Hydroxypropyl methylcellulose

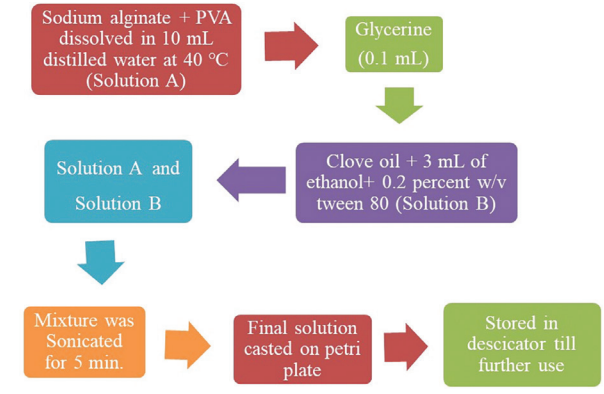

Figure 2. Schematic representation of the preparation of the secondary layer

PVA: Polyvinyl alcohol

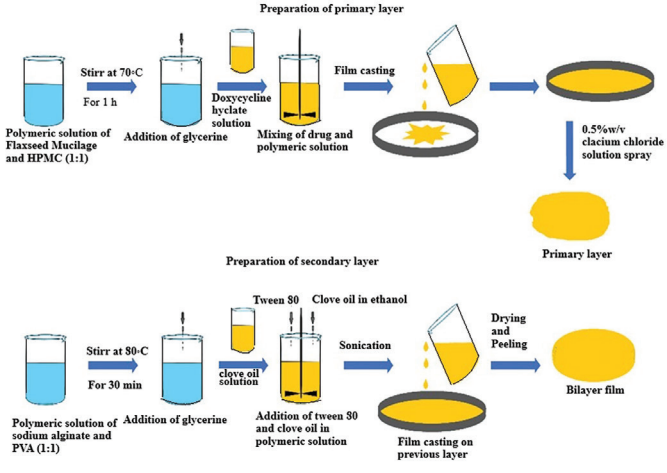

Figure 3. Schematic representation of the preparation of the bilayer film

HPMC: Hydroxypropyl methylcellulose, PVA: Polyvinyl alcohol

Table 1. Formulations of secondary layer oil-loaded films S1-S8

Formulation	Sodium alginate (mg)	PVA (mg)	Glycerin (mL)	Clove oil (mg)	Distilled water (mL)
S1	400	300	0.1	10	10
S2	200	400	0.1	10	10
S3	200	200	0.1	10	10
S4	200	300	0.1	10	10
S5	400	400	0.1	10	10
S6	400	200	0.1	10	10
S7	300	400	0.1	10	10
S8	300	200	0.1	10	10

PVA: Polyvinyl alcohol

Table 2. Formulation of the bilayer film (B)

Formulation	Flaxseed mucilage (mg)	HPMC (mg)	Sodium alginate (mg)	PVA (mg)	Doxycycline hyclate (mg)	Clove oil (mg)	Glycerin (mL)	Distilled water (mL)
Primary layer (D)	100	100	-	-	40	-	0.1	20
Secondary layer (S)	-	-	200	200	-	50	0.1	10

PVA: Polyvinyl alcohol, HPMC: Hydroxypropyl methylcellulose

to a 100 mL volumetric flask; the final volume was made with pH 6.8 phosphate buffer. A 1 mL aliquot was removed from the solution and diluted to 10 mL with phosphate buffer pH 6.8. The absorbance of the resulting solution was measured at 271.3 nm using a ultraviolet (UV)-visible spectrophotometer (Shimadzu-1800). A similar method was followed for the second film loaded with clove oil by recording the absorbance at 283 nm. For the bilayer film, absorbance was recorded at 271.3 and 283 nm for doxycycline hyclate and clove oil, respectively.[23]

Disintegration time

The film was cut into 9.0 × 9.0 mm² and placed in a petri plate containing 5 mL purified water, and the time needed to completely disintegrate the secondary film was recorded. The average of three determinations of results was noted.[24]

Surface morphology

The surface morphology of the film was spotted by optical microscopy (Metzer, India) and scanning electron microscopy (SEM) (JEOL JSM- 6360A scanning microscope, Tokyo, Japan). Optical microscopy was used to observe the transactional view of the bilayer film with 100x power lenses. For SEM, the specimen sample was mounted on metal stubs with a double-sided adhesive band, and gold was sputtered on the specimen to confirm sufficient electrical conductivity. Images were taken using an Everhart-Thornley detector with 10 kV excitation energy.[25]

Folding endurance

Films were cut into 1.0 × 1.0 cm² and continually creased at the same point until disruptions. The number of counts film that could be creased without breaking was noted.

Tensile strength and elongation at failure percentage (EF%)

A texture analyzer (CT-3 Brookfield, USA) was used to investigate the tensile strength of the film. A sample of 4 cm^2 was taken and secured between two clamps of probe texture analyzer-dual grip assembly. The bottom clamp was detained immobile, and the film was stretched apart by the top clamp at a speed of 2.0 mm/s to a distance of 6 mm with a trigger load of 0.05 N. The force required to break the film was recorded. Data assemblage and calculations were performed using Texture Pro CT V1.3 Build 14 software. The tensile strength at break rate was calculated using the formula:

Tensile strength (N/cm^2) = Breaking force (N)/cross-sectional area of sample (cm^2)

Elongation at break %, a measure of the percentage of a film that has ruptured, was determined using the following equation:

$$\text{Elongation at break \%} = \frac{\text{Increase film lengath at break } (\Delta L)}{\text{Inital film lengath } (L)} \times 100$$

In vitro bioadhesion force

The bioadhesion force was estimated using a texture analyzer (CT-3/100, Brookfield, USA) equipped with a 100 g load cell. Bioadhesive force was recorded in porcine buccal mucosa. The mucosal membrane was cut and the underlying connective tissue was separated. It was thoroughly cleaned with pH 6.8 phosphate buffer and secured between two circular disks positioned at the bottom perspex support. The mucosal membrane was exposed to the probe *via* a top spherical disk with a void of 12.7 mm diameter. Discs were placed in jacketed glass containers composed of pH 6.8 phosphate buffer and maintained at 37 ± 1 °C. The membrane was equilibrated at this temperature for 30 min. The buccal film was firmly secured using thread on the bottom side of the probe. The circular

cavity and probe were brought into line to safeguard the film originating in intimate contact with the mucosal membrane. Prior to the study, buccal film was hydrated with pH 6.8 phosphate buffer. A load of 90 g was applied, and the probe was lowered at a speed of 0.5 mm/s to contact tissue for 120 s. It was removed at a speed of 2 mm/s.[26] Data assemblage and calculations were performed using Texture Pro CT V1.3 Build 14 software. Ahesiveness and adhesive force were used to evaluate the strength of bioadhesion of the film. Bioadhesion force (N) was calculated using the following formula:

Bioadhesion force (N) = Bioadhesive strength (g)/1000

Swelling studies

Films were weighed individually, and the initial weight was noted (W1). Films were placed separately in a petri dish enclosing pH 6.8 phosphate buffer. Samples were isolated from petri plates hourly, and extra buffer was wiped carefully using filter paper. Hydrated films were weighed (W2). The swelling index was determined by the following formula:

$$\text{Swelling index (\%)} = \left(\frac{W2-W1}{W1}\right) \times 100$$

In vitro drug release

Film was kept in a dialysis bag filled with 1 mL of pH 6.8 phosphate buffer and held in 50 mL phosphate buffer 6.8 maintained at 37 °C with shaking in a thermostatic horizontal shaker at 75 rpm. Aliquots of 1 mL were removed at time intervals of every 2 min interval for 10 min to analyze clove oil and 0.5 h, 1 h, 2 h, 3 h, 4 h, 5 h, 6 h, 7 h, 8 h to quantify doxycycline hyclate. Sink conditions were maintained by replacing an identical quantity of the pre-warmed buffer solution. Samples were investigated using a UV spectrophotometer at 271.1 and 283 nm for doxycycline hyclate and clove oil, respectively. Drug release experimentation was completed in triplicate, and the mean was reported. The release of doxycycline hyclate was fitted in different kinetic models such as first order, zero order, Higuchi and Korsmeyer-Peppas and R^2 value was determined.

In vitro antimicrobial activity of the periodontal film

The drug-loaded film was studied for its antimicrobial activity against *Escherichia coli* (ATCC25922) and *Staphylococcus aureus* (ATCC25323) using the Kirby-Bauer diffusion technique. Concisely, sterile Mueller-Hinton Agar (MHA) was poured into plates up to a depth of 4 mm under sterile conditions using a laminar air flow unit. After solidification, plates were dried for 30 min in incubation to remove excess moisture from the surface. The inoculum of *S. aureus* and *E. coli* was selected and inoculated on surface MHA agar separately with a wire loop and spread with the help of a sterile spreader. After stabilization of culture, wells of each 6 mm diameter were pressed with a sterile cork borer and removed from the petri dish. Disc-shaped polymeric films B and D equivalent to 4 mg/0.5 mL were placed into wells and incubated at 35-37 °C for 24 hous. After 24 h, the zone of inhibition was measured using a zone reader.[27]

RESULTS

Periodontitis results in pain and inflammation surrounding teeth because of infection to gingival tissue, resulting in a need to counteract pain and eradicate infection. Owing to its antimicrobial properties, doxycycline hyclate was selected as the model drug. The combination of eugenol with antibiotics was reported to derive a synergistic effect.[28] Eugenol is reported to be present in clove oil; hence, in the current study, clove oil was used along with doxycycline hyclate. Mucilage from flax seeds was isolated by a simple process and characterized. The yield and ash value of mucilage were found to be 6.3% and 4.2%, respectively. The isolated sample showed the presence of carbohydrates and protein. These results were in agreement with the evaluation of flaxseed mucilage carried out by Kaewmanee et al.[29] The first layer of bilayer film was tried to develop by flax seed mucilage alone, but due to the high viscosity of mucilage, the obtained film was sticky and difficult to peel off from the petri dish. Hence, the first layer of film was prepared by combining flax seed mucilage and HPMC. A film composed of a higher concentration of HPMC was stiffer, less flexible, non-uniform, and might require a longer time to prepare; hence, a low concentration of HPMC was selected. Earlier studies also suggested that films prepared with a lower concentration of polymer were visually more homogeneous and thinner, and drug distribution in the film was uniform. Sodium alginate forms a clear transparent, flexible film, but the brittleness of sodium alginate restricts its use as an excellent film former; hence, it was combined with PVA, which is highly elastic and biocompatible. Some researchers reported that blends of this polymer were found to enhance the mechanical strength of the film and that the resulting product is highly hydrophilic. The formulation of mucoadhesive bilayer films containing doxycycline hyclate and clove oil was carried out (Figure 4a), and further films were evaluated. All films were transparent, free from creases, flexible, and had a characteristic clove oil odor. In the film casting technique, drying was carried out at a gentle rate; hence, aggregation and creases on the film surface were not noticed. Doxycycline hyclate is freely soluble in water and polymers also form clear solutions; hence, the obtained films were transparent. Flax seed mucilage and sodium alginate had a slightly yellowish to off-white color; hence, the final films also exhibited the same color (Figure 4b). Incorporation of glycerin as a plasticizer in films resulted in flexible films, whereas films produced without glycerin were brittle. Morphology of the film was not affected by the addition of glycerin.

Surface pH

Extreme pH can cause local irritation and discomfort in the periodontal cavity. The film pH was 6.4, which was well suited with the oral cavity. Indicating films were inert and compatible with the oral cavity.

ATR-FTIR

This test was performed to determine compatibility between excipient and drug. The spectra of doxycycline hyclate showed characteristic peaks at 1665.65, 1328.27 cm^{-1} conforming

to the C=O group; peaks between 3537.02 and 3812.43 cm^{-1} represented C-H, N-H, and O-H stretching; and a peak at 1456.39 cm^{-1} showed presence of C-H and N-H in-plane bend vibrations. 1217.98 cm^{-1} peak indicated C-N stretching. These results were found to be in agreement with research carried out by other researchers.[30] In addition to this United States Pharmacopeia (USP) monograph suggesting bands for doxycycline hyclate tablets at 935, and 659 cm^{-1}, drug sample showed bands at 990.61 and 659.62 cm^{-1}. Physical mixture of flaxseed, HPMC, and doxycycline hyclate shows characteristic peaks of doxycycline hyclate, indicating intactness of the drug in the presence of excipients. The primary layer (D) also resembles peaks of doxycycline hyclate with slight shifting of peaks. Slight shifting of the peaks might be attributed to physical interactions due to the formation of the composite. The spectra of clove oil showed peaks at 3000.25 cm^{-1} and 3634.58 cm^{-1} owing to O-H stretching, 1657.35 cm^{-1} representative of the C-H stretching vibration of benzene, eugenol methyl C-H deformation vibration denoted at 1365.87 cm^{-1}, 1758.24 cm^{-1} peak resembled the C=O carboxylic acid stretching vibration, and phenolic hydroxyl C-O stretching vibration appeared at 1278 cm^{-1}. The C-O-C aromatic ether vibration was denoted at 1033.21 cm^{-1}. The spectra indicated the presence of eugenol and ether groups, and the benzene ring and phenolic hydroxyl peaks confirmed the presence of eugenol. Spectra were found in agreement with spectra reported in other research work.[31] Second layer S3 film also showed the presence of similar groups, and an additional peak of PVA at 2932.57 cm^{-1} was observed. S3 film spectra closely resemble the spectra of clove oil, indicating the intactness of clove oil in the film. Various spectra are shown in Figure 5.

Thickness and weight

The thickness and weight of the film were determined to confirm the uniformity of the film and to ensure the even distribution of the polymeric solution throughout the petridish. Film thickness is an important physical parameter that potentially influences the feeling of comfort in the periodontal cavity, barrier properties, dose accuracy, disintegration, and dissolution. The average film thickness and weight of the primary layer (D) were 0.21 ± 0.06 mm and 0.143 ± 0.07 g, respectively. For the second layer (S), the thickness and weight were found to be between 0.21 and 0.28 mm and 0.123-0.189 g, respectively (Table 3). PVA shows a highly ordered crystalline structure and was responsible for producing soft, thin films with high flexibility. The thickness and weight of bilayer film (B) were 0.34 ± 0.062 mm and 0.143 ± 0.07 g, respectively. The thickness of the bilayer film was suitable to insert into a periodontal cavity having a width smaller than 0.5-3 mm.

Drug content

The drug content of the primary layer was 98% and doxycycline hyclate found in the bilayer film was 97%. For the doxycycline hyclate tablet, USP had a specified limit of 90 to 120%. Clove oil content in the film was found to be in the range of 80%-92% (Table 3). The film containing the lowest amount of polymer showed the maximum amount of clove oil entrapment as the polymeric solution was less viscous. Oil has been miscibilized easily in the polymer and homogeneously mixed throughout the blend. Surprisingly, a higher concentration of polymeric solution showed less clove oil; these results might be attributed to the uneven distribution of the drug in the viscous polymeric solution. Nevertheless, all films showed more than 80% clove oil entrapment.

Disintegration time

Official guidelines are deficient in determining the disintegration time of films. Pharmacopoeia describes standard disintegration tests for conventional dosage forms, but for films when this method was tried, the film adhered to the wall of the tube, and small pieces float inside the tube, which made visual detection difficult. Due to these practical difficulties, erroneous results might be obtained. Generally, for films, the disintegration test is done by two methods: the slide frame method and the petri dish

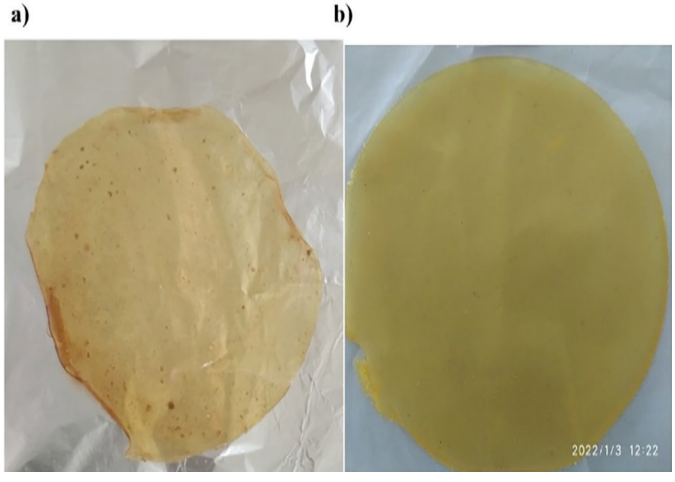

Figure 4. a) Plain flaxseed mucilage-based doxycycline hyclate loaded film (D), b) Bilayer film (B) Composed of doxycycline hyclate in the primary layer and clove oil in the secondary layer

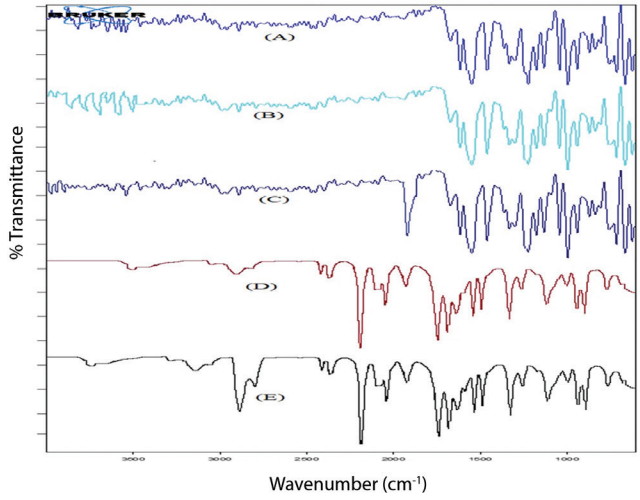

Figure 5. ATR-FTIR spectra of (A) doxycycline hyclate, (B) physical mixture of doxycycline hyclate, HPMC, and flaxseed, (C) formulation of primary layer (D1), (D) clove oil, and (E) formulation of S3 layer

ATR: Attenuated total reflection, FTIR: Fourier transform infrared radiation, HPMC: Hydroxypropyl methylcellulose

method, out of which the petri dish method was adopted for the current study. The disintegration time for the primary layer was 8 h, indicating slower penetration of the solvent due to the high viscosity of the polymers. This was a promising property to maintain film at the site of administration for prolonged drug release. It was proposed that secondary films should disintegrate faster than the primary layer and release clove oil to counteract inflammation and pain. The disintegration time for the secondary layer (S) was recorded and found to be in the range of 8.46 ± 0.74-11.86 ± 0.08 minutes. Water molecules rapidly penetrated the films, causing dispersion of the film into small pieces that ultimately released clove oil at a faster rate than doxycycline hyclate. Rapid penetration of water into the secondary film might be the result of the lyophobic nature of sodium alginate and PVA. From these results, the optimized ratio of sodium alginate and PVA was selected as 200:200, and further tests were carried out on the optimized bilayer film.

Surface methodology studies

Because this property could not be identified directly, optical microscopy was used to confirm the creation of two distinct layers in the bilayer films. The bilayer films had two different layers, as illustrated in Figure 6. SEM analysis (Figure 7) revealed a distinct structure of the film with a smooth matrix and good integrity without any pores or cracks.

Folding endurance

It is an index to investigate the mechanical properties and flexibility of a film. The optimal value of folding endurance eases the manufacturing and administration of films. A direct relation exists between the folding endurance and mechanical properties of the film. The folding endurance of the primary layer (D) and bilayer was (B) 218 ± 16 and 304 ± 18 times, respectively. Bilayer films exhibit higher folding endurance, indicating more flexibility and mechanical strength.

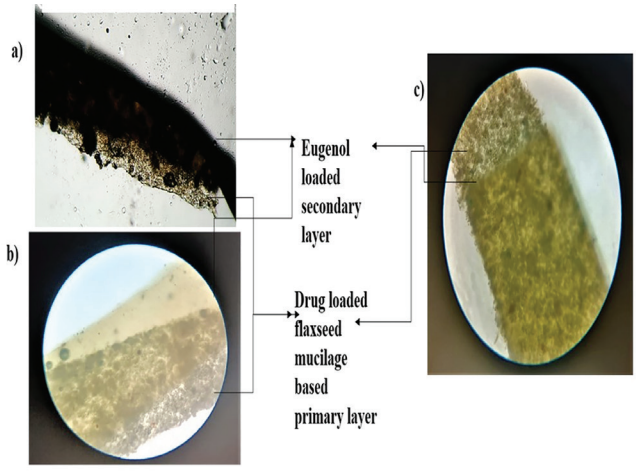

Figure 6. Optical microscopy of bilayer film a, b and c showing a transverse sectional view of the bilayer film under 100x magnification power

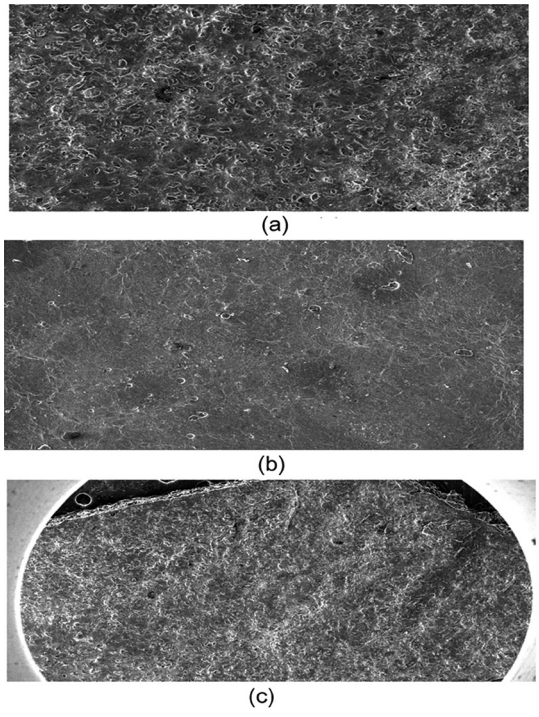

Figure 7. Scanning electron microscopic images showing the surface morphology of bilayer film a) primary layer containing doxycycline hyclate, b) secondary layer containing eugenol, c) bilayer film B

Table 3. Properties of single-layer oil-loaded films: Clove oil content (%), folding endurance, film thickness (mm), % clove oil release after 10 min, weight uniformity (g), disintegration time (min.)

Formulation code	Clove oil content (%)	Folding endurance	Film thickness (mm)	% Clove oil release after 10 min.	Weight uniformity (g)	Disintegration time (min.)
S1	80 ± 1.25	196 ± 0.18	0.22 ± 0.06	60 ± 1.29	0.123 ± 0.03	10.13 ± 0.98
S2	85 ± 1.36	201 ± 0.12	0.25 ± 0.06	39.43 ± 1.36	0.145 ± 0.01	8.46 ± 0.74
S3	92 ± 1.54	213 ± 0.15	0.28 ± 0.06	68.028 ± 1.02	0.167 ± 0.06	7.89 ± 0.45
S4	81 ± 2.61	210 ± 0.11	0.21 ± 0.06	47.32 ± 2.24	0.189 ± 0.04	11.84 ± 1.26
S5	83 ± 1.52	205 ± 0.13	0.24 ± 0.06	44.92 ± 1.21	0.132 ± 0.09	8.95 ± 0.39
S6	80 ± 2.21	209 ± 0.10	0.27 ± 0.07	53.8 ± 1.29	0.165 ± 0.07	9.36 ± 0.06
S7	82 ± 1.24	200 ± 0.14	0.23 ± 0.04	42.39 ± 1.27	0.149 ± 0.02	11.86 ± 0.08
S8	87 ± 1.87	204 ± 0.16	0.26 ± 0.08	38.45 ± 1.32	0.187 ± 0.05	10.12 ± 0.47

All the readings were taken in triplicate, (n= 3, mean ± SD), SD: Standard deviation, min: Minute

Approximately similar values were reported for HPMC films along with Eudragit RL 100 and Carbopol-934.[32] The secondary layer (S) showed folding endurance in the range of 190 ± 0.15 to 213 ± 0.13 times, which was found to be higher than the 145 and 152 reported in earlier research.[33] All films had a good value of folding endurance, showing that the films are flexible with good mechanical strength.

Tensile strength and EF%

The maximum resistance of the film to break under an applied load is the tensile strength, which is an index to confirm the mechanical strength of the film. For the primary layer (D) and bilayer (B), the tensile strength was 4.11 ± 0.04 and 4.16 ± 0.02 N/cm^2, respectively. The largest shift in the film length before breakage is called elongation at break. Maximum deformation a film can experience before breaking, which symbolizes the film's ductility and resistance to distortion. It is defined as the maximum distortion a film could undergo before it fails or breaks. EF for the primary layer (D) and bilayer (B) were 5.14 ± 1.6 and 6.12 ± 1.5% respectively. The amount of drug in the film also affects the mechanical properties of the film; in the current study, the dose of drug is less; hence, the mechanical properties of the optimized film were found to be good. Bilayer film has excellent mechanical properties than primary layer. Figure 8 shows that time required for bilayer film for tensile strength was more as compared to primary layer of film. These results were found to be in agreement with research carried out Ghavami-Lahiji et al.[34]

In vitro bioadhesion bio adhesion force

In our earlier studies, we reported flax seed as a mucoadhesive polymer.[35] Other researchers have also reported that flaxseed mucilage has mucoadhesive potential. HPMC has been widely explored as a mucoadhesive agent. Mucoadhesive drug delivery methods for periodontal disease would have significant advantages such as simplicity of entry into the periodontal pocket and good retention within it. For primary (D) and bilayer films (B), the bioadhesive force was found to be 4.24 ± 0.04 N and 4.58 ± 0.06 N, respectively. This value was found to be slightly better than studies carried out for HPMC/PEG 400/CP.[36]

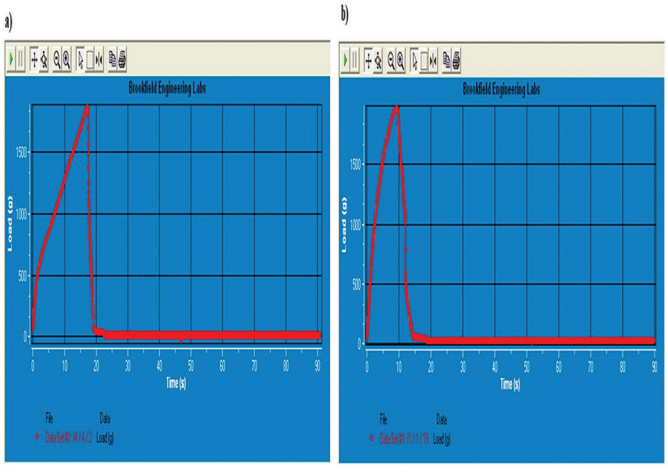

Figure 8. Graph of CT3 texture analyzer of tensile strength: a) bilayer periodontal film formulation and b) single primary layer film

Swelling index

For natural polymers that exhibit swelling-controlled release, swelling is a crucial component of drug release. Swelling studies play a substantial role in bioadhesive properties because swelling of polymers contributes to polymer chain disentanglement and relaxation, which initiates the diffusion of polymeric chains into the mucus membrane for the process of bioadhesion. A swelling study for the primary layer and bilayer film was carried out and varied from 6.65 to 13.9 and 6 to 16.5%, respectively. When flaxseed polymer comes in contact with aqueous medium, polymer chains undergo relaxation and interpenetration, causing swelling. Further expansion of the polymeric matrix may initiate the generation of slippery mucilage, consequently leading to the early release of the drug that has been trapped therein. Figure 9 illustrates the swelling index of films. The swelling index of the bilayer film increased steadily until 25 min and reached equilibrium. At the end of 30 min, the swelling index started declining at a very slow rate. These results might be attributed to the slow erosion of polymers. The swelling index of the primary layer ranged between 6.5% and 13.9%, increased until 30 min and retained equilibrium until 35 min after which it started eroding at a very slow rate. The rate of hydration of the bilayer film was found to be higher than that of the primary layer, as in addition to flaxseed and HPMC, it was also composed of highly swellable sodium alginate. Both B and D films had a good swelling index up to 3 h, after which the swelling index declined slightly, possibly due to polymeric erosion of both layers. The surface area and rate of solvent diffusion in films might be major contributing factors for initiating swelling of films. These results can be correlated with the mucoadhesion study where the bilayer film showed slightly higher mucoadhesion compared with the primary layer. Increased swelling resulted in relaxation of the polymeric chain and exposure of the polymer at the bioadhesive site. A faster swelling bilayer initiated the rapid formation of adhesive bonds.

In vitro drug release

Release of clove oil from the immediate release layer was evaluated for 10 min. Release of clove oil was found in range of 38.45 to 60% and found to be dependent on the concentration

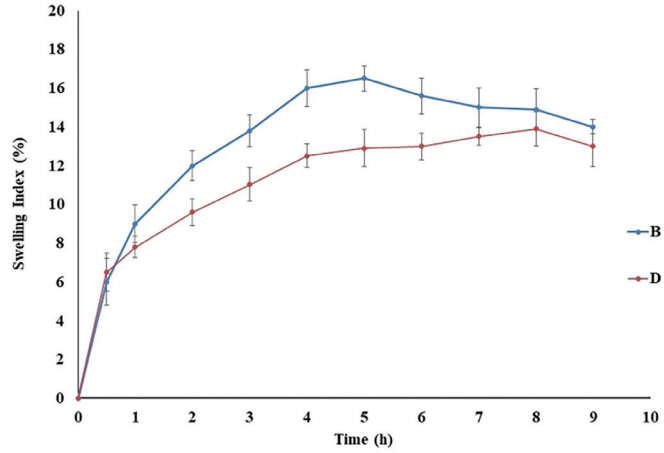

Figure 9. Swelling ratio of B and D films

of polymers. The highest concentration of sodium alginate and PVA (400:400) released only 44% of clove oil. Formulation containing an equal amount of sodium alginate and PVA at the lowest concentration (200:200) released 68% clove oil. *In vitro* drug release from different batches is depicted in Figure 10. Hence, formulation S3 containing a lower number of both polymers was selected as an optimized formulation to prepare the bilayer. Both sodium alginate and PVA are hydrophilic. They undergo swelling at a rapid rate in contact with phosphate buffer 6.8 and release clove oil. The current study also expects a faster release of clove oil to counteract pain and inflammation.

Approximately 33.82% of the drug escaped from film primary layer D at initial 3 h followed by a cumulative 93.71% drug release of up to 8 h. For the bilayer film (B), 29.81% of the drug was released at the initial 3 h and 91.58% at the end of 8 h from the sustained release layer (Figure 11). Immediate release layer showed 69.25% release of clove oil within 10 min from the bilayer film (B). Clove oil is insoluble in aqueous medium. It acted as an additional hurdle for diffusion of media in the B film and additionally contributed to the sustained release of doxycycline hyclate. The obtained results were in agreement with earlier studies on bilayer films, where components of another layer (clove oil) had an impact on the release of actives from the primary layer.[19] Flaxseed mucilage and HPMC have been reported as sustained release polymers. Both forms a very viscous gel upon contact with the dissolution media, and the doxycycline hyclate molecules dissolve in the media and then gradually diffuse out. This process of dissolution and diffusion was time-consuming; hence, a sustained release effect was achieved. The release of doxycycline hyclate at a slower rate was desired to provide a continuous antibacterial shield. Drug release was fitted in different kinetic models such as first order, zero order, Korsmeyer-Peppas, and Higuchi. R^2 value for different kinetic models were 0.9821, 0.9924, 0.872, and 0.8406, respectively. The release mechanism of the drug was in a concentration-dependent manner and it followed first-order kinetics. The obtained results were found to be in agreement with research carried out for metronidazole-loaded films for periodontal treatment.[37]

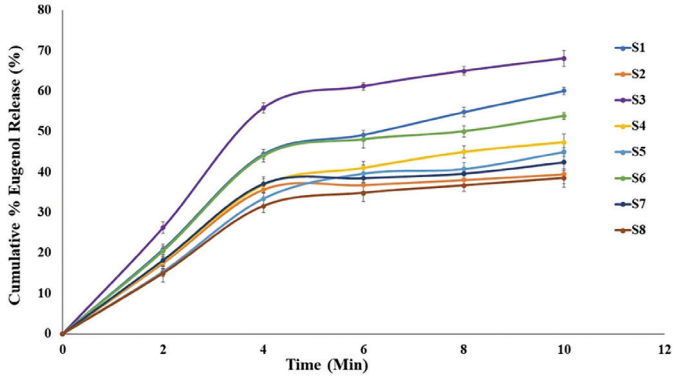

Figure 10. Cumulative drug release profile of the immediate release film

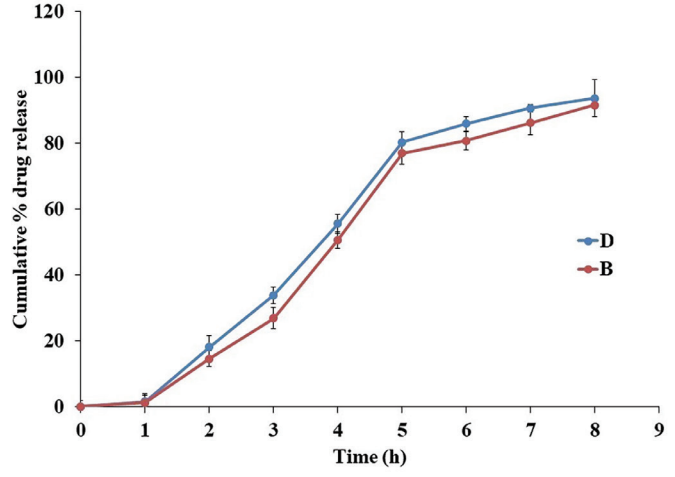

Figure 11. Cumulative drug release profile of the B and D films

In vitro antimicrobial activity of the periodontal film

The *in vitro* antimicrobial activity of the periodontal film was tested using the Kirby-Bauer disk diffusion method. This procedure is routinely adopted for the susceptibility testing of microbial isolates because it gives reliable results comparable to those of the standard epsilometer test and is useful to test the clinical efficacy of antibiotics. This test was based on the fact that for a given antibiotic, the zone of inhibition is related to minimum inhibitory concentration. To conduct the test, MHA was used. MHA is a non-differential and non-selective medium. It is composed of acid hydrolysate and beef extract, which acts as a nutrient source. Starch is incorporated to trap any toxic metabolites produced by microbes. Starch hydrolysis generates dextrose, which acts as an energy source. The rate of diffusion of antibiotics is enhanced in the presence of starch. Agar acts as a solidifying agent. *E. coli* (ATCC25922) and *S. aureus* (ATCC25323) bacteria were used to measure the zone of inhibition on both films to determine their antibacterial activity (ATCC25323) (Figure 12).

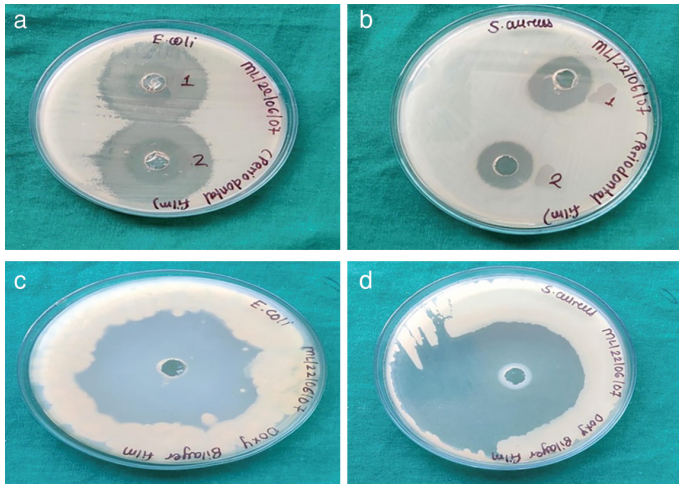

Figure 12. Antimicrobial activity of films: a. effect of primary layer film containing doxycycline hyclate (1) and clove oil (2) on *Escherichia coli*, b. effect of primary layer film containing doxycycline hyclate and clove oil on the zone of *Staphylococcus aureus*, c. effect

The zone of inhibition was calculated from four samples, and it was found that the primary layer (D) exhibited a zone of inhibition of 16.4 ± 1.25 mm for *the E. coli* and 11.5 ± 2.21 mm for the *S. aureus*. In contrast, clove oil-loaded films (S) showed zones of inhibition of 16.6 ± 1.84 mm and 12.1 ± 2.16 mm on *E. coli* and *S. aureus* species. The zone of inhibition for bilayer film (B) was found to be 22.5 ± 1.28 and 20.8 ± 2.47 mm for *E. coli* and *S. aureus*, respectively. The effect of the formulation on gram-negative bacteria was greater than that on positive bacteria. The bilayer film indicated a slightly higher zone of inhibition compared with the primary layer film of doxycycline hyclate. The antimicrobial effect contributed to the combined activity of clove oil and doxycycline hyclate. Periodontitis is mainly caused by *Aggregatibacter, Actinomycetemcomitans,* and *Porphyromonas gingivalis* infection and is a gram-negative bacterium. Antibacterial studies revealed that the bilayer film had a more profound effect on gram-negative bacteria, indicating the effectiveness of the bilayer film in controlling periodontal infection.

DISCUSSION

The diamentions, pH and mechanical strength of bilayer film was suitable to insert in periodontal pocket. All the films exhibited good drug entrapment. Disintegration time for immediate release layer was sufficient to exert preliminary therapeutic effect and treatment goal will be effectively achieved by sustained release layer. Primary layer and bilayer films showed good mucoadhesive strength and swelling owing to polymer properties. Antimicrobial studies were suggestive of microbicidal activity of films on gram-positive and gram-negative bacteria which could be beneficial to counteract periodontal infection.

CONCLUSION

Mucoadhesive bilayer films were developed for the twin delivery of clove oil and doxycycline hyclate as immediate and sustained release layers, respectively, for the treatment of periodontitis. Clove oil layer was developed to control pain and inflammation, and sustained antimicrobial effect was contributed by the doxycycline hyclate layer. The primary layer was composed of flax seed and HPMC and was found to be effective in retarding doxycycline hyclate release. The formulation containing an equal amount of sodium alginate and PVA showed better disintegration, and hence, it was selected as an optimized batch for the immediate release of clove oil. Bilayer films prepared by casting primary and secondary layers showed promising effects as antibacterial agents. Hence, it can be concluded that the bilayer formulation was effective in treating periodontal conditions.

Acknowledgement

The authors are grateful to Savitribai Phule Pune University for providing technical provision to perform scanning electron microscopic studies.

Ethics

Ethics Committee Approval: There is no requirement for ethical approval as animals were not used in current study.

Informed Consent: There is no requirement for informed consent as study was not conducted on helthy human volunteers/patients.

Authorship Contributions

Concept: U.Y.K., C.R.G., A.P.P., N.P.P., Design: U.Y.K., C.R.G., N.P.P., N.M.M., Data Collection or Processing: U.Y.K., C.R.G., A.P.P., N.P.P., A.P.P., Analysis or Interpretation: U.Y.K., A.P.P., K.R.K., P.D.C., N.M.M., Literature Search: U.Y.K., C.R.G., N.P.P., Writing: U.Y.K., C.R.G., A.P.P., N.P.P.

Conflict of Interest: The authors have no relevant financial or non-financial interests to disclose.

Financial Disclosure: The authors declared that this study received no financial support.

REFERENCES

1. Sanz M, Aiuto FD, Deanfield J, Fernandez-Aviles F. European workshop in periodontal health and cardiovascular disease-scientific evidence on the association between periodontal and cardiovascular diseases: a review of the literature. European Heart Journal Supplements. 2010;12:3-12.
2. Yucel-Lindberg T, Båge T. Inflammatory mediators in the pathogenesis of periodontitis. Expert Rev Mol Med. 2013;15:e7.
3. Park JB. Effects of doxycycline, minocycline, and tetracycline on cell proliferation, differentiation, and protein expression in osteoprecursor cells. J Craniofac Surg. 2011;22:1839-1842.
4. Ioannou I, Dimitriadis N, Papadimitriou K, Vouros I, Sakellari D, Konstantinidis A. The effect of locally delivered doxycycline in the treatment of chronic periodontitis. A clinical and microbiological cohort study. J Oral Maxillofac Res. 2010;1:e1.
5. Bogren A, Teles RP, Torresyap G, Haffajee AD, Socransky SS, Wennström JL. Locally delivered doxycycline during supportive periodontal therapy: a 3-year study. J Periodontol. 2008;79:827-835.
6. Mohammadi Nejad S, Özgüneş H, Başaran N. Pharmacological and toxicological properties of eugenol. Turk J Pharm Sci. 2017;14:201-206.
7. Leem HH, Kim EO, Seo MJ, Choi SW. Antioxidant and anti-inflammatory activities of eugenol and its derivatives from clove (Eugenia caryophyllata Thunb.) J Korean Soc Food Sci Nutr. 2011;40:1361-1370.
8. Leite AM, Lima EdO, Souza ELd, Diniz MdFFM, Trajano VN, Medeiros IAd. Inhibitory effect of beta-pinene, alpha-pinene and eugenol on the growth of potential infectious endocarditis causing gram-positive bacteria. Revista Brasileira de Ciências Farmacêuticas. 2007;43:121-126.
9. Oyedemi SO, Okoh AI, Mabinya LV, Pirochenva G, Afolayan AJ. The proposed mechanism of bactericidal action of eugenol, ∝-terpineol and g-terpinene against *Listeria monocytogenes*, *Streptococcus pyogenes*, *P*roteus vulgaris and *Escherichia coli*. Afr J Biotechnol. 2009;8:1280-1286.
10. Barbary O, El-Sohaimy S, El-Saadani MA, Zeitoun AM. Extraction, composition and physicochemical properties of flaxseed mucilage. J Adv Agric Res. 2009;14:605-621.
11. Khalloufi S, Corredig M, Goff HD, Alexander M. Flaxseed gums and their adsorption on whey protein-stabilized oil-in-water emulsions. Food Hydrocoll. 2009;23:611-618.

12. Kelemen A, Katona B, Módra S, Aigner Z, Sebe I, Pintye-Hódi K, Zelkó R, Regdon G Jr, Kristó K. Effects of sucrose palmitate on the physico-chemical and mucoadhesive properties of buccal films. Molecules. 2020;25:5248.

13. Pamlényi K, Kristó K, Jójárt-Laczkovich O, Regdon G Jr. Formulation and optimization of sodium alginate polymer film as a buccal mucoadhesive drug delivery system containing cetirizine dihydrochloride. Pharmaceutics. 2021;13:619.

14. Nagarkar R, Patel J. Polyvinyl alcohol: A comprehensive study. Acta Pharm. 2019;3:34-44.

15. Qureshi D, Sahoo A, Mohanty B, Anis A, Kulikouskaya V, Hileuskaya K, Agabekov V, Sarkar P, Ray SS, Maji S, Pal K. Fabrication and characterization of poly (vinyl alcohol) and chitosan oligosaccharide-Based blend films. Gels. 2021;7:55.

16. Fekri N, Khayami M, Heidari R, Jamee R. Chemical analysis of flaxseed, sweet basil, dragon head and quince seed mucilages. Res J Biol Sci. 2008;3:166-170.

17. Nurdianti L, Rusdiana T, Sopyan I, Putriana NA, Aiman HR, Fajria TR. Characteristic comparison of an intraoral thin film containing astaxanthin nanoemulsion using sodium alginate and gelatin polymers. Turk J Pharm Sci. 2021;18:289-295.

18. İnal Ö, Yapar EA, Baykara T. Physical properties and *in vitro* release studies on sotalol monolithic films prepared by eudragit polymers. Turk J Pharm Sci. 2010;7:151-160.

19. Li A, Khan IN, Khan IU, Yousaf AM, Shahzad Y. Gellan gum-based bilayer mucoadhesive films loaded with moxifloxacin hydrochloride and clove oil for possible treatment of periodontitis. Drug Des Devel Ther. 2021;15:3937-3952.

20. Khan G, Yadav SK, Patel RR, Nath G, Bansal M, Mishra B. Development and evaluation of biodegradable chitosan films of metronidazole and levofloxacin for the management of periodontitis. AAPS PharmSciTech. 2016;17:1312-1325.

21. Marin MM, Albu Kaya MG, Iovu H, Stavarache CE, Chelaru C, Constantinescu RR, Dinu-Pirvu CE. Obtaining, evaluation, and optimization of doxycycline-loaded microparticles intended for the local treatment of infectious arthritis. Coatings. 2020;10:990.

22. Junmahasathien T, Panraksa P, Protiarn P, Hormdee D, Noisombut R, Kantrong N, Jantrawut P. Preparation and evaluation of metronidazole-loaded pectin films for potentially targeting a microbial infection associated with periodontal disease. Polymers (Basel). 2018;10:1021.

23. Basu B, Mankad A, Dutta A. Methylphenidate fast dissolving films: development, optimization using simplex centroid design and *in vitro* characterization. Turk J Pharm Sci. 2022;19:251-266.

24. Bhyan B, Jangra S, Kaur M, Singh H. Orally fast dissolving films: innovations in formulation and technology. Int J Pharm Sci Rev Res. 2011;9:9-15.

25. Kandekar UY. Exploiting natural polymer reinforced microspheres and investigating its characteristics for sustained release. IInt J Pharm Sci Res. 2020;11:3367-3378.

26. Wong CF, Yuen KH, Peh KK. An *in vitro* method for buccal adhesion studies: importance of instrument variables. Int J Pharm. 1999;180:47-57.

27. Pandit A, Khandagale K, Nakhate V, Dharmadhikari N. Antifungal topical gel of leaf extract of *Amaranthus viridis* L. for treatment of cutaneous candidiasis. Indian Drugs. 2019;56:39-44.

28. Hemaiswarya S, Doble M. Synergistic interaction of eugenol with antibiotics against Gram negative bacteria. Phytomedicine. 2009;16:997-1005.

29. Kaewmanee T, Bagnasco L, Benjakul S, Lanteri S, Morelli CF, Speranza G, Cosulich ME. Characterisation of mucilages extracted from seven Italian cultivars of flax. Food Chem. 2014;148:60-69.

30. Yadav SK, Mishra B. Preformulation studies on combination of ornidazole and doxycycline in pharmaceutical dosage forms: infra-red spectroscopy and simultaneous ultra-violet method development. J Chem Pharm Res. 2016;8:564-573.

31. Hongfang G, Hui Y, Chuang W. Controllable preparation and mechanism of nano-silver mediated by the microemulsion system of the clove oil. Results in Phys. 2017;7:3130-3136.

32. Semalty M, Semalty A, Kumar G. Formulation and characterization of mucoadhesive buccal films of glipizide. Indian J Pharm Sci. 2008;70:43-48.

33. Lakshmi P, Lavanya D, Ali MH. Effect of synthetic super disintegrants and natural polymers in the preparation of donepezil hydrochloride fast disintegration films. Int Curr Pharm J. 2014;3:243-246.

34. Ghavami-Lahiji M, Shafiei F, Najafi F, Erfan M. Drug-loaded polymeric films as a promising tool for the treatment of periodontitis. J Drug Deliv Sci Technol. 2019;52:122-129.

35. Kandekar UY, Chaudhari PD, Chandrasekhar KB, Pujari RR. Exploration of mucoadhesive microparticles by using Linum usitatissimum mucilage. Lat Am J Pharm. 2019;38:2463-2472.

36. Peh KK, Wong CF. Polymeric films as vehicle for buccal delivery: swelling, mechanical, and bioadhesive properties. J Pharm Pharm Sci. 1999;2:53-61.

37. Shafiei F, Ghavami-Lahiji M, Jafarzadeh Kashi TS, Najafi F. Drug release kinetics and biological properties of a novel local drug carrier system. Dent Res J (Isfahan). 2021;18:94.

Turk J Pharm Sci 2024;21(2):152-158
DOI: 10.4274/tjps.galenos.2023.47105

ORIGINAL ARTICLE

Clinical Pharmacist-Led Medication Review in Hospitalized Confirmed or Probable Patients with COVID-19 During the First Wave of COVID-19 Pandemic

Duygu ÜNDER[1], Cüneyd ENVER[1], Muhammed Yasir DEMİRCİ[1], Yunus Emre AYHAN[1], Betül ÖZGAN[1], Enes Emir İLERLER[1], Betül OKUYAN[1], Buket ERTÜRK ŞENGEL[2], Derya KOCAKAYA[3], Uluhan SİLİ[2], Elif TÜKENMEZ TİGEN[2], Sait KARAKURT[3], Volkan KORTEN[2], Mesut SANCAR[1]*

[1]Marmara University Faculty of Pharmacy, Department of Clinical Pharmacy, İstanbul, Türkiye
[2]Marmara University Faculty of Medicine, Department of Infectious Diseases and Clinical Microbiology, İstanbul, Türkiye
[3]Marmara University Faculty of Medicine, Department of Pulmonary Medicine, İstanbul, Türkiye

ABSTRACT

Objectives: Drug-related problems (DRPs) result in serious problems among hospitalized patients, high rates of morbidity and mortality, and increased healthcare costs. This study aimed to identify DRPs by clinical pharmacist-led medication review in hospitalized probable patients with coronavirus disease-2019 (COVID-19) during the first wave of the COVID-19 pandemic.

Materials and Methods: This retrospective cross-sectional study was conducted at the COVID-19 inpatient services of a tertiary university hospital in Türkiye for 3 months (between March 2020 and June 2020) and included hospitalized confirmed or probable COVID-19 patients. The World Health Organization and Turkish Ministry of Health Guidelines case definitions were used to define confirmed and probable COVID-19 patients. Six clinical pharmacy residents provided medication review services during their education and training. DRPs were classified based on the Pharmaceutical Care Network Europe V9.00. The physician's acceptance rate of clinical pharmacists' recommendations was assessed.

Results: Among 202 hospitalized patients with probable or confirmed COVID-19, 132 (65.3%) had at least one drug-related problem. Two hundred and sixty-four DRPs were identified. Drug selection (85.6%) and dose selection (9.2%) were the most common causes of these problems. Among the 80 clinical pharmacist interventions, 48.8% were accepted by the physicians.

Conclusion: Clinical pharmacists identified a significant number of DRPs during the COVID-19 pandemic, particularly those related to drug interactions and drug safety, such as adverse drug reactions. This study highlights the importance of detecting and responding to DRPs in the COVID-19 pandemic.

Keywords: COVID-19, medication review, clinical pharmacist, drug-related problem, PCNE

INTRODUCTION

The first case infected with severe acute respiratory syndrome coronavirus 2 (SARS-CoV-2) was reported in Wuhan (China) in December 2019 and spread worldwide, causing a coronavirus disease-2019 (COVID-19) pandemic.[1] Since the pandemic began, 346 million COVID-19 cases have been reported globally, with a total of 5.5 million deaths.[2] Although many vaccination options are available, and many countries have vaccinated a significant number of their people, the COVID-19 pandemic continues to be a major public health problem.[3]

Several clinical trials have continued to evaluate the efficacy and safety of specific drugs in COVID-19 patients.[4] Repurposed

*Correspondence: sancarmesut@yahoo.com, Phone: +90 216 777 52 00, ORCID-ID: orcid.org/0000-0002-7445-3235
Received: 20.03.2023, Accepted: 06.06.2023

drugs for COVID-19 are given to treat patients at home, leading to adverse drug events or drug-drug interactions.[5] During the COVID-19 pandemic, clinical pharmacists continue to provide services such as medication review, medication reconciliation, patient education and counseling, and therapeutic drug monitoring in hospitalized patients with COVID-19.[6-7]

Pharmaceutical Care Network Europe (PCNE) defines the medication review as "a structured evaluation of a patient's medicines with the aim of optimizing medicines use and improving health outcomes".[8] Pharmacists play an essential role in medication review, detecting, and resolving drug-related problems (DRPs) on the level of patients and/or healthcare professionals.[9] DRPs are associated with medication errors, adverse drug events, and adverse drug reactions (ADRs).[10-11] Age, sex, presence of comorbidities, the number of drugs, and length of hospital stay are related factors for DRP.[10] Medication review services have also been provided for COVID-19 patients by clinical pharmacists.[1]

Postgraduate education programs in clinical pharmacy (M.Sc. and Ph.D.) has been maintained in Türkiye since 1991. A clinical pharmacist specialist education and training program was initiated by the Republic of Türkiye Ministry of Health in 2018. However, clinical pharmacy services are not yet included as essential requirements at hospitals in Türkiye.

To the best of our knowledge, this is one of the first studies determining DRPs in patients admitted to COVID-19 inpatient services during the first wave of the COVID-19 pandemic in Türkiye. This study aimed to identify DRPs by clinical pharmacist-led medication review in patients admitted to COVID-19 inpatient services during the first wave of the COVID-19 pandemic and evaluate the physicians' acceptance rate of the pharmacist's recommendation.

MATERIALS AND METHODS

This retrospective cross-sectional study was conducted in COVID-19 inpatient services, including infectious diseases, pulmonary medicine, and internal medicine wards of a tertiary university hospital in İstanbul, Türkiye, for three months (between March 2020 and June 2020). All patients (> 18 years old) hospitalized for confirmed or probable COVID-19, who stayed at the hospital for more than 24 hours, used at least one drug during their hospitalization, and received the clinical pharmacist-led medication review service during their hospitalization were included. Patients transferred to the intensive care unit during the first 24 hours of hospitalization were excluded from the study. Our study was conducted in 4 clinics; the total number of beds was 60 and 8 doctors, 2 doctors in each clinic, worked. Three clinical pharmacists worked in the clinics alternately, while 3 clinical pharmacists supported the study remotely. The study protocol was approved by the local Clinical Research Ethical Committee of the Marmara University Faculty of Medicine (approval number: 09.2020.668, date: 12.06.2020).

Six clinical pharmacy residents provided medication review services during their education and training at Marmara University during the COVID-19 pandemic. DRPs were evaluated and recorded by at least two different clinical pharmacists based on electronic hospital records and clinical pharmacist notes. Drug-related problems detected by the clinical pharmacist were verbally reported to the physician.

The patient's demographic (including age and sex), clinical (including comorbidities), and laboratory data (including complete blood count, lactate dehydrogenase, creatinine, coagulation tests, procalcitonin, C-reactive protein), the result of real-time reverse transcriptase-polymerase chain reaction (PCR) test from nasopharyngeal specimens were anonymously recorded to the patient follow-up and evaluation form. Biochemical data were recorded on the first day of hospitalization. In all patients, the Charlson comorbidity index was calculated.[12]

The World Health Organization (WHO) and Republic of Türkiye Ministry of Health Guideline case definitions were used to define confirmed and probable COVID-19 patient.[13,14] The Turkish Ministry of Health guide defined a confirmed case as "among the cases that meet the definition of a probable case, cases with SARS-CoV-2 detected by molecular methods". Those who have clinical findings and/or contacts with patients diagnosed with COVID-19 are defined as "probable cases".[14]

Clinical pharmacist residents assessed all medication orders of hospitalized patients with confirmed and probable COVID-19. Potential drug-drug interactions were evaluated using Lexicomp® Drug Interactions (Wolters Kluwer Health Inc., 2020), Micromedex® Drug Information, and Drug Interactions (Truven Health Analytics Inc., 2020). International guidelines in UpToDate Drug Information and Micromedex Drug Information and the national guideline of COVID-19 for adult patients published by the Turkish Ministry of Health were used to evaluate the appropriateness of drugs. Drug-related problems were classified using the PCNE V9.00-Turkish Version.[15] PCNE, one of the most widely used classification systems, was used to classify DRP in hospital practice.[9,16] PCNE has been translated into various languages in countries where clinical pharmacy is practiced[15,17] and consists of five parts: problem, cause, intervention, intervention acceptance, and status. The "status of DRP" could not be evaluated in PCNE because the study was retrospective. The type and reason for all drug-related problems, the rate of clinical pharmacists' recommendations, and the physician's acceptance rate of clinical pharmacists' recommendations were assessed.

Statistical analysis

Sample size not calculated. Descriptive variables were represented as mean [standard deviation (SD)] and/or median [interquartile range (IQR)] for continuous variables and number (%) for ordinal and nominal variables. Based on the findings of the Kolmogorov-Smirnov test, Mann-Whitney U test was used to compare the two groups. Categorized data were analyzed using the chi-square or Fisher exact tests. $p < 0.05$ was considered significant. Spearman's rank analysis was used to determine the correlation between continuous variables.

RESULTS

The study included 202 hospitalized patients with COVID-19. The PCR test results of 195 of them were identified as 112 confirmed cases and 83 probable cases. The mean age was 59.2 ± 19.3 years, with 52% females. The median (IQR) number of drugs taken *per* patient was 6.0 (4.0-8.0), and polypharmacy (patients receiving more than five drugs concomitantly) was observed in 62.9%. Among these patients, the median (IQR) hospital stay was 7.0 (4.0-11.0) days. The majority of patients had more than three comorbidities (49%), and 1260 drugs were evaluated in this study. The most commonly used drugs were hydroxychloroquine 87.1%, enoxaparin 70.3%, azithromycin 28.2%, and favipiravir 26.2% (176/202, 142/202, 57/202, and 53/202, respectively). The number of patients with two or more DRPs was 74 (36.6%). Patients with DRP had a higher total number of drugs than patients without DRP ($p < 0.05$). Table 1 summarizes the differences between the variables and the main causes of DRPs. There was a positive moderate correlation between the number of DRPs and the total number of drugs and a positive weak correlation between the Charlson comorbidity index [r= 0.317 and r= 0.214, respectively, ($p < 0.01$)]. In Table 2, there was no significant difference in

Table 1. Patients' characteristics (n= 202)

Characteristics	Total patients (n= 202) n (%)	Patients with DRP (n= 132) n (%)	Patients without DRP (n= 70) n (%)	p
Sex				
Male	97 (48.0)	62 (47.0)	35 (50.0)	NS
Female	105 (52.0)	70 (53.0)	35 (50.0)	
Age				
Median	59.0 (18.3)	58.8 (1.6)	60.1 (2.1)	
Older patients (≥ 65 years old)	78 (38.6)	51 (38.6)	27 (38.6)	NS
Charlson comorbidity index				
Median (IQR)	2.0 (1.0-4.0)	3.0 (1.0-4.0)	2.0 (1.0-4.0)	NS
Total number of medications				
Median (IQR)	6.0 (4.0-8.0)	6.0 (4.0-8.8)	5.0 (3.0-7.0)	< 0.01
Classification based on total number of medications				
< 5	76 (37.6)	45 (34.1)	31 (44.3)	NS
≥ 5	126 (62.4)	87 (65.9)	39 (55.7)	
Duration of hospitalization (day)				
Median (IQR)	7.0 (4.0-11.0)	7.0 (4.0-11.0)	7.0 (5.0-14.5)	NS
Result of SARS-CoV-2 RT-PCR				
Positive	112 (55.4)	72 (54.6)	40 (57.2)	NS
Negative	83 (41.1)	54 (40.9)	29 (41.4)	
Unknown/missing data	7 (3.5)	6 (4.5)	1 (1.4)	
Number of patients who received COVID-19 treatment				
Yes	182 (90.1)	118 (89.4)	64 (91.4)	NS
No	20 (9.9)	14 (10.6)	6 (8.6)	
The most commonly used medication in the management of COVID-19				
Hydroxychloroquine	176 (87.1)	115 (87.1)	60 (85.7)	NS
Enoxaparin	142 (70.3)	93 (70.5)	49 (70.0)	NS
Azithromycin	57 (28.2)	42 (31.8)	15 (21.4)	NS
Favipiravir	53 (26.2)	30 (22.7)	23 (32.9)	NS
Oseltamivir	7 (3.5)	4 (3.0)	3 (4.3)	NS
Tocilizumab	5 (2.5)	1 (0.8)	4 (5.7)	NS

IQR: Interquartile range, DRP: Drug-related problem, SARS-CoV-2: Severe acute respiratory syndrome coronavirus-2, RT-PCR: Reverse transcriptase-polymerase chain reaction, NS: No significant

biochemical parameters between patients with and without DRPs ($p > 0.05$).

The median number of DRPs/patients was 1.3. In Table 3, the incidence of DRPs was "treatment effectiveness" (55 of 264 DRPs; 20.8%), followed by "treatment safety" (140 of 264 DRPs; 53.0%). Within the "treatment effectiveness" category, "untreated symptoms or indication" was the dominant category (46 of 140; 32.9%). A total of 270 DRP causes were identified (Table 3). "Drug selection" category was the primary cause of DRPs (231 of 270; 85.6%), followed by "drug dose" (25 of 270; 9.3%). Among drug selection problems, the most common DRPs were "inappropriate combination of drugs or drugs and herbal medication", "no indication for drug" and "no drug treatment despite existing indication" (108 of 231, 46.8%; 54 of 231, 23.4% and 47 of 231, 20.3%; respectively). The combination of azithromycin and hydroxychloroquine constitutes 52.8% of drug-drug interactions. Of the 112 planned interventions, 91.1% were at the prescriber level. According to the PCNE classification, 80 (71.4) interventions were proposed to the prescriber. Thirty-nine (48.8%) interventions were accepted, and the acceptance status of 33 (41.3%) interventions was unknown. Only 8 (10.0%) interventions were rejected.

DISCUSSION

This is one of the first retrospective cross-sectional studies to describe the prevalence of drug-related problems in patients admitted to a COVID-19 service in Türkiye. More than half of the hospitalized patients had at least one DRP during the first wave of the COVID-19 pandemic. Patients having DRP had a higher number of drugs. The most common DRPs were related to drug and/or dose selection. Less than half of the clinical pharmacy residents' recommendations were accepted by the physicians.

In our study involving COVID-19 patients, the incidence of DRP was found to be similar to another study performed on COVID-19 patients (1.4 DRP/patient).[18] Similar rates of DRP have been detected in studies involving COVID-19 patients.[5,19,20] DRP rates were found to be higher in studies conducted before the COVID-19 pandemic.[21] The reason for our low DRP rates may be that the study was planned retrospectively during a period under pandemic conditions. Problems with drug safety were identified, including most DRPs, potential drug interactions, ADRs, and high doses. Similar to other studies, the most frequently detected DRP was "treatment safety" (53%) and then "treatment effectiveness" (20%).[19,20] Drug interactions accounted for approximately 40% of the total causes of DRP; the reason for this high rate compared with other studies may be the frequent use of hydroxychloroquine and azithromycin, which are drugs used in the COVID-19 pandemic. The risk of QT prolongation is increased with the combined use of hydroxychloroquine and azithromycin; most clinical pharmacists' recommendations have been this interaction. Proton pump inhibitors (PPIs) are often overprescribed, and overprescribing has continued in the COVID-19 pandemic. Clinical pharmacists advise physicians to optimize PPI use. Long-term use of PPIs has been associated with adverse events such as pneumonia. Analysis of clinical pharmacist interventions in COVID-19 units found that PPI was overprescribe in a similar study.[5] In our study, similar rates of "no drug indication" and "no drug treatment despite the current indication" were found among DRP causes, and it is thought that this may be due to the difficulty of medication reconciliation in pandemic conditions.

In previous studies, DRPs were associated with the presence of comorbidity and polypharmacy.[19-22] The absence of relationships with other variables may be due to the small sample number of patients and DRPs detected.

Half of the interventions proposed because of DRPs were accepted in our study. In different studies conducted before the pandemic, the acceptance rate of the interventions was found to be higher.[21,22] During the COVID-19 pandemic, clinical pharmacists continued to provide services such as medication

Table 2. Patients' biochemical parameters related to COVID-19 (n= 202)

Biochemical parameters	Total patients (n= 202) median (IQR)	Patients with DRP (n= 132) median (IQR)	Patients without DRP (n= 70) median (IQR)	p
ALT	18.0 (11.0-35.0)	17.0 (10.0-36.0)	26.0 (12.5-35.0)	NS
AST	31.0 (21.0-42.0)	20.0 (30.0-42.0)	35.0 (24.0-45.5)	NS
LDH	272.0 (205.0-368.2)	258.0 (201.0-349.0)	311.0 (217.0-427.0)	NS
Ferritin	177.0 (67.4-427.4)	215.0 (67.0-423.2)	138.4 (68.4-467.6)	NS
Procalcitonin	0.1 (0.1-0.3)	0.1 (0.1-0.3)	0.1 (0.1-0.2)	NS
CRP	46.5 (12.9-84.2)	40.1 (12.7-95.6)	48.4 (13.3-81.0)	NS
D-dimer	0.9 (0.5-1.6)	0.9 (0.5-1.9)	0.9 (0.5-1.4)	NS
PT	14.0 (13.0-15.6)	14.0 (12.9-15.6)	14.2 (13.4-15.9)	NS
aPTT	29.6 (27.2-31.8)	2.0 (2.0-3.0)	29.6 (26.4-32.1)	NS
Creatinine	0.9 (0.7-1.1)	0.9 (0.7-1.1)	0.8 (0.7-1.0)	NS

ALT: Alanine aminotransferase, AST: Aspartate aminotransferase, LDH: Lactate dehydrogenase, CRP: C-reactive protein, PT: Prothrombin time, aPTT: Activated partial thromboplastin time, IQR: Interquartile range, DRP: Medication-related problem, NS: No significant

Table 3. DRP based on PCNE V9.00 (n= 132)

	Detailed classification (Code V9.0)	n (%)
The type of DRP (Code V9.0) (n= 264)		
Treatment effectiveness (P1)	Untreated symptoms or indications (P1.3)	46 (17.4)
	Effect of drug treatment not optimal (P1.2)	9 (3.4)
Treatment safety (P2)	Adverse drug event (possibly) occurring (P2.1)	140 (53.0)
Others (P3)	Unnecessary drug treatment (P3.2)	60 (22.7)
	Unclear problem/complaint. Further clarification is necessary (P3.3)	7 (2.6)
	Problem with the cost-effectiveness of the treatment (P3.1)	2 (0.8)
Causes (Code V9.0) (n=270)*		
Drug selection (C1)	Inappropriate combination of drugs or drugs and herbal medication (C1.4)	108 (40.0)
	No indication for the drug (C1.3)	54 (20.0)
	No drug treatment despite existing indication (C1.6)	47 (17.4)
	Inappropriate drug (within guidelines but otherwise contra-indicated) (C1.2)	11 (4.1)
	Inappropriate drug according to the guidelines/formulary (C1.1)	4 (1.5)
	Too many drugs prescribed for indication (C1.7)	4 (1.5)
	Inappropriate duplication of the therapeutic group or active ingredient (C1.5)	3 (1.1)
Drug form (C2)	Inappropriate drug form (for this patient) (C2.1)	3 (1.1)
Dose selection (C3)	Drug dose too high (C3.2)	12 (4.4)
	Drug dose too low (C3.1)	6 (2.2)
	Dosage regimen, too frequent (C3.4)	5 (1.8)
	Dosage regimen, not frequent enough (C3.3)	1 (0.4)
	Dose timing instructions incorrect, unclear, or missing (C3.5)	1 (0.4)
Drug use process (C6)	Inappropriate timing of administration and/or dosing intervals (C6.1)	5 (1.8)
Related patient transport (C8)	Insufficient clinical information about the patient (C8.4)	1 (0.4)
Other (C9)	No obvious cause (C9.3)	3 (1.1)
	No or inappropriate outcome monitoring (including therapeutic drug monitoring) (C9.1)	2 (0.8)
Proposed interventions (Code V9.0) (n= 112)		
At the prescriber level (I1)	Intervention proposed to the prescriber (I1.3)	54 (19.9)
	Prescriber informed only (I1.1)	48 (17.7)
At the drug level (I3)	Drug stopped I3.5	5 (1.8)
	Dosage changed to... (I3.2)	2 (0.7)
	Drug changed to... (I3.1)	1 (0.4)
	Formulation changed to... (I3.3)	1 (0.4)
	Instructions for use changed to... (I3.4)	1 (0.4)
Acceptance of the intervention proposals (Code V9.0) (n= 80)		
Intervention accepted (by prescriber or patient) (A1)	Intervention accepted and fully implemented (A1.1)	22 (27.5)
	Intervention accepted; implementation unknown (A1.4)	12 (15.0)
	Intervention not accepted: no agreement (A2.2)	7 (8.8)
	Intervention accepted, partially implemented (A1.2)	4 (5.0)
	Intervention accepted but not implemented (A1.3)	1 (1.3)
	Intervention not accepted: other reason (specify) (A2.3)	1 (1.3)
Other (no information on acceptance) (A3)	Intervention proposed, acceptance unknown (A3.1)	33 (41.3)

*More than one cause was determined for each DRP, DRP: Medication-related problem, PCNE: Pharmaceutical Care Network Europe

reconciliation, medication review, therapeutic drug monitoring, patient education, and counseling for patients hospitalized with COVID-19 over the phone or by working remotely.[7,23] The limited performance of clinical pharmacy services due to situations such as the inability to take a medication history from the patient, the patients being in isolation conditions, the clinical pharmacist's inability to visit the patient and remote work, and the daily change of the physicians who follow the patients and the pharmacists who make suggestions may have caused the acceptance rates to be low. Because of the first wave of the pandemic, the strict implementation of protective measures, and the remote working conditions, acceptance rates could not be followed very well in resolving drug-related problems. In addition, a published articlestated that the acceptance rate of the recommendations made by pharmacists during the pandemic was lower than before the pandemic due to less effective communication and the need for more intensive follow-up to be accepted.[7]

Due to the interventions being proposed verbally, the proposal and following the acceptance status made during the transfers between the physicians and pharmacists may have been skipped. In this regard, the WHO recommends that patients' status, medication, and treatment plans be communicated in detail using a standard communication technique during care transitions to ensure a standardized handover.[5]

Clinical pharmacists can quickly develop telehealth strategies by analyzing the current situation with their professional expertise in pandemics. In this context, it can provide innovative pharmacy services such as telehealth counseling, guideline development, health education *via* multi-media, and evidence-based drug evaluation.[23]

In subsequent studies, clinical pharmacists may continue to participate in services such as medication reconciliation, medication review, discharge education, and medication counseling, as they did in periods other than the pandemic, but this time taking more precautions. If the necessary infrastructure is provided, the aforementioned services can also be delivered to patients by phone or video calls.

This study had limitations due to the retrospective and observational definition of DRPs. The study was conducted in a single center with a small number of patients; therefore, the results obtained here may not be generalizable. In the follow-up of the patients, inaccurate information was removed, and the information that was sure to be correct was evaluated. We could not determine for each patient whether an adverse drug case identified in the patient record and clinical pharmacist note is actually related to that medication or not. Therefore, adverse drug events may be underreported. However, our study is important because it shows that DRPs continue in pandemic conditions and there is a need for clinical pharmacy services.

CONCLUSION

While this study draws attention to the importance of DRPs in the treatment of COVID-19, it also revealed that clinical pharmacists should work as a part of the healthcare team in very difficult conditions such as pandemics. Further studies will be helpful to determine DRP levels in COVID-19 patients.

Ethics

Ethics Committee Approval: The study protocol was approved by the Local Clinical Research Ethical Committee of the Marmara University Faculty of Medicine (approval number: 09.2020.668, date: 12.06.2020). The required permission to conduct this study was obtained from the Ministry of Health, The Republic of Türkiye.

Informed Consent: Since the study was retrospective, informed consent was not obtained from patients and/or caregivers.

Authorship Contributions

Concept: D.Ü., C.E., M.Y.D., Y.E.A., B.Ö., M.S., Design: D.Ü., C.E., M.Y.D., Y.E.A., B.Ö., S.K., V.K., M.S., Data Collection or Processing: D.Ü., C.E., M.Y.D., Y.E.A., B.Ö., E.E.İ., B.E.Ş., D.K., U.S., E.T.T., Analysis or Interpretation: D.Ü., C.E., M.Y.D., B.Ö., V.K., M.S., Literature Search: D.Ü., C.E., M.Y.D., Y.E.A., B.Ö., E.E.İ., Writing: D.Ü., C.E., M.Y.D., Y.E.A., B.Ö., E.E.İ., B.Ö., B.E.Ş., D.K., U.S., E.T.T., S.K., V.K., M.S.

Conflict of Interest: The authors have no relevant financial or non-financial interests to disclose.

Financial Disclosure: The authors declared that this study received no financial support.

REFERENCES

1. Zhu N, Zhang D, Wang W, Li X, Yang B, Song J, Zhao X, Huang B, Shi W, Lu R, Niu P, Zhan F, Ma X, Wang D, Xu W, Wu G, Gao GF, Tan W. China novel coronavirus investigating and research team. A novel coronavirus from patients with pneumonia in China, 2019. N Engl J Med. 2020;382:727-733.
2. World Health Organization. COVID-19 weekly epidemiological update. https://www.who.int/publications/m/item/weekly-epidemiological-update-on-covid-19---25-january-2022 (accesed 25 Jan 2022).
3. World Health Organization. Coronavirus disease 2019 (COVID-19): case definitions, updated in public health surveillance for COVID-19. https://www.who.int/publications/i/item/WHO-2019-nCoV-Surveillance_Case_Definition-2020.2 (accessed 10 Aug 2020).
4. Li L, Li R, Wu Z, Yang X, Zhao M, Liu J, Chen D. Therapeutic strategies for critically ill patients with COVID-19. Ann Intensive Care. 2020;10:45.
5. Perez M, Masse M, Deldicque A, Beuscart JB, De Groote P, Desbordes J, Fry S, Musy E, Odou P, Puisieux F, Lambert M, Scherpereel A, Décaudin B. Analysis of clinical pharmacist interventions in the COVID-19 units of a French university hospital. Eur J Hosp Pharm. 2022;29:30-35.
6. Paudyal V, Cadogan C, Fialová D, Henman MC, Hazen A, Okuyan B, Lutters M, Stewart D. Provision of clinical pharmacy services during the COVID-19 pandemic: experiences of pharmacists from 16 European countries. Res Social Adm Pharm. 2021;17:1507-1517.
7. Surapat B, Sungkanuparph S, Kirdlarp S, Lekpittaya N, Chunnguleum K. Role of clinical pharmacists in telemonitoring for patients with Coronavirus disease 2019 (COVID-19). J Clin Pharm Ther. 2021;46:236-239.
8. Griese-Mammen N, Hersberger KE, Messerli M, Leikola S, Horvat N, van Mil JWF, Kos M. PCNE definition of medication review: reaching agreement. Int J Clin Pharm. 2018;40:1199-1208.

9. Blenkinsopp A, Bond C, Raynor DK. Medication reviews. Br J Clin Pharmacol. 2012;74:573-580.
10. Kefale B, Degu A, Tegegne GT. Medication-related problems and adverse drug reactions in Ethiopia: A systematic review. Pharmacol Res Perspect. 2020;8:00641.
11. Strand LM, Morley PC, Cipolle RJ, Ramsey R, Lamsam GD. Drug-related problems: their structure and function. DICP. 1990;24:1093-1097.
12. Charlson ME, Pompei P, Ales KL, MacKenzie CR. A new method of classifying prognostic comorbidity in longitudinal studies: development and validation. J Chronic Dis. 1987;40:373-383.
13. World Health Organization. Coronavirus disease 2019 (COVID-19): situation report, 61. Geneva. 2020. https://www.who.int/docs/default-source/coronaviruse/situation-reports/20200321-sitrep-61-covid-19.pdf (accessed 10 Aug 2020).
14. T.C. Sağlık Bakanlığı COVID-19 (SARS-CoV-2 enfeksiyonu) Rehberi, Bilim Kurulu Çalışması. Genel bilgiler, epidemiyoloji ve tanı. 2020. https://covid19.saglik.gov.tr/TR-66337/genel-bilgiler-epidemiyoloji-ve-tani.html (accesed 10 Aug 2020).
15. Pharmaceutical Care Network Europe (PCNE). The definition of drug-related problems. 2020. https://www.pcne.org/upload/files/417_PCNE_classification_V9-1_final.pdf (accessed 10 Aug 2020).
16. Saldanha V, Randall Martins R, Lima SIVC, Batista de Araujo I, Gouveia Oliveira A. Incidence, types and acceptability of pharmaceutical interventions about drug related problems in a general hospital: an open prospective cohort. BMJ Open. 2020;10:e035848.
17. Schindler E, Richling I, Rose O. Pharmaceutical Care Network Europe (PCNE) drug-related problem classification version 9.00: German translation and validation. Int J Clin Pharm. 2021;43:726-730.
18. Barceló-Vidal J, Carballo N, De Antonio-Cuscó M, Fernández-Sala X, Echeverría-Esnal D, Acín P, López-Mula C, Comella-Anaya L, González-Colominas E, Luque S, Ferrández O. Potential drug related problems in the time of COVID-19. Eur J Hosp Pharm. 2021;28:105-106.
19. Chappe M, Corvaisier M, Brangier A, Annweiler C, Spiesser-Robelet L. Impact of the COVID-19 pandemic on drug-related problems and pharmacist interventions in geriatric acute care units. Ann Pharm Fr. 2022;80:669-677.
20. Gourieux B, Reisz F, Belmas AS, Danion F, Fourtage M, Nai T, Reiter-Schatz A, Ruch Y, Walther J, Nivoix Y, Michel B. Prescribing practices of lopinavir/ritonavir, hydroxychloroquine and azithromycin during the COVID-19 epidemic crisis and pharmaceutical interventions in a French teaching hospital. Eur J Hosp Pharm. 2021;28:242-247.
21. Abunahlah N, Elawaisi A, Velibeyoglu FM, Sancar M. Drug related problems identified by clinical pharmacist at the Internal Medicine Ward in Turkey. Int J Clin Pharm. 2018;40:360-367.
22. Li Q, Qu HJ, Lv D, Yeh MK, Sun S, Li L, Liao Y. Drug-related problems among hospitalized patients with COPD in mainland China. Int J Clin Pharm. 2019;41:1507-1515.
23. Li H, Zheng S, Liu F, Liu W, Zhao R. Fighting against COVID-19: Innovative strategies for clinical pharmacists. Res Social Adm Pharm. 2021;17:1813-1818.

Turk J Pharm Sci 2024;21(2):159-166
DOI: 10.4274/tjps.galenos.2023.89457

ORIGINAL ARTICLE

Analyzing the Iatrogenic Triad: Discovering Strategies for Preventing Harm in the Elderly

Vinodkumar MUGADA[1]*, Srinivasa Rao YARGUNTLA[2], Satya Sai Srinivas ALLADA[1], Kamala Kumari PARAVASTU[2], Stephanie Margaret PUVVADA[1]

[1]Vignan Institute of Pharmaceutical Technology, Department of Pharmacy Practice, Duvvada, India
[2]Vignan Institute of Pharmaceutical Technology, Department of Pharmaceutics, Duvvada, India

ABSTRACT

Objectives: The iatrogenic triad is a significant global health problem in the elderly population. This study aimed to evaluate the iatrogenic triad in the elderly and identify potential preventive measures to mitigate its occurrence.

Materials and Methods: A preliminary observational study was conducted on 150 ambulatory elderly patients to assess potentially inappropriate medications (PIMs), polypharmacy, and drug interactions. The AGS Beers Criteria 2019, Polypharmacy, Medication Complexity Regimen Index (MRCI), and Micromedex (a drug information software) were used to assess the harmful triad. Before and after data collection, we observed, identified, and unfolded potential strategies to avoid the harmful triad in the elderly population.

Results: MRCI is 30.49 ± 13.77, suggesting a moderate level of complexity in the drug regimens of elderly patients. Among the PIMs identified by the AGS Beer criteria for 2019, glimepiride (45) and diclofenac (23) were found to be the most frequently prescribed. Moderate-level drug-drug interactions were identified between aspirin and metoprolol (20), metoprolol and metformin (13), and aspirin and enalapril (11). All drug-ethanol and drug-food interactions were rapid and often unknown to patients. Furthermore, the study found that MRCI and polypharmacy were significantly associated with the number of PIMs and drug interactions ($p < 0.01$). Based on data collection, this study identified three possible ways to prevent the iatrogenic triad in elderly patients: interaction, collaboration, and continuing education.

Conclusion: In conclusion, this study sheds light on medication regimen complexity, PIMs, and drug interactions in elderly patients. The study also highlights three possible ways to prevent the iatrogenic triad: interaction, collaboration, and continuing education. By implementing these strategies, healthcare providers can help prevent harm and improve the quality of care for elderly patients.

Keywords: Aged, potentially inappropriate medication list, drug interactions, polypharmacy, medication regimen complexity index

INTRODUCTION

The iatrogenic triad, which consists of potentially inappropriate medications (PIMs), polypharmacy, and drug-drug interactions (DDI),[1] is a significant concern in the field of geriatrics. PIMs refer to the use of a medicine for which the risks outweigh the potential benefits, particularly, when more effective alternatives are available.[2] High prevalence rates of PIM usage (ranging from 18 to over 40%) have been observed across various healthcare settings.[3]

Moreover, older patients frequently use a greater number of medications, leading to polypharmacy. This increased medication use is likely to result in PIM in this population. Furthermore, PIM usage has been associated with hospitalization[4] and mortality,[5] underscoring the importance of addressing this issue in geriatric care.

Co-morbidities and polypharmacy (> 5 medications) are the primary factors contributing to an increased risk of DDI in elderly patients. Furthermore, age-related changes in drug pharmacodynamics and pharmacokinetics may increase the likelihood of developing DDI.[6] To assess the complexity of medication regimens, the medication regimen complexity index (MRCI) is employed. This validated 65-item scoring system considers the number of medications, dosage

*Correspondence: viptpharmd@gmail.com, Phone: +91 7095197222, ORCID-ID: orcid.org/0000-0002-9364-9874
Received: 20.03.2023, Accepted: 06.06.2023

forms, administration instructions, frequency of dosing, and restrictions on food dosing.[7] In addition, polypharmacy and higher medication complexity are responsible for approximately 50% of medication non-adherence rates in elderly patients.[8]

DDIs, such as when anticoagulants intensify blood thinner effects, can increase the MRCI, introducing more variables such as dosage timing. This increased complexity can hinder medication adherence; patient juggling multiple medications might miss doses. Therefore, minimizing DDIs and managing MRCI are crucial to promote adherence, thereby optimizing health outcomes.

To date, no outpatient studies have investigated the impact of pharmacist intervention on the MRCI in the elderly population.[9,10] However, drug interactions, if unavoidable, can be managed through increased awareness and knowledge. In a study by Bories et al.[11] a higher prevalence of PIMs and severe to moderate DDIs were observed in the hospital settings compared with nursing homes and primary care, independent of polypharmacy rates.

To the best of our knowledge, there is a scarcity of research in India that investigates drug-alcohol and drug-food interactions in patients and seeks to identify potential methods to prevent the iatrogenic triad. Our study assessed PIMs, drug interactions, and medication regimen complexity in elderly patients. Through our investigation, we identified three potential strategies that may help prevent or mitigate the harmful triad in this population, emphasizing the need for continued research and intervention development in this area.

Study design, study site, and duration of the study

A descriptive cross-sectional study was conducted on 150 elderly patients attending outpatient departments at a government-funded, 1.000-bed hospital. This facility charges a nominal amount for diagnostic and other medical services while providing necessary medications at no cost to the patients. Owing to its operation in the public sector and its status as one of the major hospitals in nearby regions, the hospital faces a disproportionate doctor-to-patient ratio. The hospital offers surgery and emergency services around the clock. The study spanned six months, from January 7 to July 7, 2022. The manuscript has been reported in accordance with the STROBE guidelines.

Study participants, sampling technique, and sample size estimation

This study focused on elderly patients who were prescribed at least one medication, irrespective of the presence of any co-existing medical conditions. Patients with time constraints were excluded from the study to ensure data reliability. A convenience sampling approach was employed to select each participant, providing a practical and efficient method for participant recruitment. Due to the study's timeline constraints, 150 patients were ultimately included in the research, allowing for a manageable sample size while still offering valuable insights into the topic.

Ethical approval

The Vignan Institute of Pharmaceutical Technology Institutional Human Ethical Committee approved the study (approval no.: VIPT/IEC/89/2022, date: 20.01.2022). The participants were informed of the objectives of the study. We assured the confidentiality of the data and obtained informed consent from each participant.

Study instruments

American Geriatric Society (AGS) Beer's Criteria, 2019[12]

The 2019 AGS Beers Criteria is an update to the 2015 Beers Criteria, providing a comprehensive list of PIMs that should be avoided in elderly patients in specific situations or, in most cases, across the board, particularly when considering certain diseases or conditions. This updated criteria includes a list of PIMs for most older adults, drugs to be avoided for those with certain conditions, DDIs to be aware of, drugs to use with caution, and guidance on dose adjustments in cases of renal failure. For each class of PIMs, the criteria outline the rationale, recommendation, quality of evidence, and strength of recommendation, ensuring a well-informed approach to medication management in geriatric care.

Micromedex[13]

Micromedex is an evidence-based medical information software that serves as a reliable source of drug interaction-related information. To emphasize the importance of addressing these interactions, our study reported drug interactions that exhibited major and moderate severity, rapid and delayed onset reactions, and good and excellent documentation. Nevertheless, in the case of drug-ethanol interactions, we also included results with fair documentation to ensure a comprehensive analysis. Furthermore, we meticulously documented the mechanism of interaction for every instance, highlighting the sophisticated and rigorous approach employed in this academic investigation.

Definitions

Major drug interaction is any life-threatening drug interaction that requires medical intervention to minimize or prevent serious adverse effects. Moderate drug interaction is any drug interaction that may intensify the patient's condition and/or require an alteration in therapy. Excellent documentation indicates that controlled studies have established the existence of the interaction. Good documentation lacks well-controlled studies but strongly suggests an interaction. Fair documentation suspects an interaction based on pharmacological considerations from lead clinicians or documentation is good for a pharmacologically similar drug.

Medication regimen complexity index[14]

The MRCI is a validated, 65-item scale designed to quantify the complexity of a patient's drug regimen. This index considers factors such as the number of prescribed medications, dosage form, frequency of administration, and additional instructions for use. Consequently, a higher MRCI score signifies a more intricate and complex medication regimen, thereby emphasizing the importance of understanding and managing medication complexity in clinical practice.

Outcomes

The primary outcome of this study was to thoroughly analyze the iatrogenic triad, which encompasses PIMs, polypharmacy (> 5 medications), and DDIs. Concurrently, the secondary outcome is to identify effective strategies that can mitigate or prevent harm caused by the iatrogenic triad in elderly patients, ultimately contributing to improved patient outcomes and enhanced quality of geriatric care. Another secondary outcome is to identify medication regimen complexity using MRCI.

Data collection

Data collection was performed in two distinct parts. The initial part encompassed gathering the demographic and clinical details of the patients, such as their age, gender, smoking and alcoholism status, department name, diagnosis of the patient's condition, and the number of prescribed drugs. The subsequent phase involved prescription auditing to identify PIMs, medication regimen complexity, and potential DDIs, following Beer's criteria (2019).

Data analysis

Quantitative data were presented as mean and standard deviation or median and interquartile range, depending on whether the data were normally distributed or not. Qualitative data are presented as frequencies and percentages. To investigate the relationship between MRCI, polypharmacy (> 5 medications), PIMs, and drug interactions, paired-samples *t*-test or Wilcoxon test was used based on the normality assumption. The *p* value, effect size, and 95% confidence interval were reported for the tests. Spearman's Rho correlation was conducted to examine the degree of association between the medication regiment complexity index, polypharmacy, and drug interactions. The level of statistical significance was set at $p < 0.05$.

Statistical analysis

Statistical analysis was performed using Jeffrey's Amazing Statistics Programme software (version 0.14.1.0).

RESULTS

A total of 150 elderly patients participated in the study. Table 1 shows that the mean age of the elderly was 69.30 ± 5.16 years, and the mean score of the MRCI is 30.49 ± 13.77. Nearly more than half of the patients were males (52.67%), with most of them being non-smokers (72%) and non-alcoholics (74.67%). Polypharmacy (use of > 5 drugs) constituted nearly three-quarters of prescriptions (72.66%). A total of 158 DDIs were detected in the patients, and 97.47% of these interactions were moderate DDIs.

According to AGS Beer's criteria, 2019, the most prescribed PIMs are glimepiride (45) and diclofenac (23) (Table 2). The most reported DDIs are aspirin and metoprolol (20), metoprolol and metformin (13), and aspirin and enalapril (11), all with a moderate level of severity of interaction (Table 3).

MRCI and polypharmacy are significantly associated with interactions and the number of PIMs. However, polypharmacy has a significantly positive correlation with the number of PIMs, whereas MRCI has a significantly positive correlation with drug interactions (Table 4). All drug-ethanol and drug-food interactions are rapid, and patients are unaware of them (Table 5).

DISCUSSION

The key results of the study revealed that the mean age was 69.30 ± 5.16 years, and the mean MRCI score was 30.49 ± 13.77. Polypharmacy was present in 72.66%, and 158 DDIs, mostly moderate, were detected. The most common PIMs were glimepiride and diclofenac. MRCI and polypharmacy significantly

Table 1. Distribution of sociodemographic and clinical details of patients (n= 150)

Characteristic	Frequency (%)
Age	69.30 ± 5.16*
MRCI	30.49 ±13.77*
Males Females	79 (52.67) 71 (47.33)
Non-smokers	108 (72)
Smokers Ex-smokers	30 (20) 12 (8)
Non-alcoholics	112 (74.67)
Alcoholics Ex-alcoholics	24 (16) 14 (9.33)
The type of department	
General medicine	74 (49.33)
Endocrinology	39 (26)
Pulmonology	14 (9.33)
Others†	23 (15.33)
Polypharmacy	
< 5	41 (27.33)
5-6	65 (43.33)
< 7	44 (29.33)
Diagnosis	
Hypertension	113 (75.33)
Diabetes mellitus	96 (64)
CAD	15 (10)
COPD	13 (8.66)
Chronic kidney disease	11 (7.33)
Hypothyroidism	10 (6.66)
DDIs (n= 158)	
Major	4 (2.53)
Moderate	154 (97.47)

†= Orthopedics, nephrology, oncology, general surgery, neurology, *mean ± SD, MRCI: Medication regimen complexity index, CAD: Coronary artery disease, COPD: Chronic obstructive pulmonary disease, SD: Standard deviation

correlated with DDIs and PIMs, with patients largely unaware of rapid drug-ethanol and drug-food interactions.

A recent study found that individuals with an MRCI score of 22 upon hospital discharge were more prone to unanticipated hospital readmissions within 30 days.[15] Another study indicated that a cut-off score of 33 on the MRCI was optimal in identifying medication-related readmission risks.[16] However, it should be noted that these thresholds may vary based on different contexts. Non-etheless, few studies,[17,18] have consistently demonstrated that polypharmacy, i.e., the use of five or more medications, is a predictor of unplanned hospitalizations.

Wimmer et al.[18] found that older adults living at home who had complex medication regimens and were taking numerous medications were more likely to experience unplanned hospitalizations. The study also revealed that the two predictors, medication regimen complexity and number of medications, had similar sensitivity and specificity in predicting unplanned hospitalizations. These results indicate that it may be possible to use these parameters to anticipate unplanned hospitalizations in the elderly. To support this, the MRCI has been recently proposed as a tool for identifying individuals who may benefit from medication therapy management.[19]

The concept of the iatrogenic triad in the elderly refers to three interrelated elements that can adversely affect the health of older adults: polypharmacy (the concurrent use of multiple medications), DDIs, and the use of PIMs.[20] A study conducted in Brazil explored the prevalence and inter-relationship of these elements in older adults. The research found that a high percentage of the elderly population was exposed to the iatrogenic triad. Specifically, 44.6% experienced polypharmacy, 72.3% were at risk of DDIs, and 42.1% were using PIMs as *per* Beers criterion. Almost one-third (29.3%) of the study participants were exposed to all three elements of the iatrogenic triad simultaneously. The study also found that frailty and having a caregiver were associated with this triad.[20]

Research has demonstrated that the iatrogenic triad is prevalent in the elderly population. For instance, a study on elderly women reported that nearly 90% of the participants used at least one

Table 2. PIMs in prescriptions according to the AGS Beers Criteria, 2019

Name of the medication	Frequency	Rationale	Recommen dation	Quality of evidence	Strength of the recommendation
Glimepiride	45	Older adults are at a higher risk of prolonged hypoglycemia	Avoid	High	Strong
Diclofenac	23	High risk of gastrointestinal bleeding or peptic ulcer disease in individuals taking oral or parenteral corticosteroids, anticoagulants, or antiplatelet agents. Induces kidney injury and increases blood pressure. Risks are dose-related	Avoid chronic use, unless other alternatives are not effective, and the patient can take a gastroprotective agent (proton-pump inhibitor or misoprostol)	Moderate	Strong
Tramadol	3	May intensify or cause (syndrome of inappropriate antidiuretic hormone) or hyponatremia	Use with caution	Moderate	Strong
Nifedipine immediate release	2	Potential for hypotensionand risk of precipitating myocardial ischemia	Avoid	High	Strong
Alprazolam	2	Age-related cognitive impairment, delirium, falls, fractures, and motor vehicle crashes.	Avoid	Moderate	Strong
Spironolactone	2	Increased potassium if creatinine clearance < 30 mL/min	Avoid	Moderate	Strong
Theophylline	2	Increased risk of theophylline toxicity with cimetidine and ciprofloxacin	Avoid	Moderate	Strong
Chlorzoxazone	1	Older adults have a poor tolerance for most muscle relaxants because of anticholinergic adverse effects, sedation, and fracture risks	Avoid	Moderate	Strong
Levetiracetam	1	CNS adverse effects, creatinine clearance ≤ 80 mL/min	Reduce dose	Moderate	Strong
Glibenclamide	1	Higher risk of severe prolonged hypoglycemia in older adults	Avoid	High	Strong

PIMs: Potentially inappropriate medications, AGS: American Geriatric Society

element of the iatrogenic triad. The study also noted a high index of continuous use medications, PIMs, and potential drug interactions, particularly among enzymatic inhibitors. It was observed that old age was associated with the presence of all elements of the iatrogenic triad, underscoring the importance of vigilant medication management in this population.[21]

According to the 2019 AGS Beer's criteria, more than half of the prescriptions in our study (54.60%) included medications that were inappropriate for elderly patients. Among such medications, the antidiabetic drugs glimepiride and glibenclamide pose a higher risk of prolonged hypoglycemia in the elderly population. The evidence supporting this recommendation is of high quality, and the recommendation itself is strongly endorsed. Prolonged hypoglycemia can lead to adverse outcomes, including bone fractures from falls, seizures, long-term cognitive impairment (such as dementia), frailty, extended hospital stays, and even mortality in hospitals.[22] It is crucial for physicians to be aware of these PIMs to avoid their use in elderly patients. If physicians are aware, there is an opportunity to replace PIMs with alternative drugs where the benefits outweigh the risks.

No scholarly research originating from India has documented any instances of drug-alcohol or drug-food interactions. Our study highlights the rapid onset and potential severity of drug-alcohol and drug-food interactions, ranging from moderate to

Table 3. DDIs according to severity, onset, documentation, and mechanismof action

DDI	Severity	Onset	Documen station	Frequency	Mechanism
Aspirin and metoprolol	Moderate	Delayed	Good	20	NSAIDS and beta-adrenergic blockers may increase blood pressure
Metoprolol and metformin	Moderate	Delayed	Good	13	Beta-blockers may inhibit or increase the blood glucose-lowering effect of antidiabetic agents and may obscure hypoglycemia symptoms
Aspirin and enalapril	Moderate	Rapid	Excellent	11	May result in decreased effectiveness of enalapril
Atenolol and metformin	Moderate	Delayed	Good	10	The blood glucose-lowering effect of an antidiabetic drug may be increased or decreased, and hypoglycemia symptoms may be obscured
Atenolol and glimepiride	Moderate	Delayed	Good	6	It may increase or decrease the blood glucose-lowering effect of the antidiabetic agent and diminish or obscure hypoglycemic symptoms
Aspirin and atenolol	Moderate	Delayed	Good	4	May result in increased blood pressure
Azithromycin and theophylline	Moderate	Delayed	Good	3	May result in increased serum theophylline concentrations
Atenolol and diclofenac	Moderate	Delayed	Good	2	May result in increased blood pressure
Aspirin and nitroglycerin	Moderate	Rapid	Good	2	Increased nitroglycerin levels and additive platelet dysfunction
Clopidogrel and esomeprazole	Major	Rapid	Excellent	1	Reduces antiplatelet activity and plasma levels of clopidogrel active metabolites
Atorvastatin and phenytoin	Moderate	Delayed	Excellent	1	Reduces atorvastatin plasma concentrations and efficacy
Clopidogrel and tramadol	Major	Rapid	Good	1	Reduces the efficacy of clopidogrel

DDI: Drug-drug interactions, NSAID: Non streoidal anti inflammatory drug

Table 4. Association and correlation among variables in the study

Measure 1	Measure 2	*p* value††	Effect size*	95% CI for effect size		Correlation†
				Lower	Upper	r: *p* value
MRCI	No. of PIM	< 0.00001	1.000	1.000	1.000	0.03: 0.773
Polypharmacy	No. of PIM	< 0.00001	1.000	1.000	1.000	0.58: < 0.0001
Polypharmacy	Interactions	< 0.00001	0.950	0.927	0.965	0.005: 0.959
MRCI	Interactions	< 0.00001	1.000	1.000	1.000	0.50: < 0.0001

†Spearman's Rho Correlation, ††Wilcoxon signed-rank test, *Effect size-effect size is given by the matched rank biserial correlation, MRCI: Medication regimen complexity index, PIM: Potentially inappropriate medication, CI: Confidence interval

major. Patients who are not educated on these interactions by a clinical pharmacist are often unaware of the associated risks, which can result in therapeutic failure. For instance, concurrent intake of food can decrease furosemide exposure and efficacy, whereas alcohol consumption while taking aspirin can increase the risk of gastrointestinal bleeding. These interactions are typically unknown to both patients and physicians, underscoring the need for clinical pharmacist involvement in such cases.

Moreover, our study identified three potential strategies to prevent the iatrogenic triad in elderly patients: interaction, collaboration, and continuing education. Notably, we found no previous studies in India that have outlined such systematic approaches for mitigating the risks associated with the iatrogenic triad in the elderly.

Interaction

Patients will have the opportunity to interact with the clinical pharmacist (Figure 1). Typically, patients are required to register as outpatients and then wait to consult with a physician. During this waiting period, the clinical pharmacist will meet the patient and collect the best possible medication history (BPMH) using a standard proforma. The BPMH includes information such as current medications, drugs discontinued within the last six months, drug allergies, over-the-counter medications, alternative medicine, vitamin and mineral supplements, herbal supplements, and recent immunization. The clinical pharmacist will record this comprehensive information in patient case sheets. The patient will then consult with the physician using the updated case sheet. Public hospitals should actively foster collaboration with pharmacy colleges to encourage their participation as stakeholders in the process of mitigating the iatrogenic triad in vulnerable populations such as the elderly. By cultivating a symbiotic relationship between these institutions, a more comprehensive approach can be employed to address and prevent potential complications arising from medical interventions.

Collaboration

Based on the information obtained from the BPMH and drug allergy records provided by the clinical pharmacist, the physician will proceed to prescribe appropriate drugs. The clinical pharmacist will then conduct a thorough review of the prescription to identify PIMs, drug interactions, and instances of polypharmacy. In cases where discrepancies are identified, both the physician and clinical pharmacist will consult established evidence and guidelines to inform their decision-making. Upon reaching a consensus, the physician will proceed to individualize and represcribe the therapy as necessary (Figure 1).

Table 5. Possible drug ethanol and drug-food interactions according to severity, onset, evidence, and mechanism

Drug-ethanol interactions					
Name of the drug	**Severity**	**Onset**	**Documentation**	**Frequency**	**Warning**
Aspirin	Moderate	Rapid	Good	8	A combination of ethanol and aspirin may increase the risk of gastrointestinal bleeding
Nitroglycerin	Moderate	Rapid	Fair	2	Hypertension may result from the concurrent use of nitroglycerin and ethanol
Cetirizine	Major	Rapid	Fair	1	Cetirizine and ethanol may cause CNS depression when used together
Amitriptyline	Moderate	Rapid	Good	1	Amitriptyline and ethanol combined may result in enhanced CNS depression
Tramadol	Major	Rapid	Fair	1	Tramadol and ethanol may cause respiratory and CNS depression when used concurrently
Drug-food interactions					
Furosemide	Moderate	Rapid	Excellent	11	Food and furosemide may reduce the efficacy and exposure to furosemide
Metoprolol	Moderate	Rapid	Excellent	26	Metoprolol concentrations may increase when combined with food
Acetaminophen	Moderate	Rapid	Good	21	Acetaminophen effectiveness may be decreased when used concurrently with cabbage
Theophylline	Moderate	Rapid	Good	4	Food and theophylline may alter theophylline concentrations
Montelukast	Moderate	Rapid	Excellent	4	The use of montelukast and grapefruit juice together may increase montelukast exposure.
Ciprofloxacin	Moderate	Rapid	Good	5	Dairy foods and ciprofloxacin may decrease ciprofloxacin concentrations.

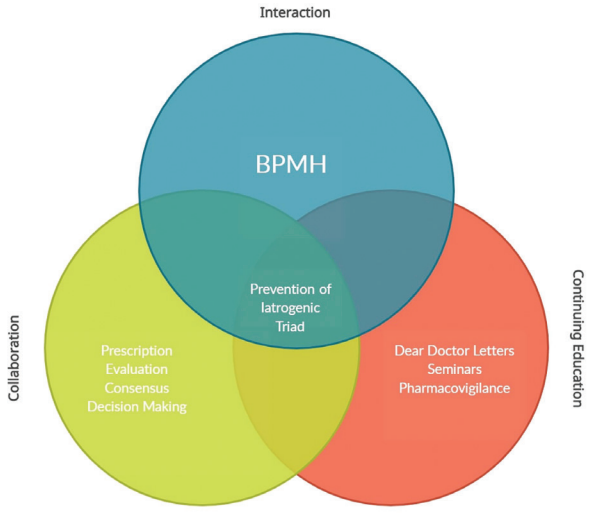

Figure 1. Interaction of outpatients, continuing education, and collaboration of physicians with a clinical pharmacist

BPMH: Best possible medication history

Collaborative interventions between pharmacists and physicians have been shown to improve the medication appropriateness index scores of elderly patients.[23] A collaborative care approach with a focus on pharmacists has been found to be effective in reducing drug-related problems, potential DDIs, and PIMs, as well as improving positive clinical outcomes related to quality-of-life measures in elderly patients with mental health concerns.[24] Moreover, interventions aimed at optimizing medication usage have been successful in reducing the risk of serious adverse drug reactions (ADRs) in older adults.[25] Nonetheless, the acceptability of pharmacist-led interventions as a means of optimizing treatment is a crucial consideration.

Continuing education

Continuing medical education is an essential tool for keeping physicians abreast of new developments and advances in medicine. This education is facilitated through various channels, such as dear doctor letters, seminars and conferences, and pharmacovigilance activities. Dear doctor letters disseminate vital information, including new drug approvals by the FDA, recent inappropriate drug usage in high-risk populations, and ADRs that commonly occur in hospitals. Clinical pharmacist-led seminars and conferences cover diverse aspects of drug safety, whereas pharmacovigilance activities enable unsolicited reporting of ADRs by healthcare and allied healthcare personnel in high-risk populations. The implementation of such measures serves to deter the prescribing or caution the use of drugs that pose potential risks to patient safety (Figure 1).

In the D-PRESCRIBE randomized trial, Martin et al.[26] established a pharmacist-led intervention group aimed at promoting educational deprescribing brochures and providing evidence-based pharmaceutical opinions to physicians. This study focused on older adults in Quebec and compared the outcomes of the intervention group with those receiving standard care. Results revealed that after 6 months, participants who received the educational intervention discontinued prescriptions for inappropriate medications. However, further research is necessary to establish the generalizability of these findings to broader patient populations.

The interplay between these three methods-interaction, collaboration, and continuing education-can significantly minimize the iatrogenic triad in the elderly. The patient-centered approach, coupled with strong professional collaboration and an emphasis on continual learning, forms a robust defense against the potential pitfalls associated with polypharmacy and complex medical care in the elderly population. They form a synergistic approach that addresses various aspects of medication safety and management. Combining these factorscan improve medication-related outcomes, reduce the iatrogenic triad, and enhance the overall well-being of the elderly population.

Study limitations

This study has some limitations. First, the small sample size is small and affects the generalizability of the results. Second, the health policy making of integrating pharmacists into patient care may require feasibility and acceptability of multiple stakeholders. However, considering the benefit of the approach and the significant number of pharmacy colleges in Andhra Pradesh, it may be possible to implement the approach in real time for optimal results.

Potential implications of the study

This study has important implications for improving the quality of care for elderly patients and preventing the iatrogenic triad. By implementing the strategies identified in this study, healthcare providers can reduce the risk of harm and improve outcomes for this vulnerable population.

Improved medication management for the elderly

The study's findings highlight the need for healthcare providers to review and adjust medication regimens for elderly patients to reduce the risk of PIMs, polypharmacy, drug interactions, and medication regimen complexity. This could lead to better health outcomes and quality of life for elderly patients.

Development of clinical guidelines

The study findings could inform the development of clinical guidelines for medication management in elderly patients. These guidelines could provide healthcare providers with a framework for assessing medication regimens, identifying PIMs, and managing drug interactions in elderly patients.

CONCLUSION

We observed the iatrogenic triad in the elderly. The iatrogenic triad in the elderly may be prevented using three possible ways that we observed in our study: interaction of patients with the clinical pharmacist to obtain the BPMH history; collaboration of the clinical pharmacist with physicians for informed decision-making and optimizing the pharmacotherapy; and continuing education activity led by a clinical pharmacist to update the knowledge on drug safety and prescribing in the physicians.

Ethics

Ethics Committee Approval: The Vignan Institute of Pharmaceutical Technology Institutional Human Ethical Committee approved the study (approval no.: VIPT/IEC/89/2022, date: 20.01.2022).

Informed Consent: We assured the confidentiality of the data and obtained informed consent from each participant.

Authorship Contributions

Concept: V.M., Design: V.M., S.R.Y., S.S.S.A., Data Collection or Processing: S.M.P., S.S.S.A., Analysis or Interpretation: V.M., S.R.Y., S.S.S.A., K.K.P., S.M.P., Literature Search: V.M., S.R.Y., S.S.S.A., K.K.P., S.M.P., Writing: V.M., S.R.Y., S.S.S.A., K.K.P., S.M.P.

Conflict of Interest: The authors have no relevant financial or non-financial interests to disclose.

Financial Disclosure: The authors declared that this study received no financial support.

REFERENCES

1. Novaes PH, da Cruz DT, Lucchetti ALG, Leite ICG, Lucchetti G. The "atrogenic triad": polypharmacy, drug-drug interactions, and potentially inappropriate medications in older adults. Int J Clin Pharm. 2017;39:818-825.
2. Renom-Guiteras A, Meyer G, Thürmann PA. The EU(7)-PIM list: a list of potentially inappropriate medications for older people consented by experts from seven European countries. Eur J Clin Pharmacol. 2015;71:861-875.
3. Motter FR, Fritzen JS, Hilmer SN, Paniz ÉV, Paniz VMV. Potentially inappropriate medication in the elderly: a systematic review of validated explicit criteria. Eur J Clin Pharmacol. 2018;74:679-700.
4. Cabré M, Elias L, Garcia M, Palomera E, Serra-Prat M. Avoidable hospitalizations due to adverse drug reactions in an acute geriatric unit. Analysis of 3,292 patients. Med Clin (Barc). 2018;150:209-214.
5. Muhlack DC, Hoppe LK, Weberpals J, Brenner H, Schöttker B. The association of potentially inappropriate medication at older age with cardiovascular events and overall mortality: a systematic review and meta-analysis of cohort studies. J Am Med Dir Assoc. 2017;18:211-220.
6. Mallet L, Spinewine A, Huang A. The challenge of managing drug interactions in elderly people. Lancet. 2007;370:185-191.
7. Brysch EG, Cauthon KAB, Kalich BA, Sarbacker GB. Medication regimen complexity index in the elderly in an outpatient setting: a literature review. Consult Pharm. 2018;33:484-496.
8. Hajjar ER, Cafiero AC, Hanlon JT. Polypharmacy in elderly patients. Am J Geriatr Pharmacother. 2007;5:345-351.
9. Elliott RA, O'Callaghan C, Paul E, George J. Impact of an intervention to reduce medication regimen complexity for older hospital inpatients. Int J Clin Pharm. 2013;35:217-224.
10. Stange D, Kriston L, von-Wolff A, Baehr M, Dartsch DC. Reducing cardiovascular medication complexity in a German university hospital: effects of a structured pharmaceutical management intervention on adherence. J Manag Care Pharm. 2013;19:396-407.
11. Bories M, Bouzillé G, Cuggia M, Le Corre P. Drug-drug interactions in elderly patients with potentially inappropriate medications in primary care, nursing home and hospital settings: a systematic review and a preliminary study. Pharmaceutics. 2021;13:266.
12. American Geriatrics Society 2019 Updated AGS Beers Criteria® for Potentially Inappropriate Medication Use in Older Adults. J Am Geriatr Soc. 2019;67:674-694.
13. MerativeTM Micromedex® Drug Interaction Checking (electronic version). Merative, Ann Arbor, Michigan, USA. Available at: https://www.micromedexsolutions.com/
14. George J, Phun YT, Bailey MJ, Kong DC, Stewart K. Development and validation of the medication regimen complexity index. Ann Pharmacother. 2004;38:1369-1376.
15. Schoonover H, Corbett CF, Weeks DL, Willson MN, Setter SM. Predicting potential postdischarge adverse drug events and 30-day unplanned hospital readmissions from medication regimen complexity. J Patient Saf. 2014;10:186-191.
16. Olson CH, Dierich M, Adam T, Westra BL. Optimization of decision support tool using medication regimens to assess rehospitalization risks. Appl Clin Inform. 2014;5:773-788.
17. Gnjidic D, Hilmer SN, Blyth FM, Naganathan V, Waite L, Seibel MJ, McLachlan AJ, Cumming RG, Handelsman DJ, Le Couteur DG. Polypharmacy cutoff and outcomes: five or more medicines were used to identify community-dwelling older men at risk of different adverse outcomes. J Clin Epidemiol. 2012;65:989-995.
18. Wimmer BC, Bell JS, Fastbom J, Wiese MD, Johnell K. Medication regimen complexity and number of medications as factors associated with unplanned hospitalizations in older people: a population-based cohort study. J Gerontol A Biol Sci Med Sci. 2016;71:831-837.
19. Clay PG. Medication regimen complexity indices: a tool to focus MTM efforts? J Am Pharm Assoc. 2014;54:664.
20. Malabu UH, Vangaveti VN, Kennedy RL. Disease burden evaluation of fall-related events in the elderly due to hypoglycemia and other diabetic complications: a clinical review. Clin Epidemiol. 2014;6:287-294.
21. Novaes PH, da Cruz DT, Lucchetti ALG, Leite ICG, Lucchetti G. The "iatrogenic triad": polypharmacy, drug-drug interactions, and potentially inappropriate medications in older adults. Int J Clin Pharm. 2017;39:818-825.
22. De Oliveira HSB, Gonzales Manso ME. The iatrogenic triad in a group of elderly women contracted to a health plan. SciELO. 2019;22:e180188.
23. Shim YW, Chua SS, Wong HC, Alwi S. Collaborative intervention between pharmacists and physicians on elderly patients: a randomized controlled trial. Ther Clin Risk Manag. 2018;14:1115-1125.
24. Stuhec M, Bratović N, Mrhar A. Impact of clinical pharmacist's interventions on pharmacotherapy management in elderly patients on polypharmacy with mental health problems including quality of life: a prospective non-randomized study. Sci Rep. 2019;9:16856.
25. Gray SL, Hart LA, Perera S, Semla TP, Schmader KE, Hanlon JT. Meta-analysis of interventions to reduce adverse drug reactions in older adults. J Am Geriatr Soc. 2018;66:282-288.
26. Martin P, Tamblyn R, Benedetti A, Ahmed S, Tannenbaum C. Effect of a pharmacist-led educational intervention on inappropriate medication prescriptions in older adults: the D-PRESCRIBE randomized clinical trial. JAMA. 2018;320:1889-1898.